POLITECNICO DI MILANO

Department of Civil and Environmental Engineering
Doctoral School in Structural, Seismic and Geotechnical Engineering

Mechanical effects of sulfate attack on concrete: experimental characterization and modeling

Supervisor

Prof. Claudia Comi

Phd Candidate

Nicola Cefis

February 2016

Nicola Cefis
Mechanical effects of sulfate attack on concrete: experimental characterization and modeling

e-mail:
nicola.cefis@polimi.it

Mechanical effects of sulfate attack on concrete: experimental characterization and modeling

A Thesis
Presented to
The Academic Faculty

by

Nicola Cefis

In Partial Fulfillment
of the Requirements for the Degree
Doctor of Philosophy
in
Structural, Seismic and Geotechnical Engineering

February 2016

Doctoral School in Structural, Seismic and Geotechnical Engineering
Department of Civil and Environmental Engineering
Politecnico di Milano

XXVIII cycle

Faculty Members

- Prof. Raffaele Ardito
- Prof. Fabio Biondini
- Prof.ssa Gabriella Bolzon
- Prof.ssa Claudia Comi (Vice-Coordinator)
- Prof. Alberto Corigliano
- Prof. Dario Coronelli
- Prof. Claudio di Prisco
- Prof. Marco di Prisco
- Prof. Roberto Felicetti
- Prof. Liberato Ferrara
- Prof. Attilio Frangi
- Prof.ssa Elsa Garavaglia
- Prof.ssa Cristina Jommi
- Prof. Pier Giorgio Malerba
- Prof. Stefano Mariani
- Prof. Roberto Paolucci (Coordinator)
- Prof. Umberto Perego
- Prof. Federico Perotti
- Prof.ssa Lorenza Petrini
- Prof. Luigi Zanzi

Abstract

When a concrete structure is located in environments naturally rich in sulfates a series of deleterious reactions can occur inside the material. During the process called sulfate attack the anions of sulfate, coming from the external environment or released by the cement paste in the presence of water can diffuse and react with the constituents of cement (gel *C-S-H* and calcium hydroxide) forming gypsum which in turn reacts with the hydrate calcium aluminates present in the cement paste. The final product of these reactions is the secondary ettringite, an expansive phase that, forming within the hardened matrix, can generate states of stress inside the material. The mechanical effects of these chemical reactions consist in a progressive decrease of the stiffness and strength of the material. This is due to two different phenomena: a chemical damage due to the leaching of silicate hydrates and calcium hydroxide and a stress-induced mechanical damage due to the expansion of ettringite in the pores. The macroscopic consequences on structural elements can be very serious, up to compromise the reliability and the safety of the entire construction. The performance of a structure subject to sulfate attack depends on a large number of strongly interacting factors both of physical-chemical nature (molar concentrations, diffusivity and reactivity) and of mechanical nature (material strength, fracture energy, ...) therefore it is very difficult to predict the real structural behavior. The objective of this thesis is the study, both from the experimental and theoretical point of view, of the mechanical effect of sulfate attack in concrete.

A first objective of this work is to obtain an adequate experimental database on concrete, under different exposure and confinement conditions. To this purpose, an experimental campaign on concrete specimens, produced with two different cements has been launched and is still ongoing. During the experimental campaign samples of concrete were placed in different exposure conditions to produce sulfate attack. Periodically weight variations and macroscopic deformations were measured and the damage of the material was indirectly measured through ultrasonic wave propagation measurements. After 400 days of immersion a series of chemical and physical characterization tests were conducted: X-ray Diffraction, Scanning Electron Microscope observations and Energy Dispersive X-ray Spectrometry.

The second objective of the thesis is the development of a model and of a numerical strategy for the chemo mechanical analysis of concrete affected by the sulfate attack. Within the framework of the Biot's theory, the concrete subject to sulfate attack is represented by the superposition of two phases: the homogenized concrete skeleton and the homogenized fluid which includes the pore solution and the expansive reaction products.

Initially the pores are totally saturated with water but, due to the reaction, acicular crystals of ettringite gradually grow and exert a isotropic pressure on the

solid matrix. The evolution of chemical species during the reaction is computed by a proper chemical model in which the diffusion process of the sulfate in the material and the reaction with the aluminates naturally present in the cement paste are simulated in a coupled form. The amount of ettringite produced is directly related to the difference between the initial and actual amount of calcium aluminates. During the chemical process a part of the solid is consumed due to the leaching and the expansive ettringite can develop in the total porosity given by the sum of the porosity naturally present in concrete and the additional porosity due the leaching process. The state laws of the constitutive model are derived from the free energy, which depends on strains, variation of fluid content and internal variables. In particular an internal variable of chemical damage and two internal variables of mechanical damage (for prevailing state of tension and compression) are introduced.

Starting from this model, valid in the case of fully saturated conditions, an extension to partially saturated condition is proposed. In the case of weakly permeable materials, like concrete, the description of the transport of moisture is carried out through a simplified model in which the only variable is the degree of saturation. The unsaturated conditions modify the kinetic of the diffusion of sulfates within the homogenized material: the model has been suitably modified to take into account the effect of the gradient of the water content on the diffusion of ions. The proposed model and approach are calibrated and validated by comparison of the obtained numerical predictions with experimental on mortar and concrete both taken from the literature and obtained in our experimental campaign.

The model showed a good capability to simulate the most important aspects of the phenomenon in different conditions. A good agreement is obtained between the experimental data and the numerical results in terms of macroscopic deformation, mass variation and depth of penetration of the salts. Furthermore, the internal pressure computed with the developed model is in reasonable agreement with that obtained through the crystallization theory.

Sommario

Quando una struttura in calcestruzzo é collocata in ambienti naturalmente ricchi di solfato puó essere soggetta ad una serie di reazioni chimiche, note con il nome di attacco solfatico, che avvengono all'interno del materiale. Durante il processo gli anioni di solfato, provenienti dall'ambiente esterno o rilasciati dal cemento in seguito a processi di innalzamento termico, entrano a contatto con l'acqua presente nei pori diffondendo nel materiale e, reagendo con i costituenti del cemento (gel *C-S-H* e idrossido di calcio), formano gesso che a sua volta reagisce con gli alluminati di calcio idrati presenti nella pasta di cemento. Il prodotto finale di queste reazione é l'ettringite secondaria, una fase espansiva che, formata nella matrice indurita, puó generare stati di sforzo all'interno del materiale. Gli effetti meccanici delle reazioni chimiche consistono in un progressivo decremento della rigidezza e della resistenza del materiale. Questo fenomeno é dovuto a due differenti meccanismi: un danneggiamento chimico causato dalla dissoluzione di silicati idrati e idrossido di calcio e un danno meccanico indotto dagli sforzi generati nel materiale dall'ettringite che espande nei pori. Le conseguenze macroscopiche sugli elementi strutturali possono essere tali da compromettere la funzionalitá e la sicurezza dell'intera costruzione. Le prestazioni di una struttura soggetta ad attacco solfatico dipendono da numerosi fattori sia di natura chimico-fisica (concentrazioni molari, diffusivitá e reattivitá) che meccanica (resistenza del materiale, energia di frattura) fortemente interagenti tra di loro; per questo motivo risulta notevolmente difficile pervenire a previsioni affidabili. L'obiettivo di questa tesi é lo studio, sia dal punto di vista sperimentale che teorico, degli effetti meccanici dell'attacco solfatico sul calcestruzzo.

Il primo obiettivo di questo lavoro é la formazione di un adeguato database sperimentale in diverse condizioni di esposizione e di confinamento. Allo scopo é stata avviata una campagna sperimentale, tutt'ora in corso, su campioni in calcestruzzo realizzati con due diversi cementi. Durante la campagna sperimentale i campioni di calcestruzzo sono stati conservati in diverse condizioni ed esposti a soluzioni con differenti concentrazioni di solfato di sodio. Periodicamente sono state eseguite misurazioni di massa e di deformazione lungo diverse direzioni; il danneggiamento del materiale é stato calcolato indirettamente tramite prove ultrasoniche. Inoltre, dopo 400 giorni di immersione, sono state eseguite prove chimiche e fisiche per la caratterizzazione del materiale: misura della penetrazione dei sali, Diffrazione a Raggi X, osservazioni al microscopio elettronico e Spettroscopie EDX.

Il secondo obiettivo di questa tesi é stato lo sviluppo di un modello e la conseguente implementazione numerica per l'analisi chimico-meccanica del calcestruzzo soggetto ad attacco solfatico. Nell'ambito della teoria di Biot sui mezzi porosi il calcestruzzo soggetto ad attacco solfatico é rappresentato come sovrapposizione di due fasi distinte: lo scheletro di calcestruzzo omogeneizzato e il fluido

omogeneizzato che include la soluzione concentrata nei pori e i prodotti di reazione espansivi.

Inizialmente i pori sono totalmente saturi di acqua ma, a causa della reazione, si ha la formazione e la crescita graduale di cristalli di ettringite che esercitano una pressione isotropa sulla matrice solida. L'evoluzione delle specie chimiche durante la reazione é calcolata tramite un modello chimico in grado di simulare il processo accoppiato di diffusione dei solfati nel materiale e di reazione con gli alluminati naturalmente presenti nella pasta di cemento. La quantitá di ettringite prodotta é direttamente correlata alla differenza tra la concentrazione iniziale e attuale degli alluminati di calcio. Durante il processo chimico una parte del solido é consumata a causa dei processi di dissoluzione e l'ettringite espansiva puó svilupparsi nella porositá totale data da un contributo legato alla porositá naturalmente presente nel calcestruzzo e da una seconda porositá dovuta al processo di dissoluzione. Le equazioni di stato del modello costitutivo sono derivate dall'energia libera espressa in funzione delle deformazioni, della variazione del contenuto fluido e delle variabili interne. Si é introdotta una variabile interna di danno chimico e due variabili interne di danno meccanico (per stati di prevalente trazione e compressione).

Partendo da questo modello, valido nel caso di materiale inizialmente saturo, é stata proposta un'estensione al caso di materiale parzialmente saturo. Nel caso di materiali debolmente permeabili, come il calcestruzzo, le descrizione del processo di trasporto dell'umiditá é stato svolto attraverso un modello semplificato in cui l'unica variabile é il grado di saturazione. La condizione di parziale saturazione modifica la cinetica del processo di diffusione dei solfati nel materiale: il modello é stato adeguatamente modificato per tenere in conto della condizione di parziale saturazione e dell'effetto del gradiente idrico nel processo di diffusione ionica.

Il modello e l'approccio proposti sono stati calibrati e validati tramite confronto con dati sperimentali relativi a malta e calcestruzzo presi dalla letteratura e ottenuti mediante campagna sperimentale in corso. Il modello mostra una buona capacitá predittiva dei principali aspetti che caratterizzano il fenomeno su differenti geometrie, condizioni iniziali e al contorno. Un buon accordo é stato ottenuto sia con i dati direttamente misurabili in laboratorio (variazione di massa, profonditá di penetrazione dei solfati, deformazioni macroscopiche) che con i valori di pressione calcolati tramite approcci alternativi basati sulla pressione di cristallizzazione.

Ringraziamenti

Fais de ta vie un rêve, et d'un rêve, une réalité.

Antoine de Saint-Exupéry

Al termine di questo percorso desidero esprimere il mio personale ringraziamento a coloro che mi hanno accompagnato in questi tre anni conferendogli quell'importanza e quel valore che solo le luci del tramonto permettono di apprezzare pienamente.

Porgo un sincero ringraziamento alla Professoressa Claudia Comi per la straordinaria cura e disponibilitá con cui ha seguito il lavoro di tesi, dalle origini fino al compimento, permettendomi una grande autonomia decisionale e al contempo trasmettendomi un metodo rigoroso e preciso di fare ricerca.

Un particolare ringraziamento va alla Professoressa Cristina Tedeschi ed alle sue collaboratrici presso il Laboratorio di Diagnostica e Analisi sui Materiali del Costruito per aver seguito ed arricchito con sempre nuovi spunti il lavoro di caratterizzazione sperimentale. In questo ambito desidero porgere un ringraziamento a Marco Cucchi e a Massimo Iscandri, del Laboratorio di Prove Materiali del Politecnico di Milano, per avermi coadiuvato nelle fasi di preparazione del setup sperimentale e alla Professoressa Maria Pia Ricciardi, del Dipartimento di Scienze della Terra e dell'Ambiente dell'Universitá di Pavia, presso la quale ho potuto eseguire le osservazioni SEM.

Desidero inoltre esprimere la mia gratitudine ad alcune persone che, seppur non direttamente coinvolte nel progetto di ricerca qui presentato, hanno lasciato in questi anni un segno indelebile: ringrazio i Professori Umberto Perego e Lorenza Petrini per la fiducia, cortesia e disponibilitá costantemente mostratami; ringrazio gli amici Deborah Briccola, Eleonora Lai e Hadi Moghadasi, per aver condiviso attimi, pensieri, preoccupazioni e speranze.

Il ringraziamento piú grande di tutti va a coloro che, con discrezione ed a voce bassa, non hanno mai smesso di essere presenti. Alla mia famiglia. A loro che mi hanno dato gli strumenti per costruirmi questa realtá. A loro a cui dedico questa tesi di dottorato.

Nicola Cefis

Contents

List of Figures

List of Tables

1 Introduction

Concrete is a heterogeneous material consisting of geological aggregates, hydraulic cement-based binder and water.The use of this material dates back to ancient Rome: famous for the structural daring and the beauty of shapes, still now intact, is the vaulted roof of the Pantheon. In the last two centuries, due to the introduction and of metal reinforcements, concrete has become one of the most important structural materials. Buildings, dams, transport infrastructures, underground structures for storage and supports for machines are just some of the applications of plain and reinforced concrete. Concrete structures have been constructed in greatly heterogeneous climatic and environmental contexts. Particularly harsh external conditions can reduce the durability of the structure through several deleterious chemical and physical processes. The consequences of these phenomena can be substantial, both in terms of load-bearing capacity and functionality (loss of stiffness, cracking, spalling). Degradation process can result from chemical reactions due to the penetration of external ions such as chlorides or sulfates or from slow expansive reactions between the components of the concrete as in the case of alkali-silica reaction or alkali-carbonate reactions. All these phenomena are strongly dependent on the porous structure of concrete and on the specific chemical composition of cement and aggregates. While in new structures designed for aggressive environments the chemical degradation can be prevented or at least mitigated by the use of special cements or additives, the safety assessment of structures built several decades ago requires a proper chemo-mechanical modeling of the phenomena.

This thesis is focused in particular on the degradation process related to the sulfate attack.

The sulfate attack in concrete consists in a complex set of reactions between sulfate ions (coming from the external environment or released from the cement after high heating) and hydrate calcium aluminates present in the cement paste. The final product of these reactions is the secondary ettringite, an expansive phase that, formed within the hardened matrix, can generate states of stress inside the material. The mechanical effects on the structural elements can be very serious up to compromise the reliability of the entire construction ([Lei et al., 2013], [Al Shamaa et al., 2014]). When a concrete structure is located in a geological site naturally rich in sulfates the phenomenon can not be avoided and one can only try to mitigate the mechanical consequences of the phenomenon of reducing the permeability, by using low-aluminates cements or by isolating the external surfaces. In any case the spread of sulfates, as the presence of aluminates in the clinker, and the resulting reaction can not be totally canceled. The present work aims to develop a constitutive model that can simulate the mechanical effects related to the delayed formation of ettringite.

1.1 Literature overview and open questions on sulfate attack

There are many studies on the chemical mechanisms and the mechanical consequences of Sulfate Attack in concrete. Although there is not unanimous agreement on the mechanisms that cause the expansion of material [Neville, 2004] many authors agree on attributing it to the formation of secondary ettringite by reaction of calcium aluminates with sulfates ([Collepardi, 2003], [Tixier and Mobasher, 2003], [Basista and Weglewski, 2008], [Roziére et al., 2009], [Planel et al., 2006]). The rate of reactions and the consequent mechanical response of material depends of environmental factors (species and concentration of sulfate, pH of the solution, humidity, temperature) and intrinsic material properties (w/c ratio, chemical composition of the cement paste, pore distribution, diffusivity properties), see e.g. [Tarcy et al., 2004], [Wee et al., 2000], [Akpinar and Casanova, 2010], [Escadeillas et al., 2007]. The computation of the amount of the reaction expansive products requires a proper diffusion-reaction model, while a mechanical model is required for the prediction of swelling and material damage. The mechanical model can be formulated in different ways. In [Tixier and Mobasher, 2003] the volumetric expansion is treated as an eigenstrain and the mechanical response is modeled by a simple uniaxial stress-strain law. In [Basista and Weglewski, 2008] a micromechanical model based on the Eshelby solution of the equivalent inclusion method is implemented to determine the eigenstrain generated by the formation of ettringite crystals in cement paste. In [Bary, 2008] the effect of expansion is modeled by an approach based on pressure crystallization, the behavior of the solid is described by a poroelasticity model and the Mazars' damage model is used

to describe concrete microcracking. In [Idiart et al., 2011(a)] concrete affected by External Sulfate Attack is modeled by at the meso-scale a two phase composite constituted by aggregates and reactive cement matrix and the degradation is describe by cohesive-crack interface elements.

1.2 Objective of thesis

The performance of a structure subject to Sulfate Attack depends on a large number of factors both of physical-chemical nature (molar concentrations, diffusivity and reactivity) and mechanical nature (material strength, fracture energy, ...). These factors strongly interact and therefore is very difficult to predict the real structural behavior. The fundamental starting point is to have an adequate experimental database in order to understand the physics of the problem and to have the necessary data to calibrate numerical models.

A first objective of this work is to obtain such experimental data on concrete, under different exposure and confinement conditions. To this purpose an experimental campaign has been launched and is still ongoing.

Several concrete specimens were fully and partially immersed in solution with different concentration of sodium sulfate. Periodically weight variations and macroscopic deformation were measured in different directions. The damage of the material was calculated indirectly through ultrasonic measurements. Chemical and physical characterization tests through X-ray Diffraction and SEM observations were conducted on samples extracted after a fixed period of immersion.

The second main objective of the thesis is the develop a model and a numerical strategy for the chemo-mechanical analysis of concrete affected by the sulfate attack. The model should accurately account for the main experimental evidences and, at the same time, should be simple enough in order to be suitable for structural applications. To this purpose a two-phase and three-phase elasto-damage model are proposed accounting for both chemical and mechanical damage.

1.3 Outline

This work is structured in six chapters besides the present Introduction.

Chapter 2 is dedicated to the presentation of the main chemical and physical issues related to the Sulfate Attack. The phenomenon is divided in two different types according the source of sulfate reactant: Internal Sulfate Attack (ISA) and External Sulfate Attack (ESA). In both cases the reactions between sulfate and calcium aluminate and the mechanical effects are reported.

Chapter 3 describes the experimental campaign carried out on concrete samples exposed to ESA. After the description of materials properties and of the curing procedures, the results in term of expansions and mass variations are presented. The final part of the chapter is devoted to the results of chemical and physical tests conducted on portions of material damaged by the reaction.

Chapter 4 presents a critical review of the principal models presented in the scientific literature for the describtion of sulfate attack.

Chapter 5 describes the weakly coupled approach for the simulation of concrete subject to Sulfate Attack in full-saturated conditions. First the diffusion and the chemical reaction are modeled by transport-reaction equations accounting for mass balance equations. These equations allow to compute the evolution in space and time of the expansive reaction products. Then, a bi-phase chemo-poro-elastic model with chemical and mechanical damage is proposed for the simulation of the mechanical behavior.

Chapter 6 extends the saturated approach to the case of partially saturated conditions. To this purpose the chemo-transport equations are modified accounting for the degree of saturation which is computed through a water diffusion analysis and a three phase damage model is proposed for the mechanical analysis.

Chapter 7 presents the numerical approach adopted in the implementation and reports a series of examples for the validation of the formulated model. The diffusion-reaction process and the mechanical behavior are simulated in the case of concrete and mortar specimens subject to ESA and ISA.

Chapter 8 contains conclusions and indications of future developments.

2

Physics and chemistry of sulfate attack

In this chapter we focus on the description of the chemical and physical aspects characterizing the sulfate attack of concrete.

As indicated by many researchers, the strength of concrete against the deleterious reactions involving the material depend, in addition to the exposure conditions, on the products formed during the first period of maturation. The processes of hydration influence the micro-structure of the hardened material and the reactivity towards different ions diffusing through the pore network. This aspect plays a crucial role in the durability of the material. The increase of the porosity corresponds to an increase of permeability and therefore accelerates the diffusion of external agents (water, salts, ...) inside the material [Powers, 1958]. A careful design of the mixture and proper curing conditions can lead to a dense and compact concrete less prone to chemical degradation. Also the addition of fillers within the material, such as the silica fume, allows to reduce the permeability improving the durability of the material [Wee et al., 2000].

The term "sulfate attack" indicates, in its most general form, the reaction between the sulfate ions and the hydrates constituents of clinker. This reaction leads to the formation of secondary ettringite within the hardened paste. At the structural level it leads to a progressive decrease of the mechanical properties of strength and stiffness. In scientific literature it is customary to distinguish, however, two types of sulfate attack depending on the origin of the pollutant: External Sulfate Attack (ESA) and Internal Sulfate Attack (ISA). In the first case the sulfate ions present in the external environment enter into the material through the porous structure. The reaction proceeds from the surface and progressively reaches the inner layers. In the second case the reaction takes place without

preliminary internal diffusion process since the sulfate ions are already present in the material. In both cases, the expansion process is possible only in the presence of water.

The formation of secondary ettringite is a phenomenon dominant only at temperatures above $10°\ C$: for lower temperatures the sulfate attack can lead to the formation of thaumasite, an even more expansive and deleterious product. This work is devoted to concrete subject to sulfate attack at temperatures above the critical value of thaumasite formation. Many of the real structures subject to sulfate attack are placed in contact with the ground and therefore protected from very low temperature. In these conditions there is no formation of thaumasite.

2.1 Chemical composition of cement

The degradation of concrete is a direct consequence of two fact: the internal porous structure of the material that allows the penetration of water and pollutants up to the inner layers and the chemical characteristics of the cement-based binder. Most of concrete used in structural engineering is made using Portland cement(Cement Type I) constituted for 95% by clinker. More recently there has been a progressive use of Portland-composite cement(Cement Type II) in which clinker is at least 65% while the rest is occupied by mineral additions such as blast furnace slag, silica fume, pozzolan, fly ash, calcined shale or limestone. This second class of cements is more resistant to chemical attacks. In the case of an aggressive environment, or particular needs of reduction in the development of heat during hydration, another class of cements is preferred, with a lower percentage of clinker: the blast furnace cement (Cement Type III) with a maximum percentage of 64% of clinker and the blast of furnace slag $36\% - 95\%$, the pozzolanic cements (Cement Type IV) with percentage of pozzolan between 11% and 55%, the composite cements(Cement Type V according to EN197-1) with maximum content of clinker equal to 64% and with simultaneous addition of blast furnace slag and pozzolanic materials. In all these types of cements the percentage of clinker tends to decrease, replaced by different binders. This fact, besides having positive implications in terms of heat of hydration, leads to a reduction of the vulnerability of the material to chemical attack. The clinker is obtained from raw materials consisting of a mixture of limestone and clays that, suitably mixed, are cooked in a rotary furnace at a temperature of about $1450°C$. This process allows to release the oxides from the raw materials which can be combined between them giving origin to the clinker: a granular material varying in size from a few centimeters to portions of millimeter. The main constituents present in raw materials and in clinker are reported in table 2.1 both in real chemical formula and in Cement Chemist Notation ([Taylor, 1997], [Hewlett, 2003], [Collepardi, 1991]).

Principal raw materials		
Name	Chemical formula	CCN
Water	H_2O	H
Sulfur trioxide	SO_3	$\bar{S}$
Calcium oxide	CaO	C
Aluminium oxide	Al_2O_3	A
Silicon dioxide	SiO_2	S
Iron oxide	Fe_2O_3	F
Clinker composition		
Name	Chemical formula	CCN
Tricalcium silicate	$(CaO)_3SiO_2$	C_3Si
Dicalcium silicate	$(CaO)_2SiO_2$	C_2Si
Tricalcium aluminate	$(CaO)_3Al_2O_3$	C_3A
Tetracalcium alumino ferrite	$4CaO{\cdot}Al_2O_3 \cdot Fe_2O_3$	C_4AF

Table 2.1: Raw materials and clinker composition

The calcium aluminates play a marginal role on the ultimate strength, which is almost entirely given by the hydrated silicates, but they reduce the firing temperature of the clinker and give the initial resistance of the material. To delay the hydration process of aluminates a small percentage of gypsum (about 5%) is usually added to the cement clinker. In the initial stage of hydration the gypsum reacts with the calcium aluminates creating a film of primary ettringite and around them. During the next hours the water penetrates beyond the layer of ettringite and reacts with tricalcium aluminate producing gel $C-A-H$. The main constituent of the gel $C-A-H$ are mono-sulphoaluminate $C_4A\bar{S}H_{12}$, tetra-hydrated aluminate C_4AH_{13}, allumino-ferrite C_4AF. The presence of hydrate calcium aluminate confers the initial strength and allows for a fast de-molding of concrete. Aluminate hydrates are, however, reactive toward sulfates: their presence represents a negative factor in term of the durability. The effective mechanical strength of concrete, necessary to meet the resistance requirements, is achieved by the hydration of silicates. The two silicates, by reacting with water, form a calcium silicate hydrate (gel $C-S-H$) and the calcium hydroxide. Only the gel $C-S-H$ provides a significant contribution to the mechanical strength while the calcium hydroxide does not influence appreciably the mechanical properties. The final strength and stiffness of the material is reached when all the silicate has transformed into gel $C-S-H$. This process has a rapid initial kinetics and then a slow kinetics.

2.2 External Sulfate Attack (ESA)

In the case of ESA the sulfate ions which are present in the external environment (ground, industrial water, stored materials) diffuse through the porous micro structure and, reacting with the hydrated constituents of cement, form expansive species. Figure 2.1 shows the cracking patter of a mortar specimen [Al-Amoudi, 2002] and of concrete cylinder after immersion in sodium sulfate solution. Figure 2.2 (a) shows the spalling in a concrete lining of a ventilation shaft.

This type of attack is manifested primarily in structural elements in contact with environments containing sodium sulfates, potassium sulfates, calcium sulfates or magnesium sulfate with a sufficient humidity to enable the activation and development of the diffusion process ([Collepardi, 2003], [El-Hachem et al., 2012], [Lei et al., 2013]). Documented examples of structures affected by ESA are galleries [Lei et al., 2013] and structures for storage of radioactive waste ([Scrivener and Young, 1997], [Sarkar et al., 2010]).

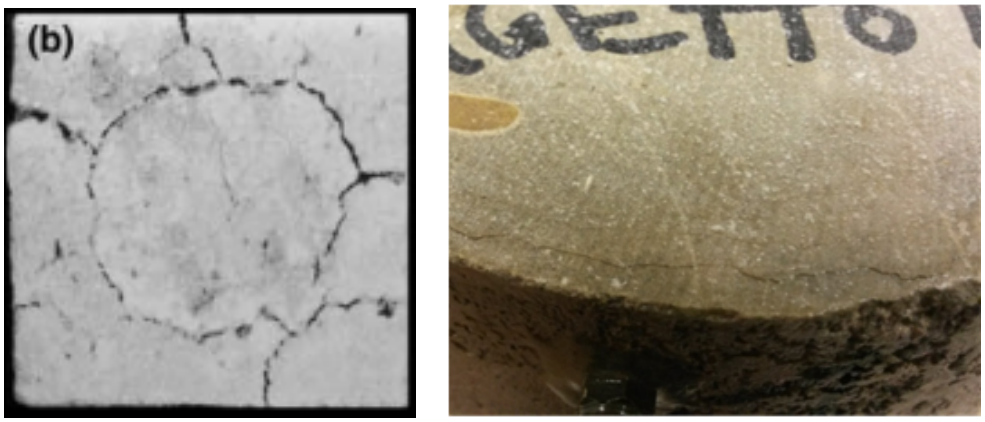

((a)) ((b))

Figure 2.1: Circumferential cracks on (a) mortar [Al-Amoudi, 2002] and (b) concrete specimens after immersion in sodium sulfate solution

2.3 Internal Sulfate Attack (ISA)

In the case of ISA the sulfate ions involved in the reactions with the components of the cement may come from an excess of gypsum, during the phase of preparation of cement or, more frequently, from the thermal decomposition of primary ettringite formed in the early time of the hydration process. This second case is often referred to in the literature as Delayed Ettringite Formation (DEF). As

widely observed in experimental campaigns the phenomenon of decomposition is triggered when the material reaches temperatures close to $70°C$ [Al Shamaa et al., 2014]. These temperatures can be reached within massive structural elements due to the heat released during the hydration process (dams, foundations) or in case of curing in oven (precast elements). Also in this case the presence of water is essential for the development of reaction ([Batic et al., 2000], [Collepardi, 2003]). A particular type of ISA is caused by the reaction between the hydration products and anions present in sulfate-rich aggregates. Typical example is the case aggregates containing iron (pirotite): the penetration of atmospheric oxygen inside the pores causes the oxidation of iron with consequent release of sulfates according the reaction:

$$2FeS_2 + 7.5O_2 + H_2O \rightarrow Fe_2(SO_4)_3 + H_2SO_4 \tag{2.1}$$

This type of attack has been detected for instance in two dams in Spain: the Graus dam and Tavascan dam. The mechanical effects consist in a considerable diffused cracking of the structures [Oliveira et al., 2013]. Figure 2.2 (b) shows the crack pattern which is visible on the inspection tunnel of the Graus dam [Leemann and Loser, 2011].

Additional sources of sulfate are the aggregates containing calcium-sulfate. The sulfates dissolve in water and react with aluminates causing the formation of ettringite.

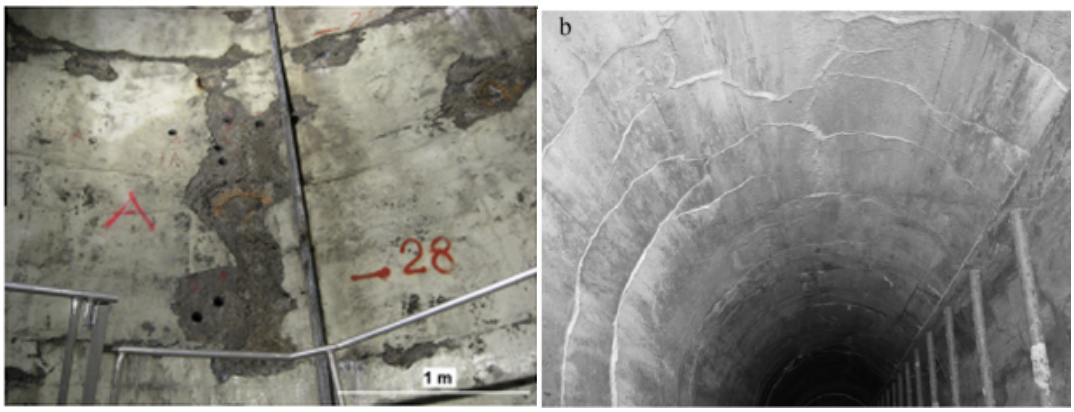

((a)) ((b))

Figure 2.2: Cracks and spalling in vertical ventilation shaft (Switzerland) due to ESA [Leemann and Loser, 2011] (a); cracks in Graus Dam (Spain) due to ISA [Oliveira et al., 2013] (b)

2.4 Chemical reactions of ettringite formation

The sulfate attack of concrete manifests itself through a set of topochemical reactions occurring between the hydrated product of cement and the sulfate ([Basista and Weglewski, 2008], [Marchand, 2003]). In the most common case the sulfates anions come from the ionic dissociation of sodium sulfate through reactions with the portlandite CH or the gel $C-S-H$ leading to the formation of gypsum $C\overline{S}H_2$ ([Marchand, 2003], [Collepardi, 2003],[Tixier and Mobasher, 2003], [Idiart et al., 2011(a)]). The initial process can be defined by the reactions:

$$CH + \mathrm{Na_2SO_4} + \mathrm{H_2O} \rightarrow C\overline{S}H_2 + 2\mathrm{NaOH} \tag{2.2}$$

$$C-S-H + \mathrm{Na_2SO_4} + \mathrm{H_2O} \rightarrow C\overline{S}H_2 + 2\mathrm{Na^{++}} \tag{2.3}$$

Then, the reactions between the gypsum and the hydrated and unreacted aluminates lead to the formation of ettringite $C_6A\bar{S}_3H_{32}$:

$$C_4A\bar{S}H_{12} + 2C\overline{S}H_2 + 16H \rightarrow C_6A\bar{S}_3H_{32} \tag{2.4}$$

$$C_4AH_{13} + 2CH + 3\bar{S} + 17H \rightarrow C_6A\bar{S}_3H_{32} \tag{2.5}$$

$$3C_4AF + 12C\overline{S}H_2 + aH \rightarrow 4\left(C_6A\bar{S}_3H_{32}\right) + 2\left[(A,F)\,H_3\right] \tag{2.6}$$

$$C_3A + 3C\overline{S}H_2 + 26H \rightarrow C_6A\bar{S}_3H_{32} \tag{2.7}$$

In reactions (2.2)-(2.7) the cement notation of table 2.1 has been used.

The amount of secondary ettringite formed through reactions (2.2)-(2.7) depends on the composition of the cement and in particular on the amount of tricalcium aluminate initially present. Several experimental campaigns ([Akpinar and Casanova, 2010], [Wee et al., 2000], [Ouyang et al., 1988]) have shown how cements with lower content of C_3A are significantly less affected by the delayed ettringite formation. Figure 2.3 shows the evolution in time of the expansion of mortar prisms cast with two different types of cement, with high and low concentration of calcium aluminate. The lower curves refer to samples fully immersed in a sodium sulfate solution with concentration of 6000 ppm, while the higher curves refer to a solution with sodium sulfate concentration of 50000 ppm.

The level of acidity of the solution has a great influence on the reaction extent. The ettringite is stable at pH values close to 10.7 [Pajares et al., 2003]. In less alkaline solutions the ettringite coexists with gypsum and for pH values close to 8 the ettringite may not be present.

2.5 Mechanical consequences

The damage of concrete caused by the sulfate attack consists of an overall expansion and microcracks formation with progressive reduction on strength and

stiffness on concrete with possible macro-cracking and spalling of the material.

This phenomenon is mainly due to two interacting effects. The first effect is the dissolution of calcium hydroxide and gel $C-S-H$ caused by the reaction with the sulfates. The gel $C-S-H$ is the main responsible of strength and stiffness in the hardened concrete and its dissolution causes micro-cracks formation. A similar phenomenon is the decalcification of calcium hydroxide by the interstitial solution poor in calcium. From the mechanical point of view the calcium hydroxide does not contribute to the strength but its consumption causes an increase in porosity facilitating the migration of aggressive species inside the material. The second main phenomenon is the formation of expansive ettringite in the pores. This phenomenon is more prominent in ESA where the penetration of sulfate, and the resulting reaction, takes place progressively: the outer layers react before and tend to expand. In this region the solid skeleton is subject to a prevailing compression state. The inner layers instead, in which the reaction has not yet occurred, tend to constrain the expansion of the outer layers and are therefore subject to tensile stresses. These efforts can overcome the resistance of the material causing cracking. This phenomenon is visible on concrete or mortar specimens immersed in sulfate solution as shown in figure 2.1.

The phenomenon of leaching and expansion due to the ettringite formation are two phenomena strongly interacting. Microscopic observations on mortar samples subject to a combination of leaching and ettringite formation show that three distinct zones can be identified, as schematically sketched in figure 2.4 [Santhanam et al, 2002]. The first zone is characterized by diffusive microcracking due to leaching and by ettringite formation. In the second zone there is no leaching and no visible damage is present, but there is delayed ettringite formation. This region tends to expand with respect to the inner part and is therefore subject to compressive stress. In the third zone the reaction is not yet developed and the material is cracked due to tensile stress arising for compatibility of deformation with the outer reactive layer. Figure 2.5 (a) shows a SEM image of the first zone, near the surface of a mortar specimen after immersion in a sodium sulfate solution. The black cracks due to leaching are visible. Figure 2.5 (b) shows a SEM image of the inner part of the same specimen. Microcracks due to tensile stresses are visible in zone 3.

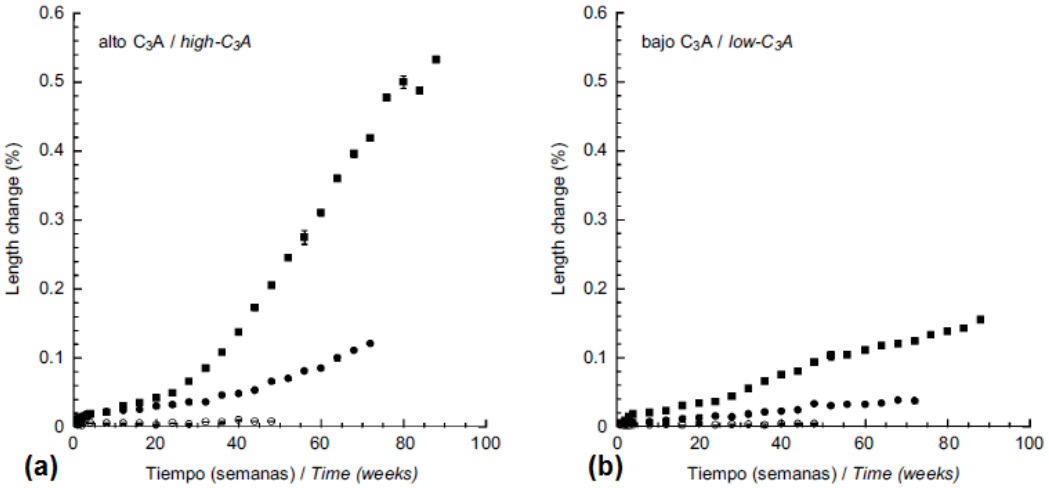

Figure 2.3: Expansion of mortar prism immersed in sodium sulfate solution [Akpinar and Casanova, 2010], (a) high C_3A content and (b) low C_3A content

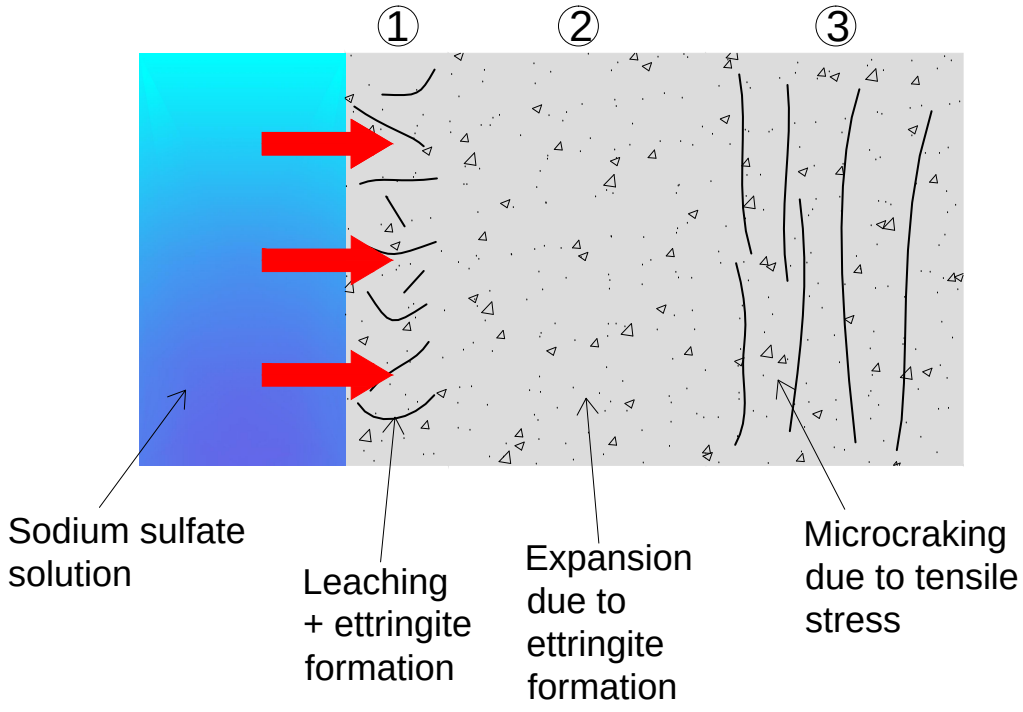

Figure 2.4: Schematic view of the three zones due to ESA

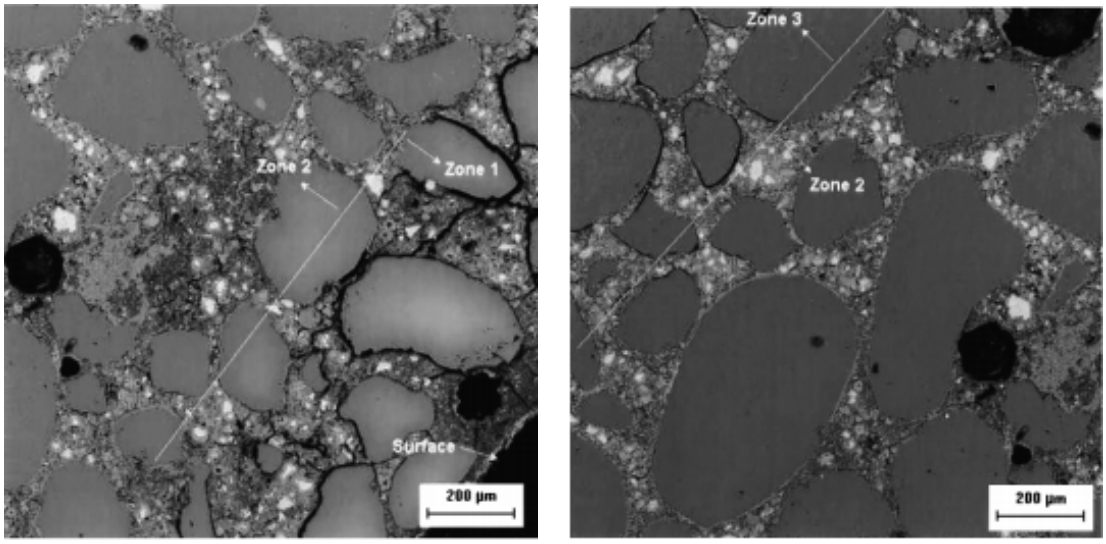

((a)) ((b))

Figure 2.5: SEM image of the three different zones [Santhanam et al, 2002]

3

Experimental characterization of concrete subject to ESA

Concrete is a heterogeneous material that consists in a balanced mixture of aggregates made rigid by a binder composed of cement and water. When the material is subject to sulfate attack, the extent and the kinetics of the chemical reactions are strongly dependent on the mineralogical composition of the cement and on the amount of the individual reactant species within the material. An adequate simulation of the mechanical behavior in time requires the knowledge of several parameters, both of chemical (composition and concentration of the reactants) and physical nature (porosity, water content, temperature).

The main purpose of the experimental campaign carried out at Politecnico di Milano is to measure the response of concrete samples subject to external sulfate attack in terms of deformation and damage evolutions in order to obtain a reliable database designed to calibrate the input parameters of the numerical model. Most of the experimental campaigns presented in the scientific literature are focused on the behavior of cement paste [Planel et al., 2006] and mortar [Akpinar and Casanova, 2010]-[Yu et al., 2013], while a few results are available for concrete.

Furthermore the vast majority of tests is performed under free expansion conditions: the influence of mechanical stress on the phenomenon has been seldom considered in experimental tests. An exception of particular interest is the experimental campaign reported in [Bouzabata et al., 2012], though referring to the internal sulfate attack.

The experimental program developed in this work involves concrete samples immersed in solutions with different concentrations of sodium sulfate Na_2SO_4 (ex-

ternal sulfate attack). The evolution of the reaction and the consequent influence on the mechanical behavior of the material are monitored by measuring the longitudinal and radial extension and the variation of mass. The evolution of the Young modulus is indirectly measured through ultrasonic wave propagation.

3.1 Materials, casting and curing

The tests are conducted on concrete specimens of different shape and composition at the Laboratory of Materials Testing of Politecnico di Milano. The first serie of samples are cylinders of diameter 15 cm and height 30 cm made with a Portland cement CEMII / A-LL 42.5 R, the second serie of samples are prisms of 8 cm $\times$ 8 cm $\times$ 16 cm made with a pure Portland cement type CEM I 52.5R.

Standard cubes of 15 cm side have also been produced with the two mixtures to assess the mechanical strength of the material at 28 days. Table 3.1 shows the chemical composition of cements in relation to the class of sulfate resistance and table 3.2 reports the mix design of the two concretes in terms of water/cement ratio, cement content, maximum size of the aggregates. The particle size distribution of the aggregates is calibrated according to the Fuller's curve.

Cement	C_3A	C_4AF	SO_3
CEM II/A-LL 42.5R	6.08%	7.90%	3.15%
CEM I 52.5R	4.22%	5.16%	3.61%

Table 3.1: Chemical composition of cements

	Compressive strength	w/c	cement content [kg/m^3]	$D_{max}[cm]$
First	C30/37	0.45	250	3.2
Second	C30/37	0.62	387	1.6

Table 3.2: Composition of concrete

The cylinders and the cubes were cast in steel molds, see fig. 3.1 ((a)) , while the prisms were cast in polyurethane molds, ad-hoc fabricated. In addition three cylinders were cast in stainless steel rings of 3 mm thickness, see fig. 3.1 ((b)).

((a)) Casting in stainless steel ring

((b)) Casting in steel molds

((c)) Samples in aging room

((d)) Preliminary mechanical testing

Figure 3.1: Preparation of test specimens

The concrete was kept for 24 hours in the molds in order to ensure a proper hardening. The samples were cured in a climatic chamber at controlled temperature ($T = 20°\ C$) and humidity ($RH = 90\%$) for 28 days, see fig. 3.1 ((c)). After curing ultrasonic measurements along 3 directions were performed on cubes. The results showed that the speed of propagation of the wave are substantially equal in the three directions, confirming the homogeneity and isotropy of samples. The measuring operation is performed in transparency using a transducer with frequency of 50 kHz according to the standard UNI EN 12504-4:2001. The mean value of the dynamic elastic modulus is estimated through the following relation [Lamond, 2006]

$$E_d = V^2 \frac{[\rho(1+\nu)(1-2\nu)]}{(1-\nu)} \tag{3.1}$$

where

ρ = density of concrete;

V = wave velocity;

ν = Poisson's ratio;

E_d = dynamic modulus of elasticity.

The relation between the static (E) and dynamic (E_d) elastic modulus of ordinary concrete can be obtained through the empirical correlation given by [Lydon and Balendran, 1986]

$$E = 0.83E_d \tag{3.2}$$

Table 3.1 reports the values obtained on three cubes in three directions (1: direction of casting, 2/3: orthogonal directions) together with the mean values and the standard deviation.

Specimen	$E_1[MPa]$	$E_2[MPa]$	$E_3[MPa]$	$E_{mean}[MPa]$	SD [MPa]
A	30797	30459	30933	30703	199
B	29433	30361	30030	29941	384
C	30539	29948	30076	30188	254

The characterization of the compressive strength of the material is carried out through mechanical testing of cubes after curing, see fig. 3.1 ((d)). The mean values of strength R measured on two cubes extracted from each cast are

Specimen	R [MPa]
A	33.33
B	26.84
C	29.88

3.2 Experimental procedure

After curing brass studs are glued on cylinders and prisms for the subsequent measurement of axial and longitudinal expansion. Twelve studs are placed on each cylinder, 4 at 90 degrees one from each other at 3 different heights, see figure 3.2 (a). As for the prisms, two studs are glued at the center of the bases for longitudinal measures while 8 studs are placed on the lateral faces to measure transversal deformation.

The samples are then placed in different storage conditions in order to observe the response of the material in different environmental of situations. Twelve free cylinders, three cylinders with rings and six cubes are fully immersed in three different conditions:

- four free cylinders, one cylinder with rings and two cubes in pure water;
- four free cylinders and two cubes in sodium sulfate solution at 5%;
- four free cylinders, two cylinders with rings and two cubes in sodium sulfate solution at 10%;

Three cylinders with the lateral surface wrapped by a plastic film and located in a climatic chamber at temperature $T = 20°C$ and $RH = 50\%$ are partially immersed at the bottom edge in two different conditions:

- one cylinder in pure water;
- two cylinders in sodium sulfate solution at 10%;

Two cylinders with the lateral and the top surfaces wrapped by a plastic film and located in a climatic chamber at temperature $T = 20°C$ and $RH = 50\%$ are partially immersed at the bottom edge in two different conditions:

- one cylinder in pure water;
- one cylinder in sodium sulfate solution at 10%;

Eight prisms are fully immersed in two different conditions:

- four prisms in pure water;
- four prisms in sodium sulfate solution at 10%;

Four prisms are located in a climatic chamber at temperature $T = 20°C$ and $RH = 90\%$ partially immersed for half height in two different conditions:

- two prisms in pure water;
- two prisms in sodium sulfate solution at 10%;

Measurements were performed initially every 14 days to accurately capture the phenomenon of water absorption. After saturation, measurements were performed every two months. The measurements on the cylinders and prisms are performed with the following procedure. The sample is extracted from the solution and, after a couple of minutes necessary to allow dripping of the solution in excess, it is weighed. After weighing, the radial/transversal and longitudinal deformation are measured. In cylindrical samples the measurements of longitudinal displacement are performed by a mechanical comparator Huggenberger while the radial deformation is measured with a electronic micrometer Mitutoyo, see figure 3.2 (b) and (c). In prismatic specimens, given the small size, both measurements are performed by the electronic micrometer Mitutoyo. Finally ultrasonic tests are performed: the samples are place horizontally on a wood rail and the time required for the wave train to traverse the specimen is measured.

((a)) Positioning of the measuring points

((b)) Measuring longitudinal expansion

((c)) Measuring radial expansion

Figure 3.2: Preparation of test specimens and strain measurements

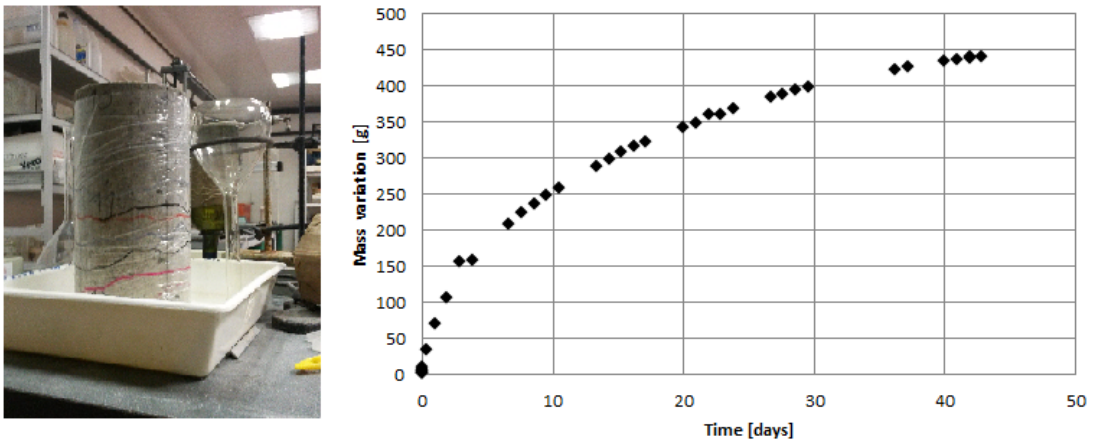

Figure 3.3: Capillary rise test: experimental set-up and evolution of the mass

3.3 Results

3.3.1 Capillary rise test

The parameters governing the diffusion of water have been calibrated on the basis of the experimental data of capillary rise tests. One cylinder partially immersed in water is stored in a climatic chamber at fixed temperature and humidity ($RH = 50\%$, $T = 20°C$). The water uptake in time is measured by weighing. The results in term of mass variation in time are showed in figure 6.1.

3.3.2 Penetration of salt

After 400 days of exposure one cube stored in sodium sulfate solution at 10% is extracted from the solution in order to characterize the penetration of salt. The preliminary operation consisted in cutting in half the cube and in the subsequent storage in a climatic chamber at $RH = 50\%$. The evaporation of water leads to the crystallization of salt which is clearly visible and measurable, see fig. 3.4.

3.3.3 Expansion and mass uptake

Fully immersed cylinders

The displacement measurements in the longitudinal and radial directions allow to characterize the time evolution of the specimens expansion due to water uptake and

Figure 3.4: Profile of salt after 400 days on the half section of the specimen

the chemical reactions. Figure 3.5 shows the evolution of the mean longitudinal and radial deformation on specimens immersed in pure water. After two months of immersion a constant value is reached denoting full saturation of the specimens. It should be noted that the difference between the radial and longitudinal asymptotic deformation is due to the swelling of the glue which affects the radial displacement.

To investigate the behavior of the glue and to characterize its swelling a simple test was performed an a metallic bar with glued studs immersed in water. The measurements in time showed an actual swelling whose asymptotic value is reached approximately after 30 days of immersion. After 15 days the deformation of the glue has already reached the 70 % of the final value. This expansion of glue was subtracted from all the radial measurements in order to obtain the actual concrete expansion. The porosity of the samples was evaluated by difference between the mass of full saturated sample and the mass of the same after drying in a climatic chamber at fix temperature and humidity. The average value of porosity obtained is 0.18.

Figures 3.6 and 3.7 show the concrete radial and longitudinal deformations measured on the cylinders immersed in different solutions. Each curve represent the mean value of 3 specimens, the bars represent the variance of the measures.

Figure 3.8 shows the increase in weight over time for the specimens immersed in the different solution. In all cases a constant value is reached after 3 months of immersion, denoting full saturation of the material.

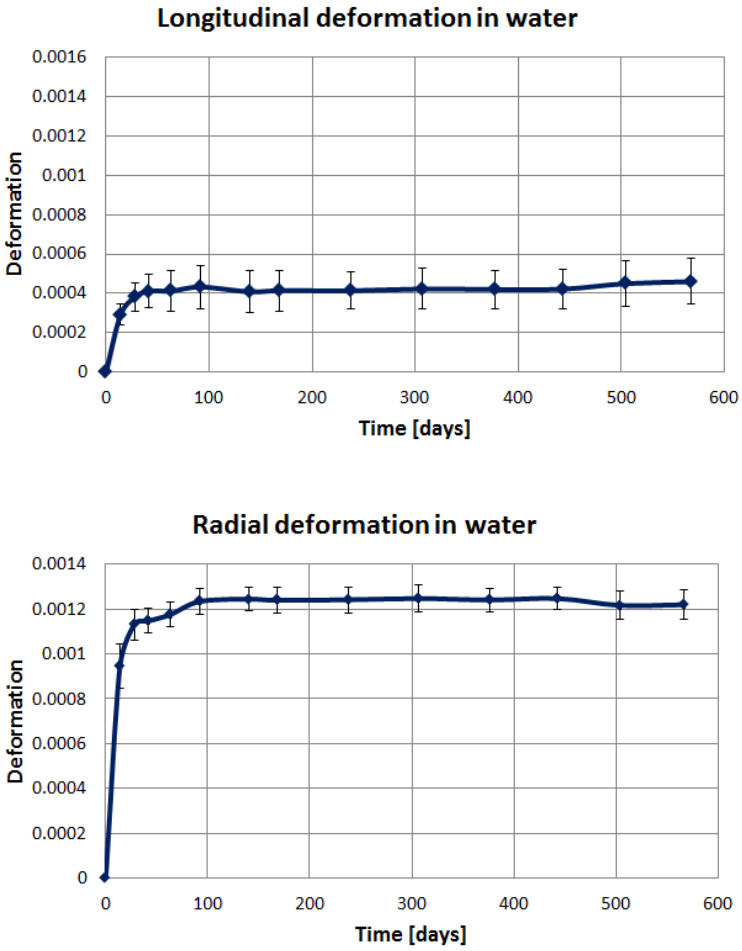

Figure 3.5: Mean longitudinal and radial deformation of cylinder stored in pure water

The deformations of the samples stored in water are due to the variation of the water content and stabilize when the specimens reach full saturation. The radial expansion has a faster evolution due to the geometry of the sample. The samples stored in sulfate solutions exhibit a continuous growth of deformation in time due to the expansive chemical reactions occurring in the material. As confirmed by SEM observation presented in section 3.4, there is a delayed ettringite formation which causes swelling. The increase of deformation is higher in the radial direction because the ratio between the length of the external layer where the reaction occurs and the total length is higher in that direction.

The effect of the sulfate concentration of the solution is very clear: after 570 days of exposure in the 5% sodium sulfate solution the radial deformation is about

0.0008, while the specimens stored in the 10% solution have a radial deformation of about 0.0012. The same remark holds for the longitudinal deformation: 0.0006 for specimens in the 5% solution and 0.0008 for those in the 10% solution. The tests are still ongoing since strains are still growing, showing that chemical reactions are still occurring.

In the case of cylinders cast in stainless steel ring the kinetics of expansion is very slow with respect to the corresponding expansion in free cylinders. This is probably due to the effect of the hoops that severely limits the diffusion of the water and the solution inside the material. For this reason no further comments relating to this set of cylinders are reported in this thesis.

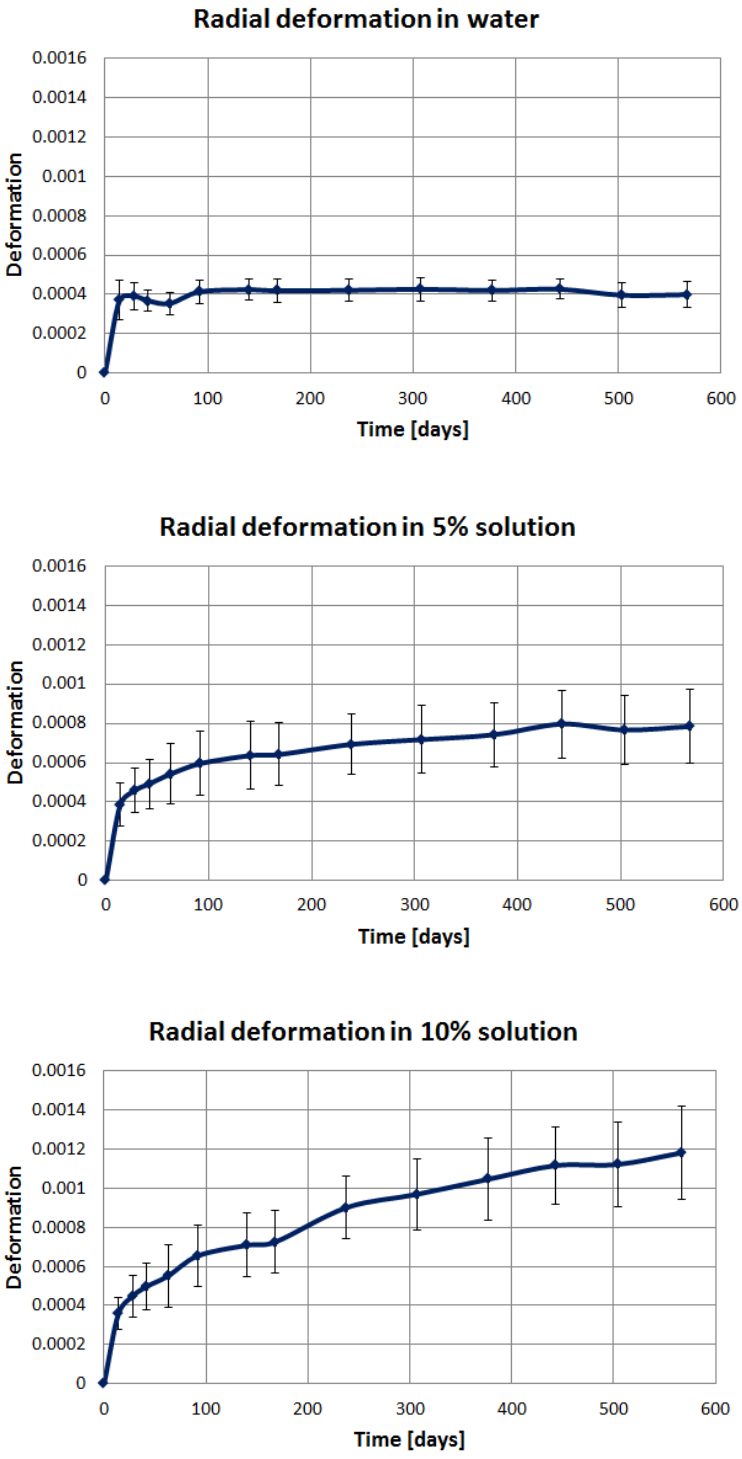

Figure 3.6: Radial deformation of cylinders

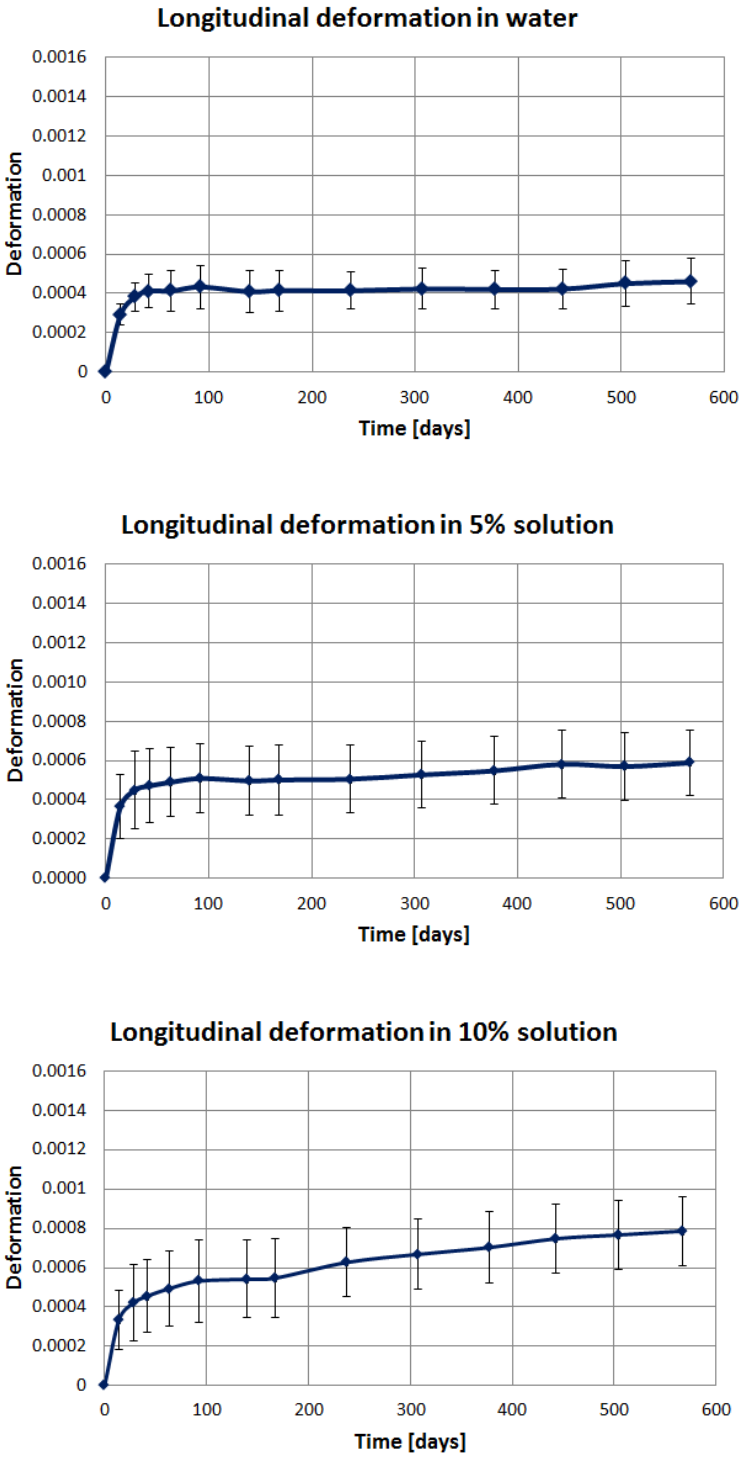

Figure 3.7: Longitudinal deformation of cylinders

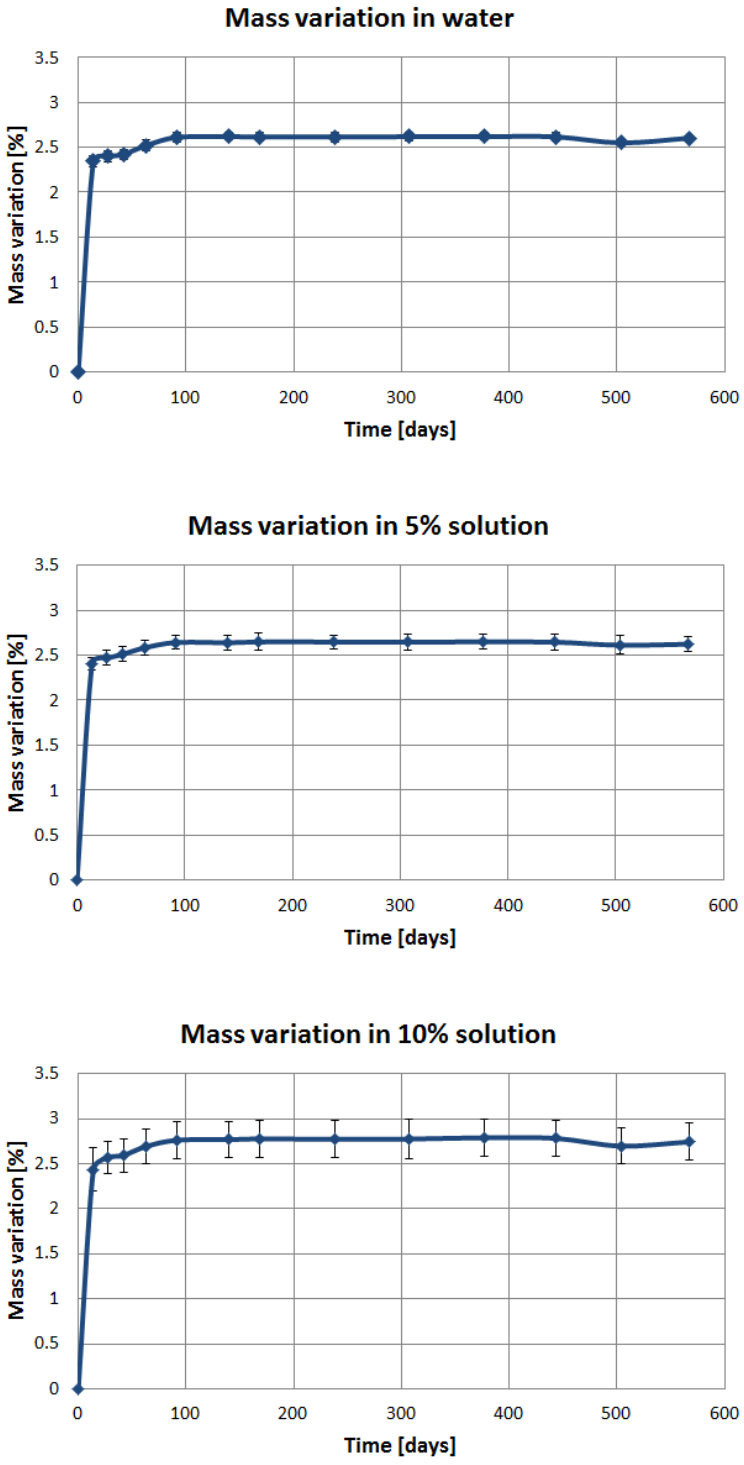

Figure 3.8: Mass variation in different exposure conditions of the cylinders

Fully immersed prisms

The prisms with the second concrete mix design were cast about 10 months later with respect to the cylinders, thus the measurements are relative to 200 days of immersion only. The experimental data in terms of transversal and longitudinal strains are shown in fig. 3.9 and 3.10 respectively both for samples in water and in 10% sodium sulfate solution. The concrete of these specimens is more reactive than that used for the cylinders, therefore the effect of the sulfate attack is very important already after few months of exposure, especially in the transversal direction, where a 0.0015 strain is reached after 180 days of immersion in a 10% sulfate solution.

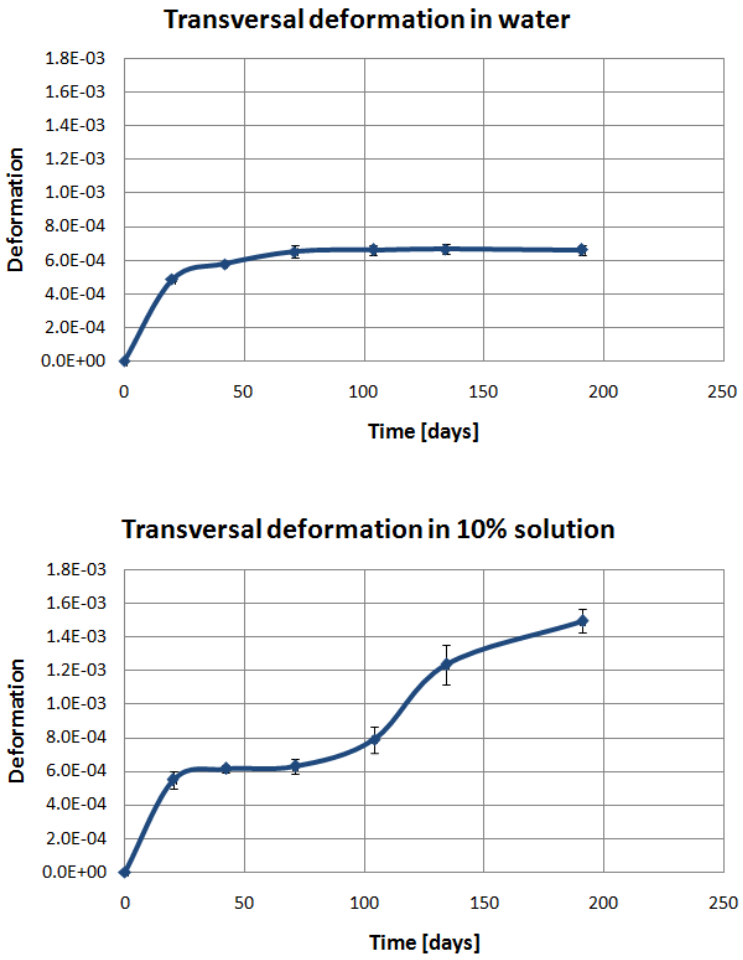

Figure 3.9: Transversal deformation of prisms totally immersed

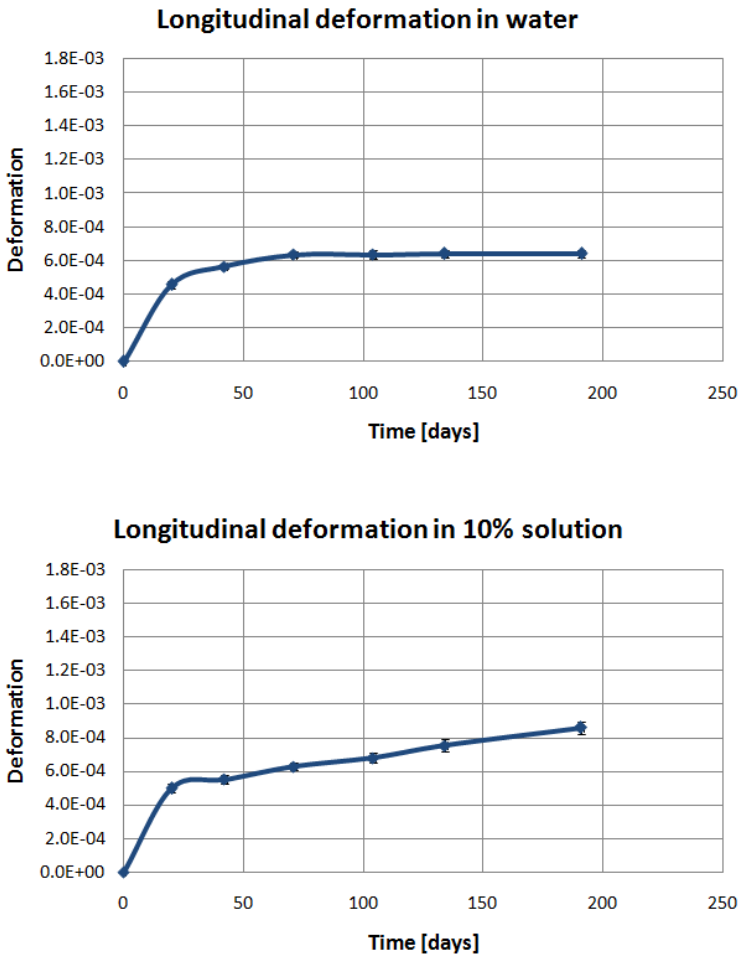

Figure 3.10: Longitudinal deformation of prisms totally immersed

Partially immersed cylinders

Some cylinders, cast in a different time but with the same geometry and mix design of those totally immersed, have been employed for partial immersion tests in a climatic chamber with $T = 20°C$ and $RH = 50\%$. Unfortunately, due to failures of the climate control, the real value of relative humidity was often different from the theoretical one. The results on these cylinders are therefore only qualitative.

Figure 3.11 shows the time evolution of mass density of the cylinder partially immersed.

The curves corresponding to samples with wrapped lateral surface, immersed in 10% sodium sulfate solution show a highly irregular trend in the first 250 days. This phenomenon can be attributed to anomalies of climatic chamber and to the

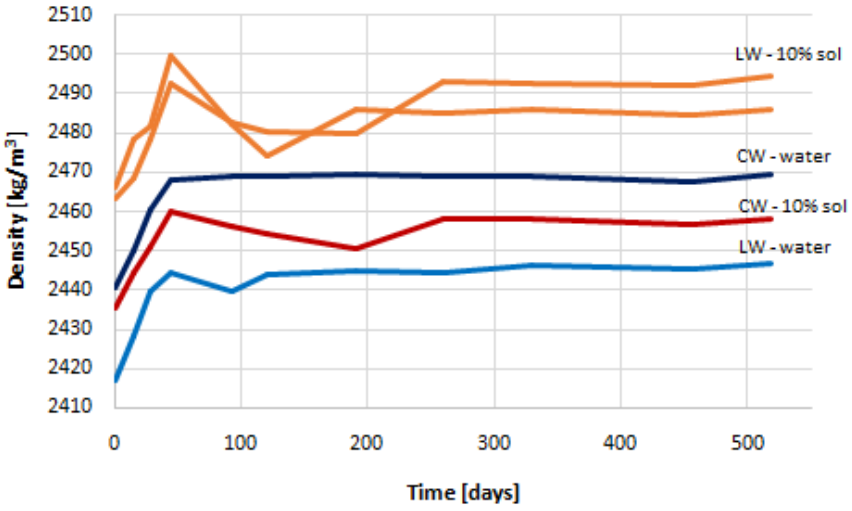

Figure 3.11: Time evolution of density in partially immersed cylinders. Light blue line: lateral wrapping (LW); blue line: complete wrapped in water (CW); orange line: lateral wrapping (LW) sides in 10% sodium sulfate solution; red line: complete wrapped (CW) in 10% sodium sulfate solution

corresponding evaporation at the top edge. The curves of specimens wrapped also at the top face (blue and red line) show a lower anomaly due to a reduced evaporation.

Figures 3.12 and 3.13 show for the bottom, mid and top level the radial deformation for cylinders in water and in 10% sodium sulfate solution with lateral wrapping and complete wrapping respectively. The time evolutions of deformation show how the reaction is present only in the lower part of the cylinders in contact with the solution. In the two upper levels the radial deformations of the cylinders in the sodium sulfate solution are even lower than that of the corresponding cylinder in water.

This phenomenon can be justified by observing that, at these low levels of humidity, the sulfate salts crystallize and occlude the pores reducing the diffusion of water. This hypothesis is supported by the appearance of efflorescence in the lower part of the samples, see figure 3.14. The upper part of the samples has a lighter color than the lower part, and this indicates that water has not reached the upper part.

The model formulated in this thesis is related to humidity levels higher than the value of sulfate salts crystallization, for this reason these tests will not be simulated.

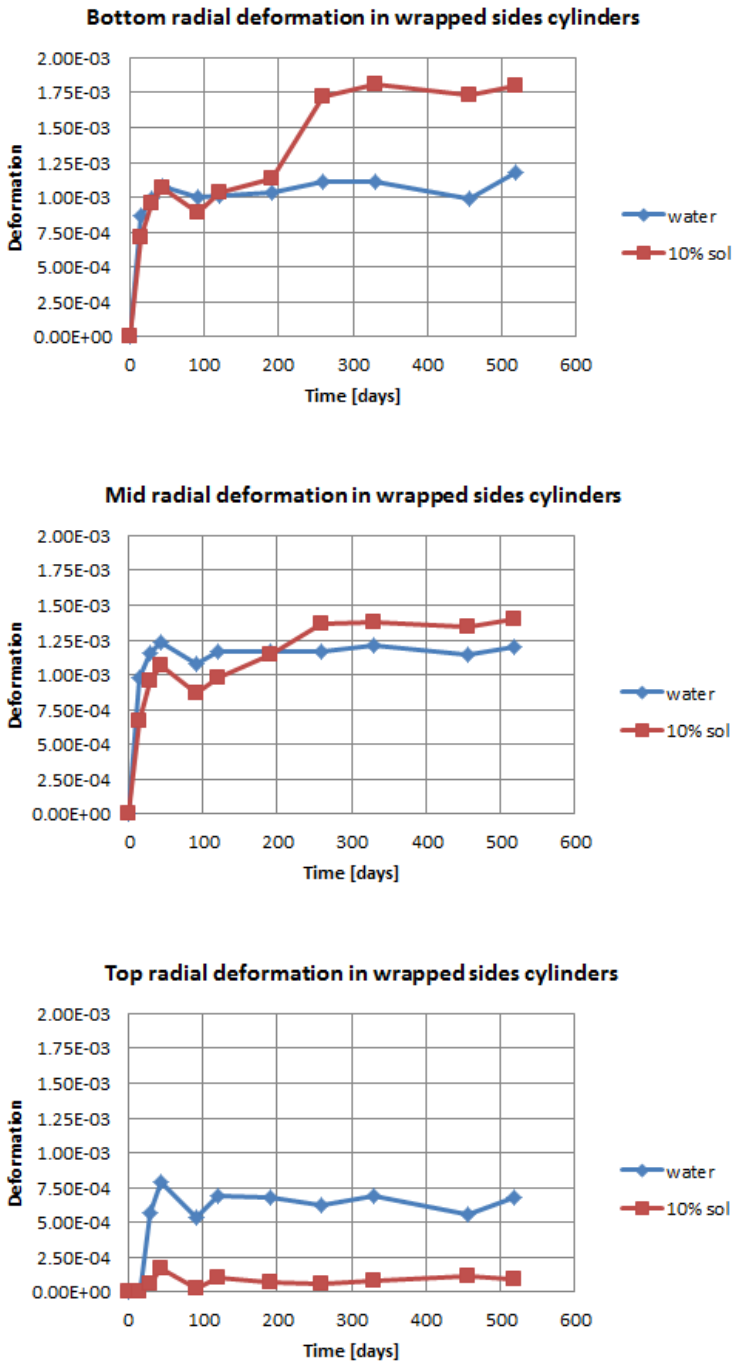

Figure 3.12: Time evolution of radial deformation of laterally wrapped cylinders at bottom, mid and top level

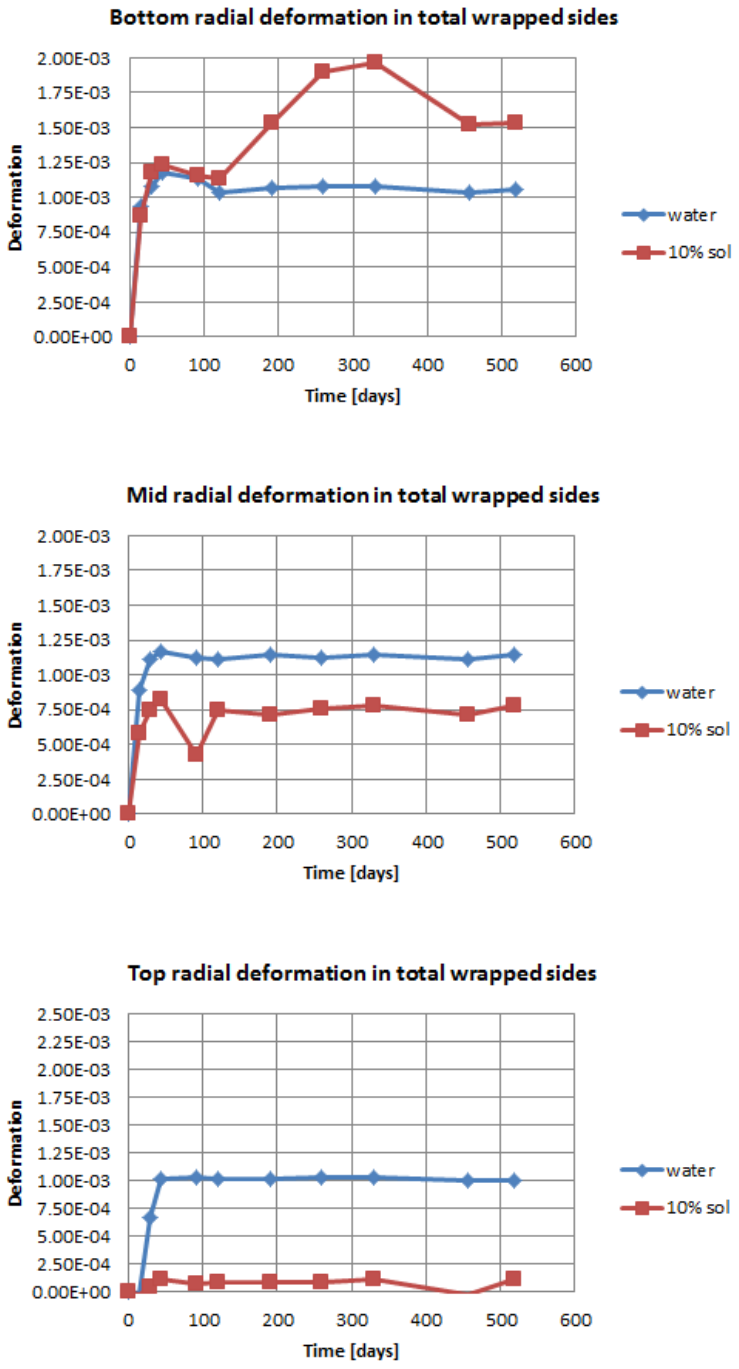

Figure 3.13: Time evolution of radial deformation of completely wrapped cylinders at top, mid and bottom level

Figure 3.14: Cylinders partially immersed in 10% sodium sulfate solution after 600 days of exposure - two cylinders (left and center) are laterally wrapped while one cylinder (right) is completely wrapped

Partially immersed prisms

The prisms partially immersed in water in a climatic chamber with $RH = 90\%$, shown in figure 3.15, progressively adsorb water and swell in the first two months until saturation is reached. Figure 3.16 shows the corresponding longitudinal strain and transversal strains at two different heights.

Figure 3.17 shows the transverse and longitudinal deformations of the prisms partially immersed in sodium sulfate solution (mass concentration 10%). The transversal deformation of the immersed portion of material includes a part of swelling caused by water absorption and, after about 50 days, the contribution due to the reaction. The transversal deformation of the zone not immersed does not show significant differences compared to the one measured on the corresponding specimens in water. In this part the reaction is not occurred. The longitudinal mean deformation over the whole specimen accounts of the local strains of the reacted and unreacted portions. Therefore its value is between the upper and lower transverse deformations.

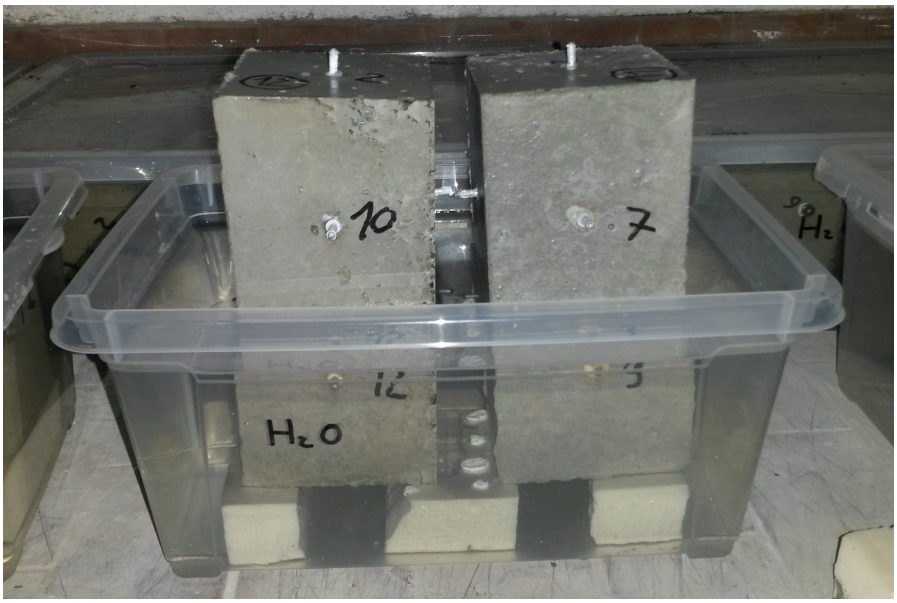

Figure 3.15: Prismatic specimens partially immersed in water

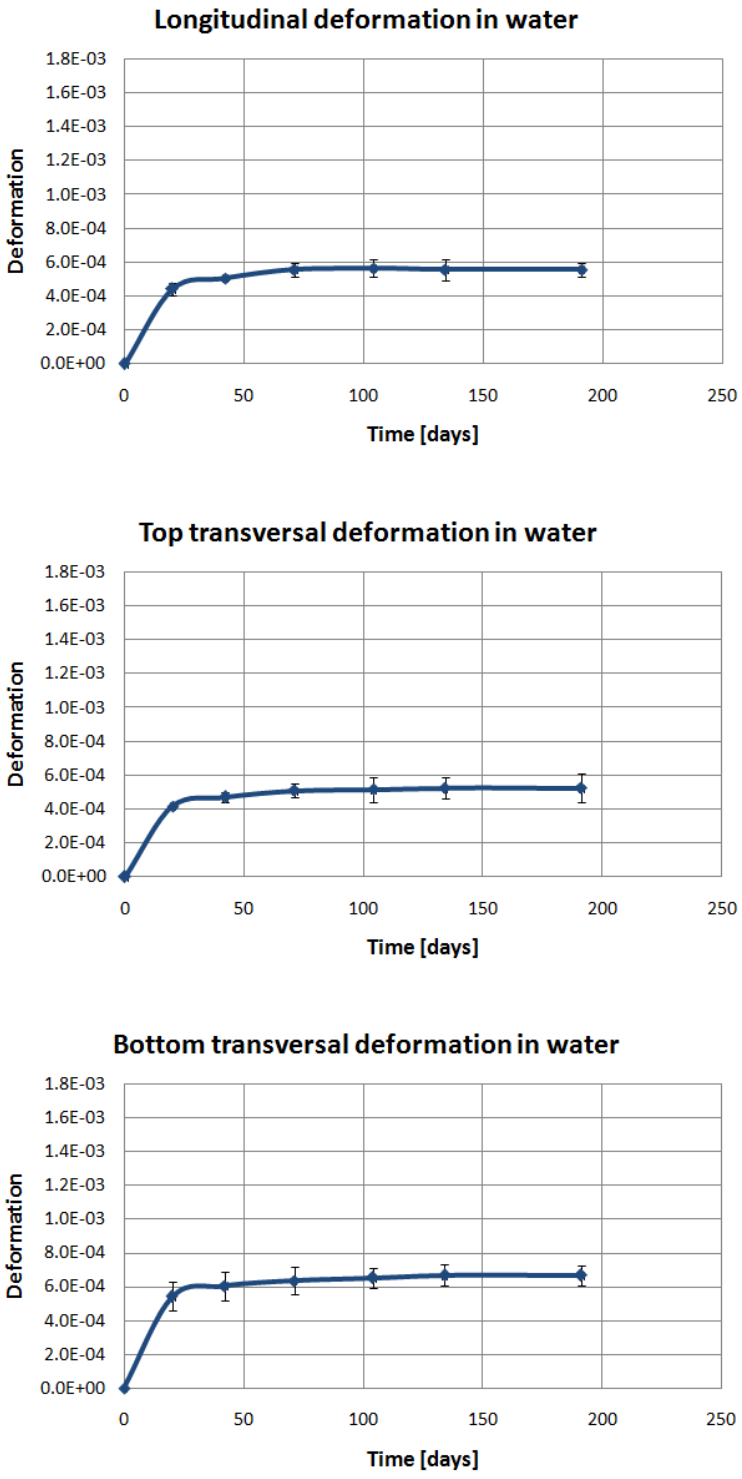

Figure 3.16: Longitudinal and transversal deformations of prisms partially immersed in water

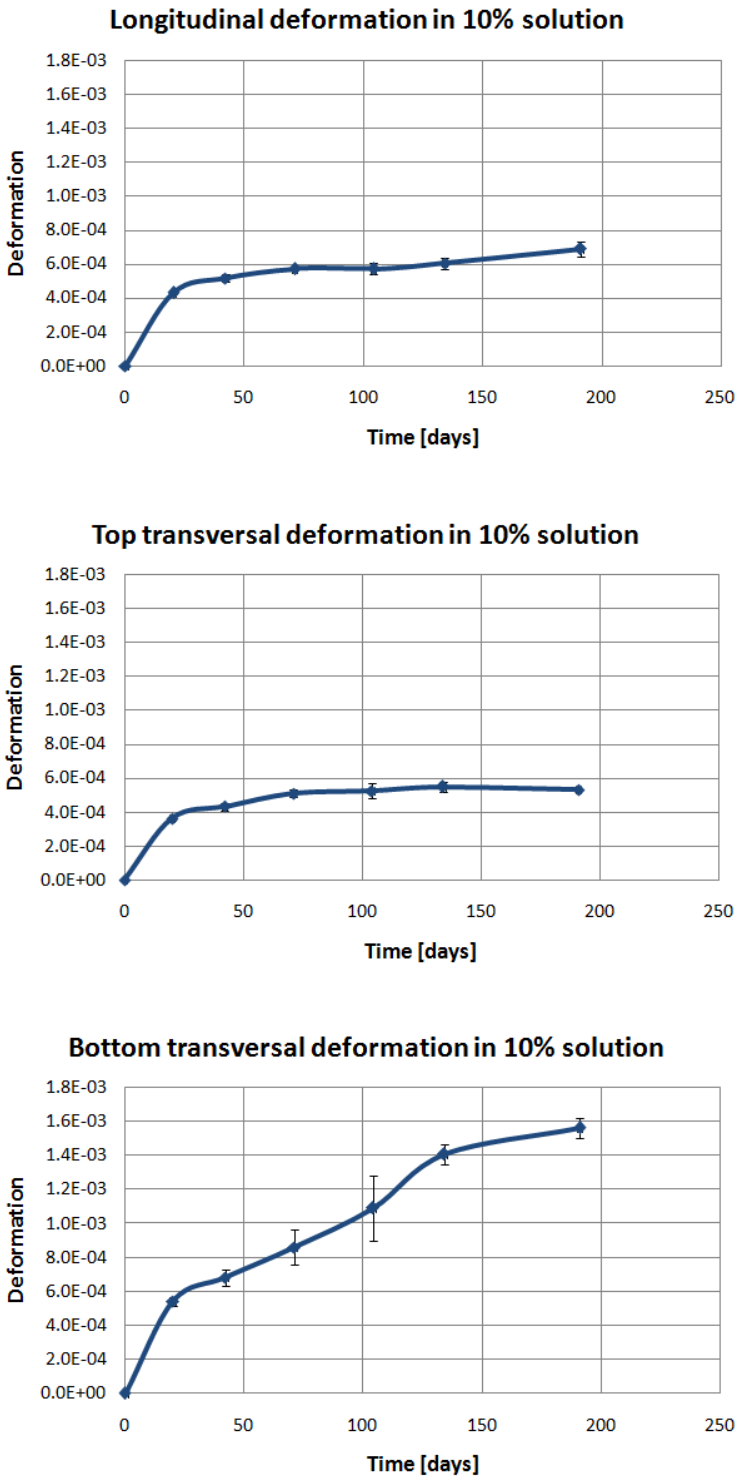

Figure 3.17: Longitudinal and transversal deformation of prisms partially immersed in sodium sulfate solution at mass concentration 10%

3.3.4 Ultrasonic measurements

After 400 days of exposure the evolution of the mechanical properties on the cylinders and the prisms are indirectly evaluated through non destructive ultrasonic test. The experimental facility is shown in fig. 3.18. In these tests a train of longitudinal waves, produced by a transducer placed in contact with one surface of specimens, propagates in the material until it reaches the receiving transducer. The travel time depends on the distance between the transducers, on the density and on the stiffness of the material. When the material is subject to damage the stiffness decreases and the travel time increases. In porous media, like concrete or rocks, another aspect to consider is the variation of acoustic impedance due to the degree of saturation [Berriman et al., 2000]-[Ohdaira and Masuzawa, 2000]. A growth in humidity is associated with an increase in speed and therefore with a higher apparent stiffness.

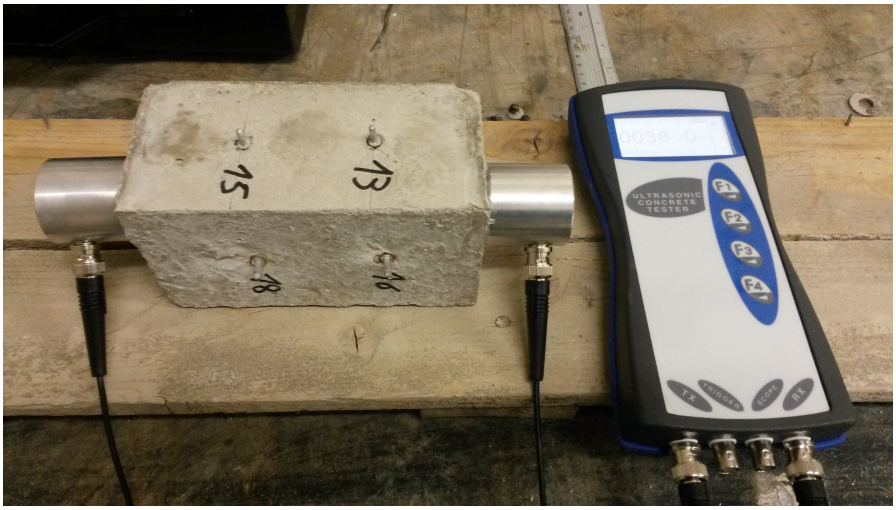

Figure 3.18: Ultrasonic test on concrete prism

In the figures 3.19 and 3.20 the mean value of elastic modulus computed by equations (3.1) - (3.2) of cylinders and prisms are shown.

Comparing the elastic moduli in the two fully saturated cases (10% sodium sulfate solution and water) we note a mean reduction of about 7.2% in case of cylinders and 7.6% in case of prisms. This indicates the development of damage inside the specimens.

Figure 3.19: Mean value of elastic modulus on cylinders in air (right bar), pure water (central bar), 10% sodium sulfate solution (left bar) after 400 days of exposure

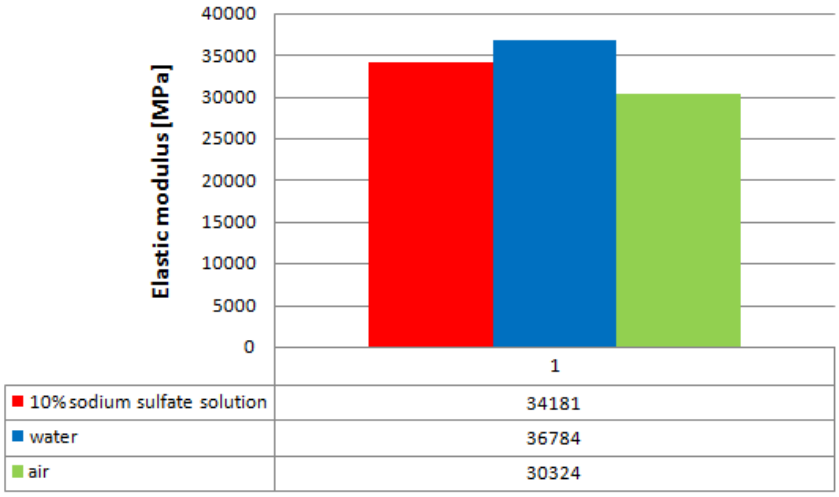

Figure 3.20: Mean value of elastic modulus on prisms in air (right bar), pure water (central bar), 10% sodium sulfate solution (left bar) after 400 days of exposure

3.4 SEM-EDS observations

In order to identify the morphology and the modifications due to the sulfate attack a series of observations with Scanning Electron Microscopy has been performed. The observations were carried out through microscope MIRA3XMU at the Department of Earth Sciences of the University of Pavia, see Figure 3.21.

Figure 3.21: SEM-EDS MIRA3XMU - Department of Earth Sciences of the University of Pavia, courtesy of prof. Maria Pia Riccardi

The electron beam is generated by a crystal of Lanthanum hexaboride heated by an electric field. The electrons are accelerated by a tension of 20 KV and suitably collimated toward the sample placed in the vacuum chamber. The interaction between the primary electrons and the atoms of the material investigated generates different particles and in particular secondary electrons and X-ray. Secondary electrons are captured by detector and converted into electrical impulses. These signals are transform in image on a computer monitor. Photons X are used to perform the Energy Dispersive X-ray Spectrometry (EDS). These rays, emitted as a consequence of excitation of the outer electrons of the material, collide with a crystal generating electric currents. The value of the energy allows a qualitative evaluation of the chemical composition of the investigated material portion.

The observation was carried out on three small samples taken from specimens stored in different conditions for 400 days:

- Sample 1: taken from the reference concrete specimen stored in a climatic chamber at $T = 20°C$ and $RH = 50\%$ and not subject to sulfate attack. The purpose of these observations is to identify the phases naturally produced during the hydration of the cement.

- Sample 2: taken from the outer edge of the cube shown in figure 3.4 immersed in a solution of sodium sulfate with mass concentration of 10% for 400 days. The purpose of these observations is to evaluate the microstructural alterations and the ettringite formation due to the penetration of sulfate ions and the reaction with the calcium aluminates.

- Sample 3: Taken from the middle part of the same cube of sample 2. The purpose of these observations is to evaluate the microstructure of a portion of the material immersed in the aggressive solution but not yet directly affected by the reaction with the sulfates.

Before inserting the samples in the microscope, the mineralization process was performed through the device shown in figure 3.22. A strand of graphite is heated to the evaporation temperature and carbon atoms are deposited on the samples.

The samples thus obtained, shown in figure 3.23 (a), are then inserted into the microscope (fig. 3.23 (b)).

Figure 3.22: Mineralization process

((a))

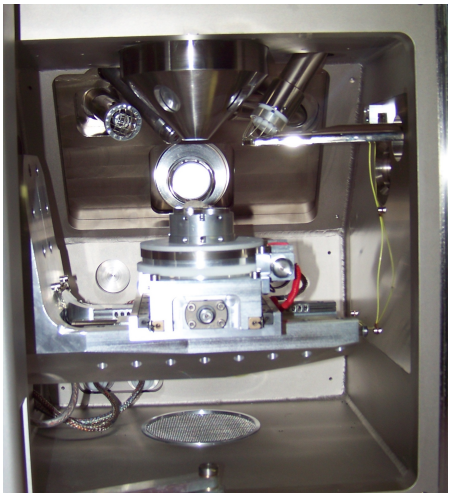

((b))

Figure 3.23: (a) Prepared samples, (b) positioning of the samples in the microscope

3.4.1 Results

The observations conducted on the sample 1 show the typical structure morphology of the cement paste. Most of the material is made of the amorphous gel of calcium silicate hydrates, see Figure 3.24 (a). Rare formations of primary ettringite are incorporated in the gel 3.24 (b).

The primary ettringite has a typical needle-like shape and can be seen in the SEM image of Figure 3.24 (b) but it cannot be identified by EDS, as the finite size of electron beam of about $3-5\ \mu m^2$ is larger than these crystals and consequently also irradiates adjacent regions. Figure 3.25 shows a close up view of the SEM image and the corresponding EDS spectrum which shows a predominant presence of calcium silicate hydrates (indicated by the main peaks of silicon and calcium in the spectrum) and a limited presence of the ettringite components (peaks of aluminum and sulfur).

Figures 3.26 (a) and (b) compare the microstructure of the samples 2 and 3 with a zoom of 959×. In Figure 3.26 (a) several micro cracks are visible and are indicated by white arrows. Microcracking is due to the stress generated by the production of expansive ettringite. No micro-cracks are visible at this scale in sample 3 taken from the inner part of the specimen, see Figure 3.26 (b)

Images at higher magnification, as that of figure 3.27, show that the cracks of the sample 2 are filled with an expansive phase. The EDS spectra centered at points 1 and 2 of figure 3.27, i.e. inside the crack and at the edge of the crack are reported in figure 3.28. One can remark that the crystals inside the crack are rich

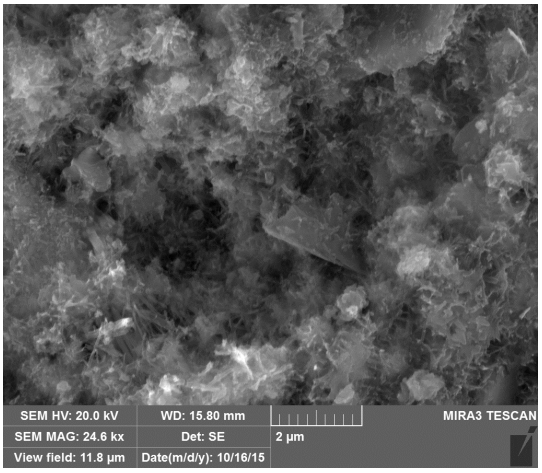

((a)) Gel *C-S-H*

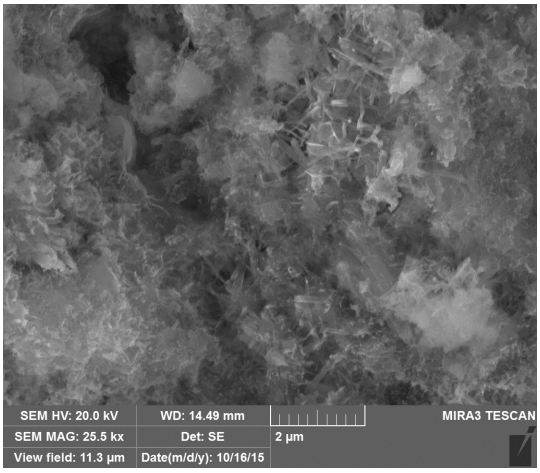

((b)) Ettringite formations inside matrix *C-S-H*

Figure 3.24: SEM of CSH matrix and small primary ettringite formation in Sample 1

in sulfur, which may indicates the presence of ettringite, while the matrix at the edge is rich in silicon, besides that in calcium, as typical in *C-S-H* gel.

Figure 3.29 (a) show the image of another portion of the sample 2, characterized by the amorphous structure of the *C-S-H* matrix with cracks which can be due to leaching. Figure 3.29 (b) shows the formation of needle-like crystal around an aggregate.

In sample 3 the structure is mainly composed of calcium silicate hydrates and there is a limited amount of ettringite. From the morphological point of view the sample 3 is quite similar to the sample 1, compare fig. 3.30 and fig. 3.24.

The EDS spectrum of samples 3, reported in figure 3.31 shows a limited amount of sulfur and is similar to that of sample 1, see fig. 3.25 (b). This confirms that the internal part of the specimen was not yet reached by the sulfate attack.

To sum up, the observations by SEM showed the presence of a newly formed crystalline phase in the external part of the specimen immersed in sodium sulfate solution. Through EDS spectra this new phase can be recognized as secondary ettringite. On the contrary no delayed ettringite formation is observed in the internal part of the specimen.

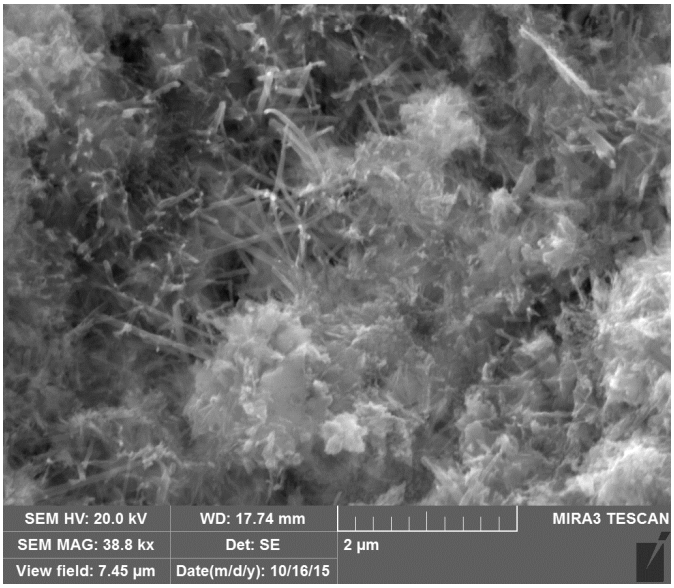

((a))

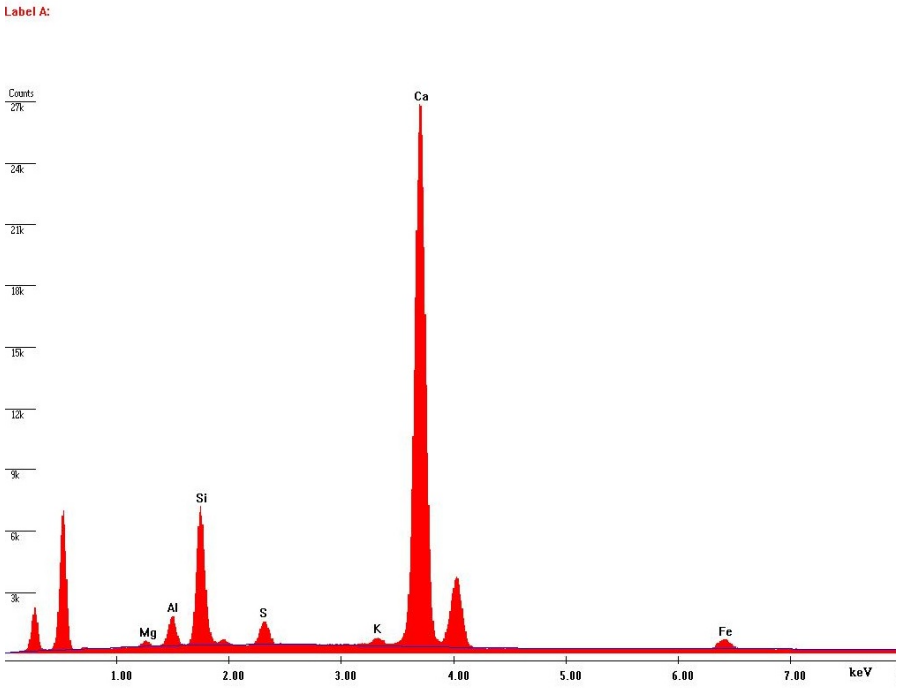

((b))

Figure 3.25: SEM and EDS of hydrated matrix in Sample 1

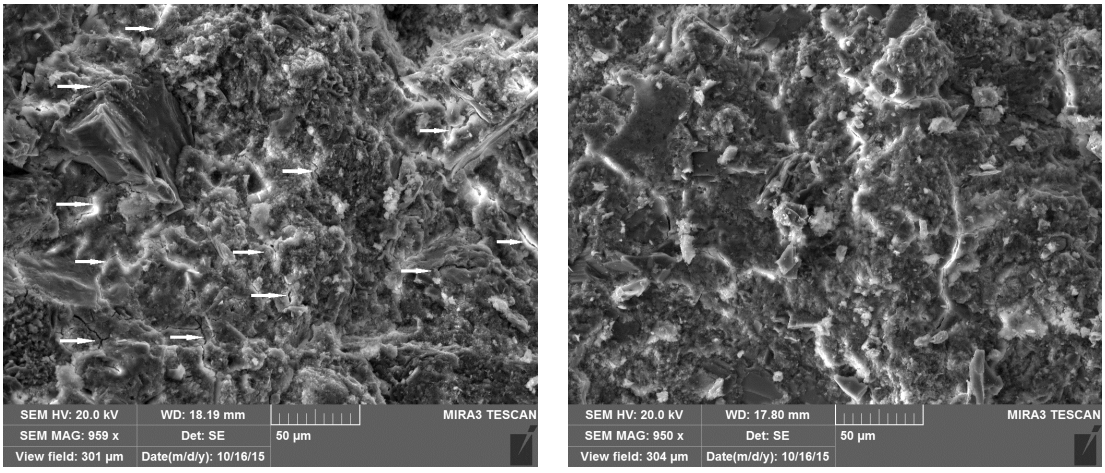

((a)) Sample 2 ((b)) Sample 3

Figure 3.26: SEM immages of Sample 2 and Sample 3 (zoom 959×)

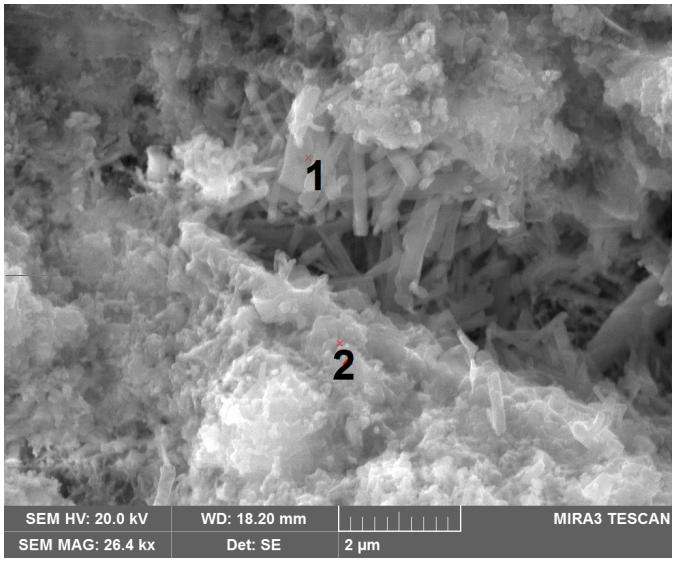

Figure 3.27: SEM image of a crack in Sample 2

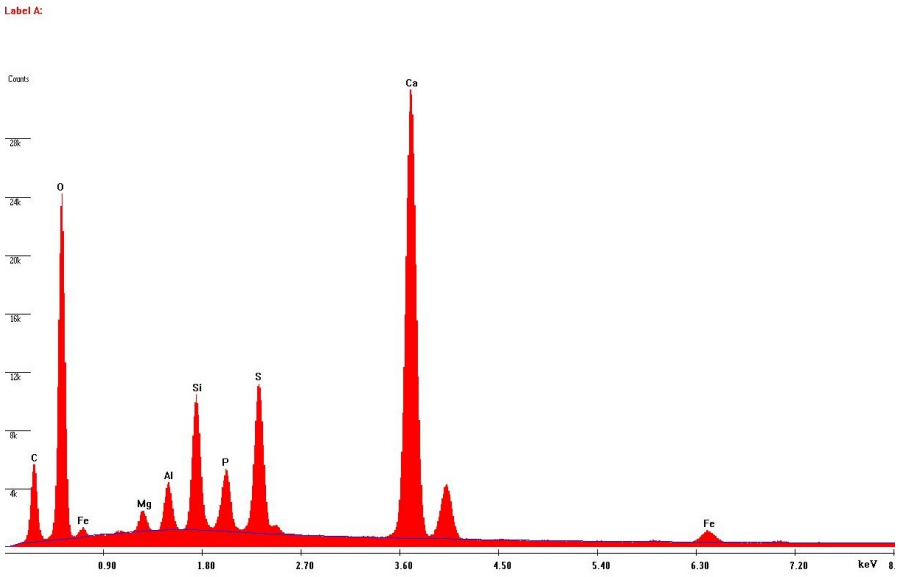

((a)) Point 1

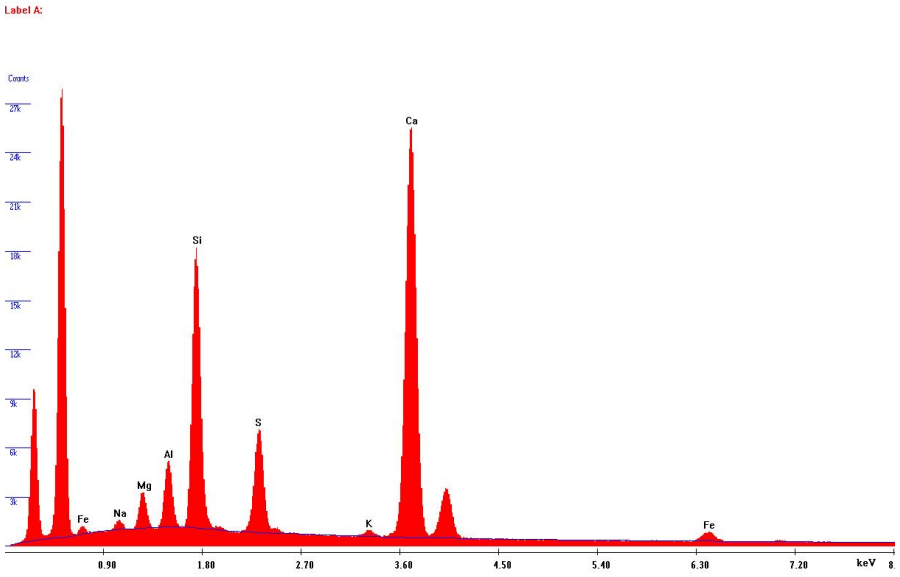

((b)) Point 2

Figure 3.28: EDS refer of point 1 and 2 in the SEM image of figure 3.27

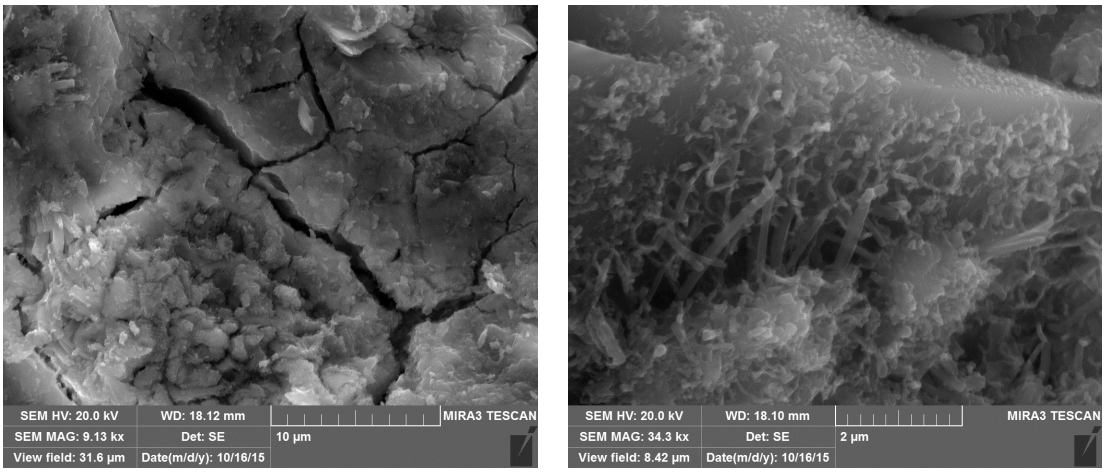

((a)) ((b))

Figure 3.29: SEM images of Sample 2: (a) amorphous *C-S-H* matrix, (b) crystal around a aggregate

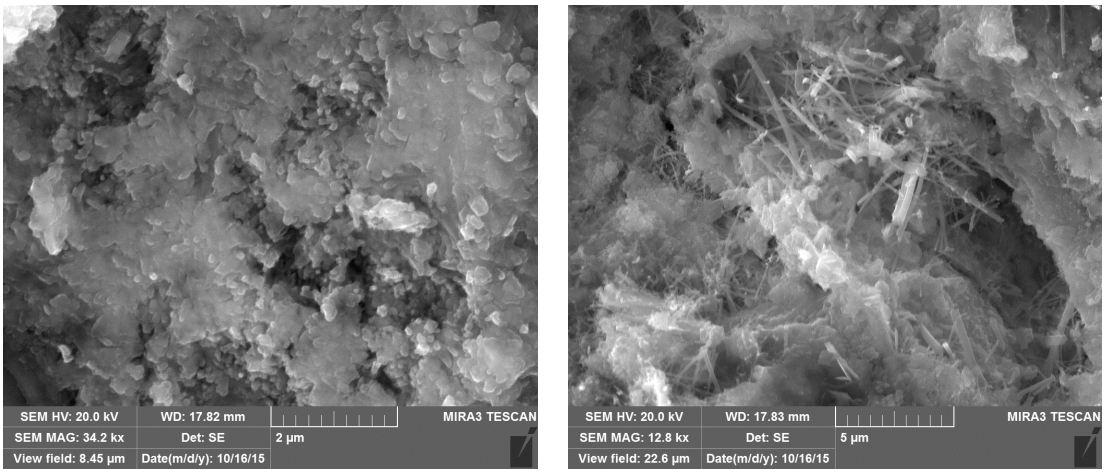

((a)) ((b))

Figure 3.30: SEM images in Sample 3: amorphous (a) and crystalline (b) morphology of calcium silicate hydrate

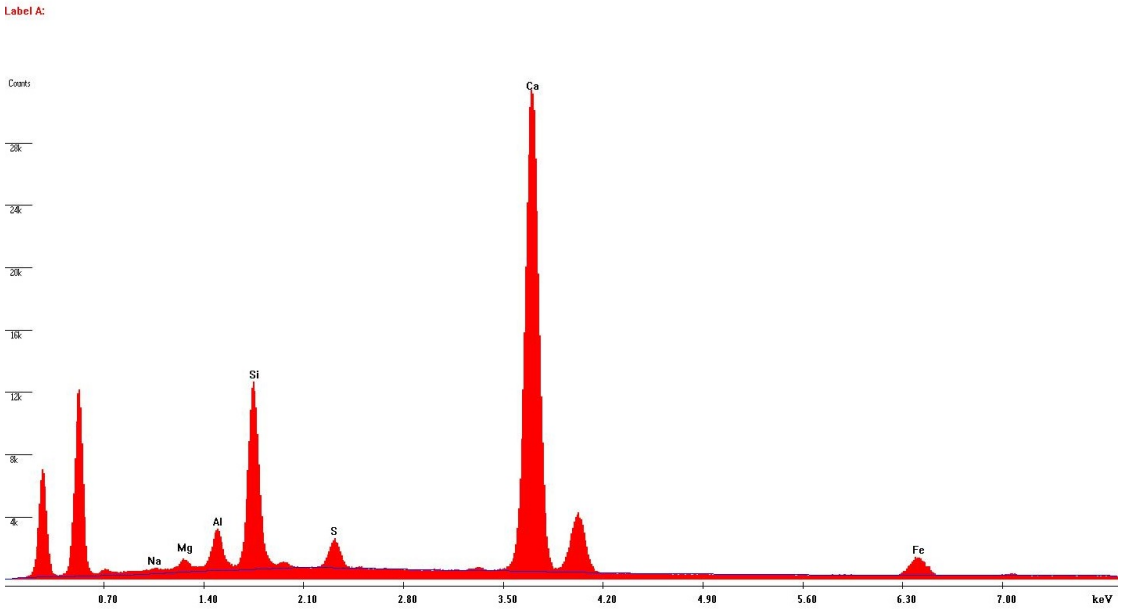

Figure 3.31: EDS of the matrix in Sample 3, corresponding to figure 3.30(a)

3.5 X-Ray Diffraction

A further confirmation of delayed ettringite formation can be obtained through X-Ray diffraction measurements. This technique consists in irradiating the sample with a collimated beam of X rays. The distance between the atoms, comparable with the wavelength of the incident radiation, causes a diffraction wave. In the case of crystalline material, the distances between the different atoms of the lattice causes a specific diffraction pattern that is characteristic of a single compound. X-Ray diffraction measurements have been carried out at the Department of Chemistry, Material and Chemical Engineering "Giulio Natta" of Politecnico di Milano on two samples taken from the same cube used in SEM-EDS measurements. One of the samples is taken near the surface, in the region affected by the SA and the other sample is taken in the centre of the specimen which is not reached by the penetrating sulfates. Figure 3.32 shows the result of the test on the first sample. Besides the minerals of the aggregates (quartz, calcite, dolomite), ettringite has been clearly identified and is reported in the table of constituents.

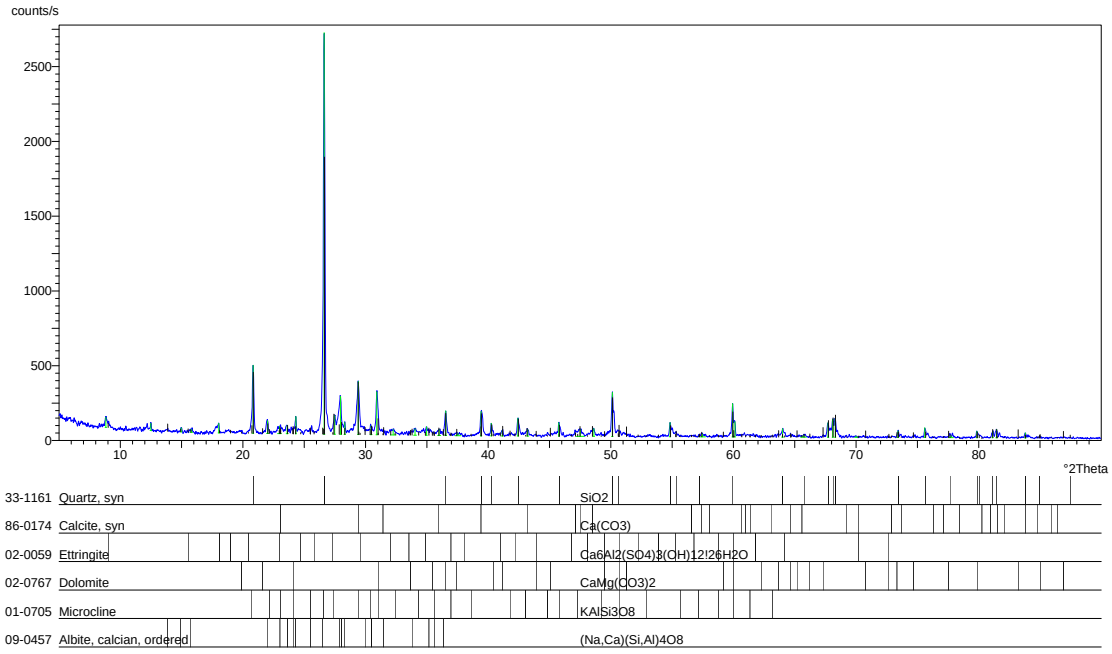

Figure 3.32: XRD of mortar powder of the external edge of cube

Figure 3.33 reports the results of the XRD on the central sample. In this case ettringite is not detected. This indicates that the amount of ettringite possibly present is below the sensitivity of the XRD measurements.

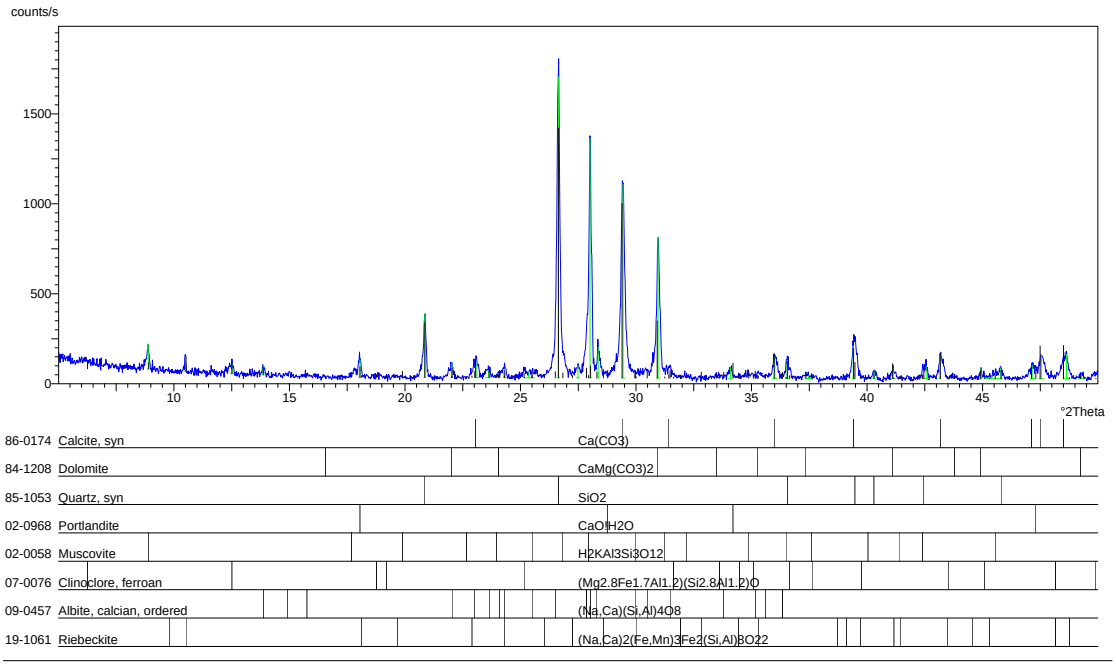

Figure 3.33: XRD of mortar powder of the center of cube

4

Mechanical models for concrete subject to Sulfate Attack: an overview

In Chapter 2 it has been shown that the mechanisms of sulfate attack are very complex due to the various interacting phenomena involved. During the external sulfate attack the degradation of concrete is due to the migration of ions inside the material and to the consequent reactions: the decalcification due to calcium leaching, the reaction between the sulfate ions and the hydrated products (portlandite and gel *C-S-H*) of cement paste with gypsum formation and the reaction between gypsum and the calcium aluminates with consequent formation of ettringite.

From the chemical point of view there is a broad consensus on the reactions leading to the formation of ettringite, but the same can not be said for the mechanisms which cause expansion. This uncertainty is reflected in the mechanical interpretations of the phenomenon and in the consequent strategies of theoretical modeling.

The common point of the different models is the need to describe the diffusion and reaction of the chemical species involved in the process in order to determine the amount of ettringite produced. An overview of these models is reported in section 4.1.

When the ettringite concentration in time and space is known the problem consists in the evaluation of swelling and degradation in concrete. Several different proposals exist in the literature to describe the mechanical consequences of sulfate attack. These models can be divided into two classes:

- Chemo-mechanical models based on topochemical reactions in which the effect of the expansion is attributed to the change in volume between reactants

and reaction products;

- Chemo-mechanical models based on the crystallization pressure in which the expansion is attributed to the formation of expansive crystals inside the pores.

This distinction stems from a different interpretation of the ettringite formation mechanism inside the material. In section 4.2 a review of mechanical model based on the two approaches is presented.

The composite and multiphase nature of concrete suggests its modeling through the theory of multi-phase porous media. This multiphase modeling is also very effective when chemical or physical swelling and degradation processes occur. In particular in the case of sulfate attack a bi-phase formulation can be used which the concrete is represented by the superimposition of two phases: the solid skeleton and the expansive products. A poroelasticity model is proposed to formulate the mechanical model presented in [Bary, 2008]. Many theories aimed at the study of the concrete subject to chemical and physical degradation phenomena are formulated by modeling the material as a multiphase media. Examples include the alkali-silica reaction ([Ulm et al., 2000], [Comi et al., 2009], [Pesavento et al., 2012]), the freezing of concrete in cold regions ([Coussy and Monteiro, 2018]), the leaching of calcium ([Gawin et al., 2007], [Gawin et al., 2009]), the effect of high temperature ([Schrefler et al., 2002]).

The theory formulated in the next chapters for concrete subject to sulfate attack are based on the mechanics of porous media.

To model the inelastic behavior of concrete, including the microcracks formation, both continuum damage models ([Comi and Perego, 2001], [Cefis and Comi, 2014]) and cohesive models [Carol et al., 2001] are used. In several recent formulations ([Segura and Carol, 2004], [Idiart et al., 2011(b)]) concrete is modeled as a composite material with inclusions (aggregates) in the cement matrix and the degradation is described by cohesive-crack interface elements. In this context with application to sulfate attack, we quote the work of [Idiart et al., 2011(a)] in which the variation of volume between reactants and products during delayed ettringite formation is accounted for.

4.1 Chemical models

The assessment of chemical concentrations of the species involved in the reaction can be conducted using two different approaches. A first technique consists in the evaluation of species locally present by minimizing the Gibbs free energy of the entire chemical system. Through minimization it is possible to calculate the chemical concentration at the equilibrium. The main disadvantage of these methods

consist in the necessity to have a thermodynamic database and in the inability to simulate the diffusion processes that govern, in a fundamental way, most of chemical phenomena in porous media.

A second approach make use of diffusion-reaction models. This approach requires a smaller number of parameters and it is therefore much easier to be calibrated by means of a few experimental data. The two main ingredients of these models are a diffusive term that describes the penetration of chemical species and a reactive term that simulates the consumption due to the reaction. A brief description of these terms is given in the following paragraphs

Diffusion on ions

Let us consider a reference volume of a porous medium in which the solid skeleton and the liquid phase coexist. The differential equation describing the diffusion process is obtained enforcing the mass conservation. In general form the equation of conservation, applied to a penetrating ion, can be written in the form:

$$\frac{\partial n_c}{\partial t} + \text{div}\,(\mathbf{j}) = 0 \tag{4.1}$$

where n_c is the molar concentration of the ion in solution (mol/m^3) and $\mathbf{j}$ is the flux. The problem is completed with the boundary conditions on the concentration and or on the flux.

At constant temperature and in the absence of electrochemical coupling between different ions in solution the kinetic of migration process is governed by the agitation of the molecules (Brownian motion). The process, which is purely diffusive, can be modeled by the Fick's first law

$$\mathbf{j} = -\tilde{D}\text{grad}(n_c) \tag{4.2}$$

where $\tilde{D}$ (m^2/s) is the diffusion coefficient, which can be experimentally measured.

In the case of non-isothermal conditions the diffusion equation must also consider the effect of the thermal gradient. The additional motion due to thermal agitation is known as thermophoresis and a mathematical description can be performed using the Soret's law ([Piazza e Parola, 2008]):

$$\mathbf{j} = -\tilde{D}\text{grad}(n_c) + n_c\tilde{D}_T\text{grad}(T) \tag{4.3}$$

where $\tilde{D}_T$ is the thermal diffusion coefficient. If in the solution are present different charged ions the diffusion process can not be described only by equations (4.2)-(4.3). In these cases the mechanism are governed by further phenomena: a difference in concentration between different points of the solution induce a motion of *diffusion* similar to the Fick term; a difference of electric potential due to an

external electric field generate a transport of charged ion and this phenomenon is known as *electric transport*; an external differences in pressure, temperature or humidity generates the motion of ions by *hydrodynamic flow*. A complete description of these phenomena to be found in the classical texts of electrochemistry ([Bard et al., 2003], [Bockris e Reddy, 2013], [Carbó, 2009]) and in [Samson and Marchand, 2007].

In the case of external sulfate attack of concrete, the dominant phenomenon is the diffusion for gradient concentration between the material and the environment. Most of the models present in the literature neglects totally other effects.

Reaction

In porous media two types of chemical reactions can take place:

- through solution reactions: the solid matrix before reacting dissolves in the solution and the reaction occurs between reactants in solution;
- topochemical reactions: the reaction takes place directly between the surfaces of the solid and the solution contained in the pores.

The reactions between the sulfate anions and the calcium aluminates of the cement paste are essentially of topochemical nature. The topochemical reaction can be represented in the form:

$$A + B \Longleftrightarrow C \tag{4.4}$$

where A and B are two reactant and C is the product of reaction. The chemical reaction and the rate of formation of reaction products change the equation of mass transport in which the term $-k\ n_{cA}\ n_{cB}$ must be added, where n_{cA} and n_{cB} are concentrations of the species involved in the reaction while k is the coefficient that defines the kinetics of the reaction.

4.2 Chemo-mechanical models on sulfate attack in concrete

4.2.1 Chemo-mechanical model based on topochemical reactions

Several models proposed in the literature assume that the expansive process is due to the volume change between the reactants (sulfate anions in solution and calcium aluminates present on the walls of pores) and the reaction products (ettringite). In a topochemical reaction the amount of overall expansion depends on the amount of ettringite produced. Many models have been proposed for the simulation of the diffusion-reaction process and for the evaluation of the expansion due to the change

of volume. In [Krajcinovic et al., 1992] a single-ion diffusion-reaction equation in terms of molar concentration of sulfate n_c $[mol/m^3]$ ions is introduced

$$\frac{\partial n_c}{\partial t} = (D_{eff}\,\mathrm{Grad}(n_c)) - kc(n_{c_a^0} - n_{c_e}) \tag{4.5}$$

where D_{eff} $[m^2/s]$ is the effective diffusion coefficient depending on microcrack evolution, k is the rate of reaction, $n_{c_a^0}$ $[mol/m^3]$ is the initial concentration of tricalcium aluminate in the hardened paste, $n_{c_e}[mol/m^3]$ is the actual concentration of ettringite. In this model it assumed that the ettringite forms around the spherical grains of aluminate and develops radially. The volumetric expansion depends on the volumetric density and on the elastic properties of ettringite, on microcrack density and on the deformation of the aluminate grain. The mechanical response of the material is assessed through an elastic perfectly brittle constitutive model for states prevailing traction.

The model proposed in [Tixier and Mobasher, 2003] and subsequently adopted in [Idiart et al., 2011(a)] considers a two-ions diffusion-reaction scheme. The general equations (2.5) - (2.7) that describe the reaction between sulfates and aluminates are condensed in a single lumped reaction

$$C_{eq} + q\overline{S} + rH \longrightarrow C_6A\overline{S}_3H_{32} \tag{4.6}$$

where C_{eq} is the equivalent grouping of calcium aluminates whose molar concentration n_c is given by

$$n_c = \sum_{i=1}^{4} \gamma_i\; n_{ci} \tag{4.7}$$

n_{ci} $[mol/m^3]$ is the actual molar concentration of each aluminate and γ_i is the ratio between the concentration of each aluminate and the total concentration of aluminates.

$$\gamma_i = \frac{n_{ci}}{\sum_{i=1}^{4} n_{ci}} \tag{4.8}$$

The diffusion-reaction model related to the lumped equation is

$$\begin{cases} \frac{dn_s}{\partial t} + k\; n_c\; n_s = \mathrm{div}(D(\mathrm{grad}(n_s))) \\ \frac{dn_c}{\partial t} + \frac{k}{q}\; n_c\; n_s = 0 \end{cases} \tag{4.9}$$

The mechanical effect of ettringite formation is taken into account by the volumetric expansion ε_{chem}. Starting from the actual molar concentration of aluminates the volumetric deformation is [Idiart et al., 2011(a)].

$$\varepsilon_{chem} = \left\langle \sum_{i=1}^{4} \left(n_c^0 - n_c\right) \frac{\Delta V_i}{V_i} \mathcal{V}_i - f \cdot \phi_0 \right\rangle \tag{4.10}$$

where $\langle \bullet \rangle$ denotes the positive part of $\bullet$, $\mathcal{V}_i$ is the molar volume of each aluminate i $[m^3/mol]$, $f \in (0.05 - 0.40)$ is a coefficient representing the portion of the pores that needs to be filled before macroscopic expansion appear, ϕ_0 is the initial porosity. The volumetric variation is [Tixier and Mobasher, 2003]:

$$\frac{\Delta V_i}{V_i} = \frac{\mathcal{V}_e}{\mathcal{V}_i + \nu_i \mathcal{V}_{gyp}} - 1 \tag{4.11}$$

This formulation of diffusive-reactive problem has been used in [Idiart et al., 2011(a)] and coupled with a meso-scale model based on zero-thickness interface elements equipped with cohesive crack constitutive laws. The concrete is considered as constituted by two materials: the homogenized mortar (cement paste and small aggregates) and the largest aggregates. The non linearity of the material is taken into account with zero-thickness interface elements introduced at all aggregate matrix interfaces and within the matrix, see figure 4.1. The constitutive law

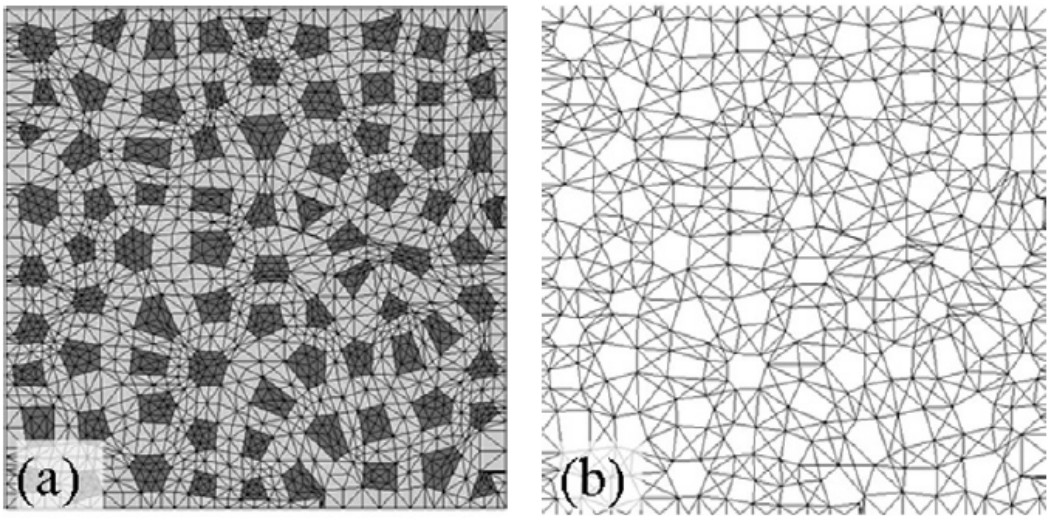

Figure 4.1: FE discretization at the meso-level (a) and arrangement of zero-thickness interface elements for the same mesh (b) [Idiart et al., 2011(a)]

for the interface elements is able to incorporate the effect of mechanical damage and aging of concrete. The initial failure surface depends on tensile strength, cohesion and friction angle. The damage of the material reduces the surface. The aging of concrete is considered in a phenomenological way through an empirical relation.

In this model the diffusive properties change due to the cracking of the material: a quadratic - linear relation between crack width and diffusivity has been introduced. This approach allows for a complete description of cracking on specimens, in good agreement with the experimental observation.

In [Sarkar et al., 2010] a more refined model was proposed for the analysis of diffusive and reactive problem. A chemical activity gradient is taken into account in the diffusive term. For each ionic species present in solution a diffusive equation can be formulated and solved simultaneously in order to obtain the molar concentration in time and space for all species. During the diffusive process some ions react with the cement hydration products and some solids dissolve or precipitate in the pore solution to maintain the chemical equilibrium. In this model the diffusive and reactive problem is solved by a sequential approach: first the diffusion equations are solved and then the chemical equilibrium is enforced.

The change in solid volume due to the reactions (leaching of calcium, depletion of aluminate and ettringite formation) is calculated as difference between actual and initial volume of each component. A positive change in volume due to ettringite formation induce deformation and crack inside the material. A isotropic scalar damage parameter proportional to the deformation is introduced to simulate the reduction in stiffness and strength and the change in diffusive properties, see figure 4.2.

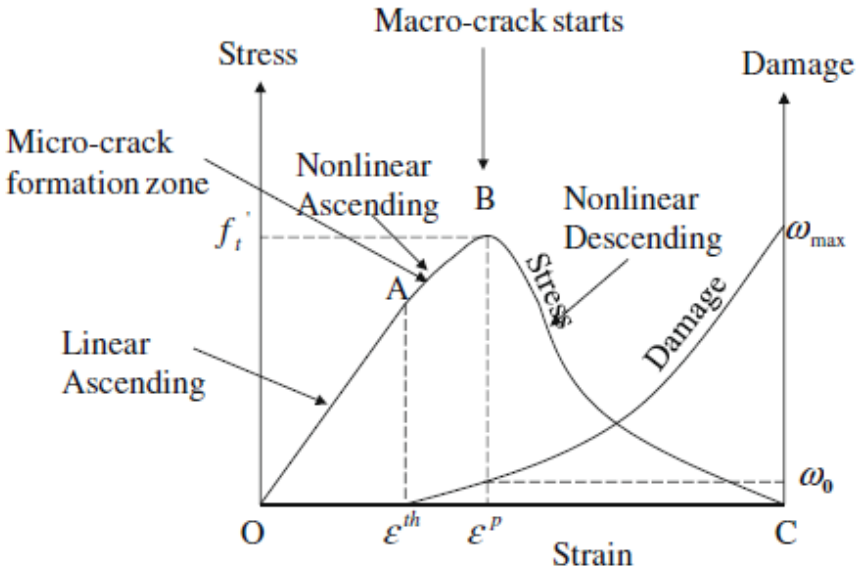

Figure 4.2: Stress-strain curve used in [Sarkar et al., 2010]

In [Basista and Weglewski, 2008] a diffusion-reaction model similar to that proposed in [Krajcinovic et al., 1992] has been adopted and enriched. The same paper presents a comparison between the values of expansion obtained considering the volume change in the topochemical reaction and that obtained considering the crystallization pressure.

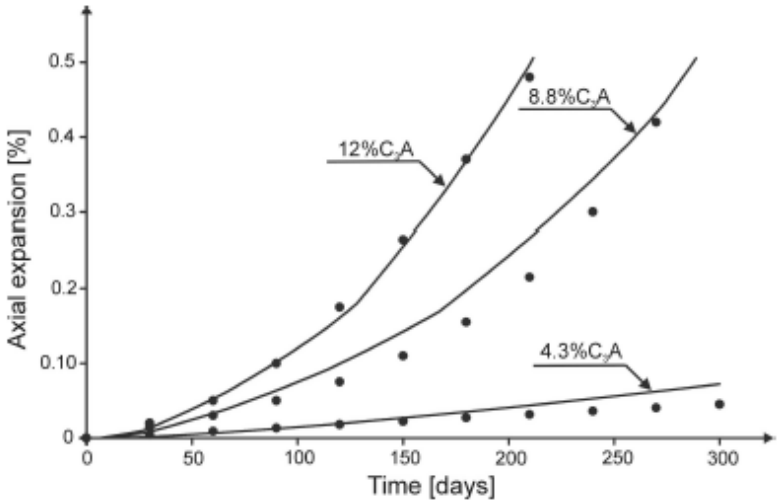

Figure 4.3: Comparison between the experimental measure and the prediction of expansion due to topochemical reaction, from [Basista and Weglewski, 2008]

4.2.2 Chemo-mechanical model based on crystallization pressure

This second class of models assumes that the expansive process is due to the crystallization pressure of ettringite inside the pores. In this case the reaction process is considered to be of through solution type. The crystallization process takes place in confined conditions and induces a pressure on the walls of pores. In general, the crystalization pressure p_c can be calculated by the relation [Bary, 2008]

$$p_c = \frac{RT}{\mathcal{V}_{crys}} ln\left(\frac{Q_{reac}}{K_{reac}}\right) \qquad \text{where } Q_{reac} = \prod_i a_i^{v_i^{reac}} \tag{4.12}$$

where $\mathcal{V}_{crys}$ is the molar volume of crystal $[m^3/mol]$, R is the gas constant $[J/(molK)]$, T is the absolute temperature $[K]$, a_i and v_i^{reac} are the activity and the stoichiometric coefficient of species in solution, K_{reac} is the equilibrium constant of the chemical reaction. The pressure can develop only in supersaturated solutions, in the presence of mechanical confinement. The action exerted by the crystallization consists in a pure hydrostatic pressure and any surface effect is neglected. The pressure calculated using the formula (4.12) is well comparable with experimental measurements but it is not sufficient to cause the real deformation of the material. A similar approach was also presented in [Yu et al., 2013]. In that paper equation (4.12) is developed accounting for the different ionic species involved in the SA. In [Basista and Weglewski, 2008] a nonsteady diffusion with a second order reaction model is implemented for the solution of chemical problem. Starting from the calculated concentrations of sulfate and ettringite, the crystallization pressure is

calculated and used to simulate the expansion of mortar prism cast with different cement and stored in sulfate solution at molar concentration $0.352 mol/l$. The results reported in figure 4.4 show how the calculated pressure is not sufficient to justify the macroscopic expansion of samples. In [Bary, 2008] the approach of

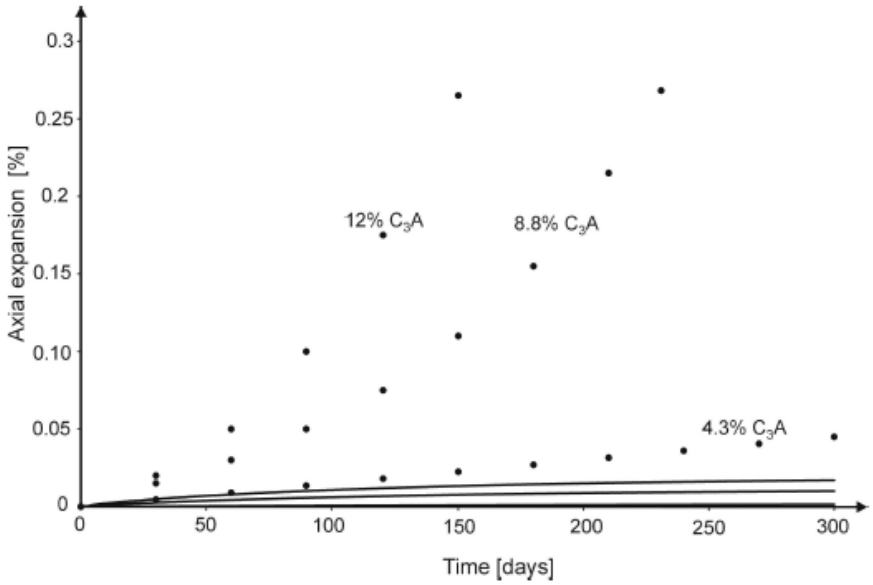

Figure 4.4: Comparison between the experimental measure and the prediction of expansion due to crystallization pressure, from [Basista and Weglewski, 2008]

pressure crystallization is adopted to simulate the expansion of mortar specimens subject to ESA. The description of the chemical process is more complex than that proposed in [Basista and Weglewski, 2008] and considers two ionic species: calcium and sulfate. The depletion of calcium is the cause of leaching and the reaction of sulfate leads to the production of ettringite. The mechanical response of material is assessed through a poro-mechanic model with Mazars' isotropic damage. Crystallization pressure is introduced in the constitutive model by a coefficient of interaction which modifies the value. The final results of the study are the distributions of molar concentrations of the species involved in the process (sulphate, calcium, gypsum, portlandite, ettringite) and the pattern of damage. Quantitative comparisons in terms of displacements are not reported.

5

Multi-phase model in fully saturated conditions

The present model for the simulation of concrete subject to sulfate attack is formulated within the theory of porous material [Coussy, 2004]. At the mesoscale the material can be represented by a superposition of two phases: the homogenized concrete skeleton including the nonreactive material (u) and the reactive part of solid matrix (c); the homogenized fluid including water (w), sulfates (s) and reactant products (e). This approach, used for the study of other chemical reactions in concrete ([Ulm et al., 2000], [Comi et al., 2009]), considers the material in conditions of total saturation. The chemical reactions here considered are the reactions of the sulfates with the aluminates which lead to the formation of ettringite crystals. The stress exerted by these crystals is assumed to be isotropic, so that the secondary ettringite is considered as a fluid-like constituent exerting a pressure on the solid skeleton.

A schematic representation of the material is shown in figure 5.1.

The total volume V of the representative volume element RVE at each instant is the sum of the volume of the solid matrix V_s and the volume of fluid inside the pores V_f. The lagrangian porosity ϕ is defined as the ratio between the volume currently filled by the fluid and the initial total volume of RVE V_0.

$$\phi = \frac{V_f}{V_0} \tag{5.1}$$

The constitutive model presented in this chapter is based on the following assumptions:

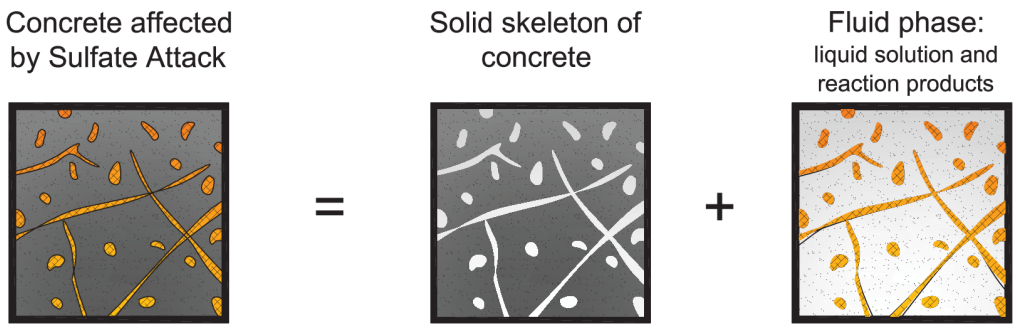

Figure 5.1: Biphase model of concrete affected by Sulfate Attack

- a single fluid phase is considered including water and reaction products;
- a single solid phase, the homogenized skeleton, is considered including aggregates and cement paste;
- fully saturated conditions are considered with the pores initially filled by water;
- the reaction products, and in particular ettringite, is modeled as a fluid like material only exerting pressure on the solid matrix;
- the chemical reactions consumes water but the pressure change due to the variation of the water content is assumed to be negligible;
- the delayed ettringite formation is a topochemical reaction and the change in solid volume together with the oriented anisotropy crystal growth causes a volume increase which is proportional to the reaction extent ;
- the calcium leaching induced by sulfate penetration is modeled by a chemical damage variable d which depends on the reaction extent ;
- the system is in isothermal conditions;
- the mechanical stress-induced damage D is modeled by two isotropic damage variables D_t and D_c.

In this chapter, after a brief introduction to the classic poroelasticity, a double porosity approach is proposed to describe the increase in porosity due to damage of the material. Through this approach we obtain the relationships between the microscopic parameters of the solid matrix and of the fluid inside the pores and

the mesoscopic parameters defined on the RVE. The state equations of the material are obtained by derivation of the expression of the free energy, appropriately formulated. Finally the equations of mass balance and the evolution equations of the internal variables necessary to fully describe the process are presented.

5.1 Elastic bi-phase model

The mechanical response of elastic multiphase materials can be described by the theory of poroelasticity [Coussy, 2004]. In this approach the solid skeleton is considered as an elastic material in which the internal dissipation is equal to zero. The temperature of the system is assumed constant during the process. Assuming a isothermal process, the condition of zero dissipation of solid skeleton can be expressed as:

$$\boldsymbol{\sigma} : d\boldsymbol{\epsilon} + p d\phi - d\Psi_s = 0 \tag{5.2}$$

where $\boldsymbol{\sigma}$ is the total stress tensor, $\boldsymbol{\epsilon}$ is the deformation tensor, p is the internal pressure exerted by the fluid on the solid skeleton, ϕ is the lagrangian porosity and Ψ_s is the free energy of the solid skeleton.

The poroelastic state equations read

$$\boldsymbol{\sigma} = \frac{\partial \Psi_s}{\partial \boldsymbol{\epsilon}}; \qquad p = \frac{\partial \Psi_s}{\partial \phi} \tag{5.3}$$

One can also introduce another potential $G_s = \Psi_s - p\phi$, as the partial Legendre Fenchel transform of Ψ_s. Substituing this definition into equation (5.2) one has

$$\boldsymbol{\sigma} : d\boldsymbol{\epsilon} - \phi dp - dG_s = 0 \tag{5.4}$$

and one can obtain the constitutive relations in the alternative form

$$\boldsymbol{\sigma} = \frac{\partial G_s}{\partial \boldsymbol{\epsilon}}; \qquad \phi = -\frac{\partial G_s}{\partial p} \tag{5.5}$$

Differentiating the relations (5.5) and using the Maxwell's symmetry condition we obtain the expression $d\boldsymbol{\sigma} = d\boldsymbol{\sigma}\left(d\boldsymbol{\epsilon}, dp\right)$ and $d\phi = d\phi\left(d\boldsymbol{\epsilon}, dp\right)$ in the form:

$$d\boldsymbol{\sigma} = \mathbf{C} : d\boldsymbol{\epsilon} - b\ dp\mathbf{1} \tag{5.6}$$

$$d\phi = b\ d\boldsymbol{\epsilon} : \mathbf{1} + \frac{dp}{N} \tag{5.7}$$

where $\mathbf{C}$ is fourth order elasticity tensor of the skeleton , b is the Biot's coefficient and N is the Biot's tangent modulus. The Biot's coefficient relates the variation of porosity $d\phi$ and the variation of volumetric deformation $\mathrm{tr}d\boldsymbol{\epsilon}$ at constant pressure

($dp = 0$). The effective stress $\boldsymbol{\sigma}'$ acting on solid skeleton can be related to the total stress $\boldsymbol{\sigma}$ through the relation

$$\boldsymbol{\sigma}' = \boldsymbol{\sigma} + bp\mathbf{1} \tag{5.8}$$

This poroelastic approach represents the starting point of the model proposed in the next paragraphs for the description of concrete subject to sulfate attack.

5.2 Double porosity model

The initial total volume V_0 of concrete before the activation of chemical reaction is given by the sum of a part occupied by the solid matrix V_{s0} and a part occupied by the fluid V_{f0}. Denoting by ϕ_0 the initial lagrangian porosity, these volumes are

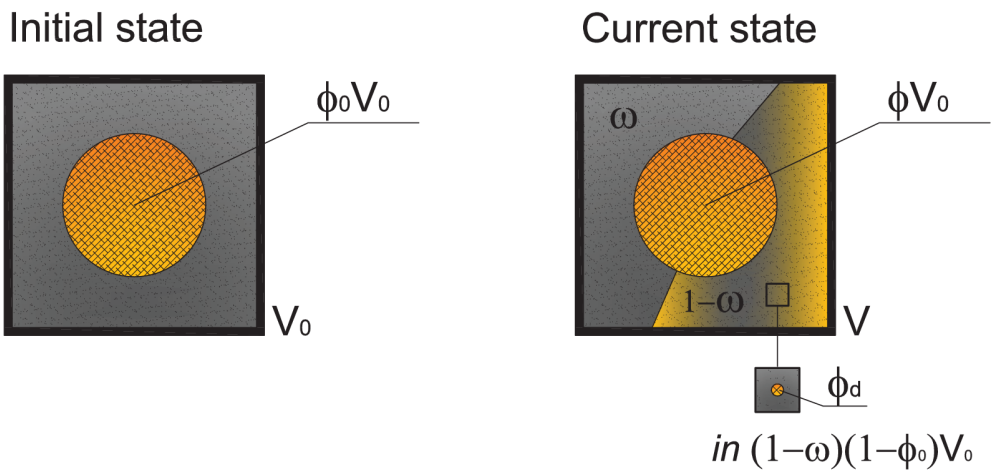

Figure 5.2: Double porosity model: initial and current state

expressed as

$$V_{s0} = (1 - \phi_0)V_0 \qquad V_{f0} = \phi_0 V_0 \tag{5.9}$$

see figure 5.2

Due to the chemical reactions of dissolution and ettringite formation, some microvoids nucleate and develop in a portion of the matrix. To describe this phenomenon we introduce a second porosity ϕ_d.

SEM images show clearly that only a portions of material is affected by dissolution phenomena while other parts are still intact. For this reason we introduce a phenomenological parameter ω, taking values between 0 and 1, and we consider that the additional porosity ϕ_d develops only in the portion $(1-\omega)$ of the matrix.

The actual total porosity $\widetilde{\phi}$ can be expressed as the sum of the porosity ϕ due to the initial porosity of the concrete and the porosity ϕ_d due to dissolution and chemical process.

$$\widetilde{\phi} = \phi + \phi_d(1-\omega)(1-\phi_0) \tag{5.10}$$

The actual volume of the solid matrix is

$$V_s = V - \widetilde{\phi} V_0 \tag{5.11}$$

5.2.1 Relation between skeleton and matrix properties

The fluid exerts an isotropic pressure on the solid skeleton. For simplicity we consider first the volumetric behavior expressed in terms of volumetric deformation $\mathrm{tr}\boldsymbol{\epsilon}$ and mean stress $\mathrm{tr}\boldsymbol{\sigma}/3$. The extension to the deviatoric part results immediate.

The volumetric strain of concrete can be expressed as

$$\mathrm{tr}\boldsymbol{\epsilon} = \frac{V}{V_0} - 1 \tag{5.12}$$

while for the solid matrix the volumetric strain reads

$$\mathrm{tr}\boldsymbol{\epsilon_s} = \frac{V_s}{V_{s0}} - 1 \tag{5.13}$$

Dividing equation (5.11) by V_0 and using (5.12) and (5.13) we obtain a relation between the total deformation and the deformation of the solid matrix

$$\frac{V}{V_0} = \frac{V_s}{V_{s0}}\frac{V_{s0}}{V_0} + \widetilde{\phi} \tag{5.14}$$

$$\mathrm{tr}\boldsymbol{\epsilon} + 1 = (\mathrm{tr}\boldsymbol{\epsilon_s} + 1)(1-\phi_0) + \widetilde{\phi} \tag{5.15}$$

$$\mathrm{tr}\boldsymbol{\epsilon} = (1-\phi_0)\,\mathrm{tr}\boldsymbol{\epsilon_s} + \widetilde{\phi} - \phi_0 \tag{5.16}$$

The total stress acting on the material at the mesoscale is given by a contribution from solid matrix $\boldsymbol{\sigma}_s$ and a contribution from fluid $\boldsymbol{\sigma}_f$. The fluid exerts a hydrostatic stress on the material, therefore the stress $\boldsymbol{\sigma}_f$ can be expressed in the form

$$\boldsymbol{\sigma}_f = -p\mathbf{1} \tag{5.17}$$

Starting from a stress free state $\boldsymbol{\sigma}^0 = \mathbf{0}$, $p^0 = 0$ and under the hypothesis of infinitesimal transformation the stress partition gives

$$\frac{\mathrm{tr}\boldsymbol{\sigma}}{3} = (1-\phi_0)\frac{\mathrm{tr}\boldsymbol{\sigma_s}}{3} - \phi_0 p \tag{5.18}$$

This stress is related to the strain in the matrix at the mesoscale, at a given level of additional porosity ϕ_d, by the relation

$$\frac{\mathrm{tr}\boldsymbol{\sigma_s}}{3} = K_s \mathrm{tr}\boldsymbol{\epsilon_s} \tag{5.19}$$

where $K_s = K_s(\phi_d)$ can be expressed in terms of the stiffness of the integer matrix K_s^0 and of the current additional porosity $\phi_d(1-\omega)$ as proposed by [Kendall et al., 1983]

$$K_s = K_s^0(1-\phi_d(1-\omega))^3 \tag{5.20}$$

The relation between mean stress and volumetric strain on the solid matrix is therefore

$$\frac{\mathrm{tr}\boldsymbol{\sigma}_s}{3} = K_s^0(1-\phi_d(1-\omega))^3 \mathrm{tr}\boldsymbol{\epsilon}_s \tag{5.21}$$

Using equations (5.6) and (5.7) the bi-phase model at the macroscopic level in the Biot's form can be written in term of overall strain $\boldsymbol{\epsilon}$ and total porosity variation $\tilde{\phi} - \phi_0$ as

$$\begin{cases} \frac{\mathrm{tr}\boldsymbol{\sigma}}{3} = K\mathrm{tr}\boldsymbol{\epsilon} - bp \\ \tilde{\phi} - \phi_0 = b\mathrm{tr}\boldsymbol{\epsilon} + \frac{p}{N} \end{cases} \tag{5.22}$$

where b is the Biot's coefficient and N is a Biot's modulus. Combining equations (5.16) - (5.22) one obtains

$$\frac{\mathrm{tr}\boldsymbol{\sigma}}{3} = K_s(1-\phi_0)\mathrm{tr}\boldsymbol{\epsilon_s} - \phi_0 p = K_s\mathrm{tr}\boldsymbol{\epsilon} - K_s(\tilde{\phi}-\phi_0) - \phi_0 p = \tag{5.23}$$

$$= K_s(\mathrm{tr}\boldsymbol{\epsilon} - b\mathrm{tr}\boldsymbol{\epsilon}) - \frac{K_s}{N}p - \phi_0 p \tag{5.24}$$

$$= \frac{K_s}{K}(1-b)\frac{\mathrm{tr}\boldsymbol{\sigma}}{3} + \frac{K_s}{K}(1-b)bp - \frac{K_s}{N}p - \phi_0 p \tag{5.25}$$

This leads to a direct relationship between macroscopic stress and pressure

$$\frac{\mathrm{tr}\boldsymbol{\sigma}}{3}\left(1 - \frac{K_s}{K}(1-b)\right) = p\left(K_s(1-b)\frac{b}{K} - \frac{K_s}{N} - \phi_0\right) \tag{5.26}$$

This identity must be respected for any value of stress and pressure: $\mathrm{tr}\boldsymbol{\sigma}$ and p are independent variables and is therefore necessary to require that the respective coefficients are zero. This leads to a relation between the Biot's parameters and the skeleton and matrix properties of materials

$$b = 1 - \frac{K}{K_s} \qquad \frac{1}{N} = \frac{b-\phi_0}{K_s} \tag{5.27}$$

The macroscopic stiffness K can be expressed in terms of the current solid matrix stiffness K_s and initial porosity ϕ_0 [Kendall et al., 1983]

$$K = (1 - \phi_0)^3 K_s \tag{5.28}$$

which, substituted into (5.27), leads to a value of b independent of ϕ_d

$$b = 1 - (1 - \phi_0)^3 \tag{5.29}$$

The modulus N turns out to depend on ϕ_d through

$$\frac{1}{N} = \frac{b - \phi_0}{K_s^0 \left(1 - \phi_d(1 - \omega)\right)^3} \tag{5.30}$$

5.2.2 Relation between Biot's parameters and fluid properties

The fluid mass inside a reference volume is given by the relation

$$m_f = \tilde{\phi} \rho_f \tag{5.31}$$

where ρ_f is the mass density of the fluid and $\tilde{\phi}$ is the total porosity occupied by the fluid. The fluid mass variation can be expressed as

$$dm_f = d\tilde{\phi}\rho_f + d\rho_f \tilde{\phi} \quad \longrightarrow \quad \frac{dm_f}{\rho_f} = d\tilde{\phi} + \frac{d\rho_f}{\rho_f}\tilde{\phi} \tag{5.32}$$

The variation of pressure can be related to the variation of mass density through the constitutive law of the fluid

$$\frac{dp}{K_f} = \frac{d\rho_f}{\rho_f} \tag{5.33}$$

where K_f is the elastic bulk modulus of the fluid. Introducing this relation in the equation (5.32) we obtain

$$\frac{dm_f}{\rho_f} = d\tilde{\phi} + \frac{dp}{K_f}\tilde{\phi} \tag{5.34}$$

Assuming that the change in the density of the fluid during the process be small, it is possible to replace the current value of density ρ_f with the initial value ρ_{f0}. This hypothesis allows the integration of the differential equation in the linearized form

$$\frac{m_f - m_{f0}}{\rho_{f0}} = \tilde{\phi} - \phi_0 + \tilde{\phi}\frac{p}{K_f} \tag{5.35}$$

Substituting (5.35) in equation (5.22) one obtains

$$\frac{m_f - m_{f0}}{\rho_{f0}} = b\mathrm{tr}\boldsymbol{\epsilon} + \left(\frac{\tilde{\phi}}{K_f} + \frac{1}{N}\right) p \tag{5.36}$$

$$= b\mathrm{tr}\boldsymbol{\epsilon} + \frac{1}{M} p \tag{5.37}$$

where M is the Biot's modulus defined by

$$\frac{1}{M} = \frac{\tilde{\phi}}{K_f} + \frac{b - \phi_0}{K_s^0 \left(1 - \phi_d(1-\omega)\right)^3} \tag{5.38}$$

Figures 5.3 and 5.4 shown respectively the evolution of Biot's Modulus M and macroscopic bulk modulus K with the value of additional porosity ϕ_d for different value of parameter $\omega = (0.0,\ 0.25,\ 0.50,\ 0.75,\ 1.0)$. The other material parameters used are reported in table 5.1.

Parameter	ϕ_0	K_s^0	K_f	b
Value	0.16	26000MPa	10000MPa	0.407

Table 5.1: Material parameters

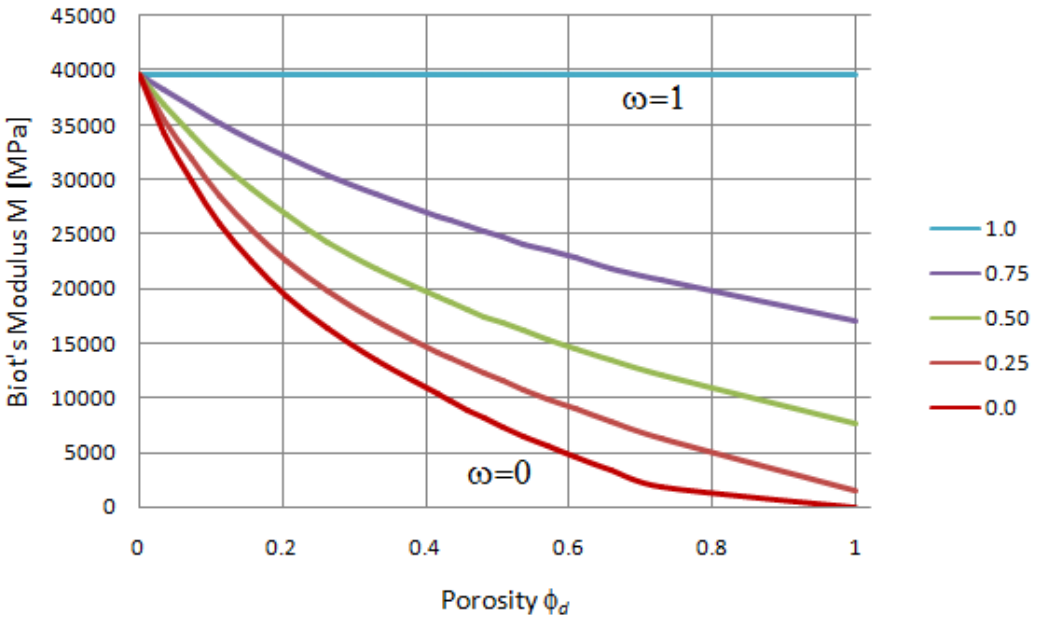

Figure 5.3: Evolution with additional porosity ϕ_d of Biot's modulus M

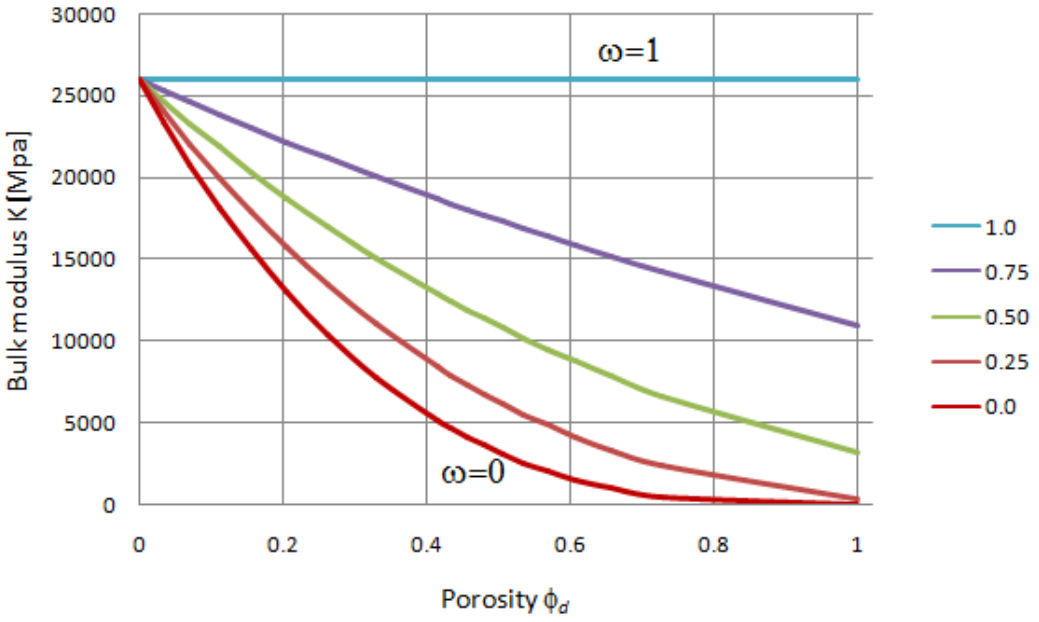

Figure 5.4: Evolution with additional porosity ϕ_d of macroscopic bulk modulus K

5.3 Compatibility and equilibrium equations

The kinematic model adopted is based on the assumption of small displacements and strains. The relation between strains and displacements is expressed in the linearized form

$$\begin{array}{ll} \boldsymbol{\epsilon} = \frac{1}{2}\left(\text{grad}\mathbf{u} + \text{grad}^T\mathbf{u}\right) & \text{in}\Omega \\ \mathbf{u} = \overline{\mathbf{u}} & \text{in}\Gamma_u \end{array} \tag{5.39}$$

where $\mathbf{u}$ is the displacement field, $\boldsymbol{\epsilon}$ is the tensor of small strains, $\overline{\mathbf{u}}$ are the displacements on the constrained boundary Γ_u of Ω.

Neglecting dynamic effects the equilibrium equations are

$$\begin{array}{ll} \text{div}\boldsymbol{\sigma} + \rho\mathbf{b} = \mathbf{0} & \text{in}\Omega \\ \boldsymbol{\sigma}\mathbf{n} = \mathbf{f} & \text{in}\Gamma_\sigma \end{array} \tag{5.40}$$

where $\boldsymbol{\sigma}$ is the stress field, $\rho\mathbf{b}$ is the body force of the mixture (solid and fluid), $\mathbf{f}$ are the external force at the boundary Γ_σ and Ω is the body volume.

5.4 Chemo-elastic model with chemical and mechanical damage

The model proposed in the previous section introduces two distinct contributions to the total porosity $\tilde{\phi}$: ϕ, which is the porosity naturally present within the porous medium and ϕ_d, which is an additional porosity due to the chemical reactions involving the reactive solid.

The development of this secondary porosity reduces the mechanical properties of the material. This phenomenon is taken into account through an internal scalar variable of chemical damage d, ranging from 0 to 1 dependent on the reaction extent. The parameter ω allows to split the solid matrix in a part subject to chemical damage and in the complementary non damaging part.

Using the relation proposed by [Kendall et al., 1983] and relative to the decrease of Young modulus due to the variation in porosity one has

$$(1-d) = (1-\phi_d)^3 \tag{5.41}$$

Introducing this relation into equation (5.20) and the result into equation (5.28) one obtains the following expression of the macroscopic bulk modulus affected by chemical damage

$$K = K(d) = (1-\phi_0)^3 K_s^0 \left(\omega + (1-\omega)(1-d)^{\frac{1}{3}}\right)^3 \tag{5.42}$$

$$= K^0 \left(\omega + (1-\omega)(1-d)^{\frac{1}{3}}\right)^3 \tag{5.43}$$

The stress-induced degradation of material properties is also considered and modeled by the isotropic damage model proposed in [Comi and Perego, 2001]. In this model two isotropic damage variables are introduced, one for prevalent state of traction (D_t) and the other for prevalent state of compression (D_c). The total mechanical damage affecting the mechanical properties of the material is computed by a combination of the two variables:

$$D = 1 - (1 - D_t)(1 - D_c) \tag{5.44}$$

No permanent strains are considered for the sake of simplicity.

The chemo-mechanical constitutive model is formulated starting from the expression of the free energy of the system Ψ. The static variables (total stress $\boldsymbol{\sigma}$ and chemical potential of expansive fluid μ) can be related to the conjugate kinematic variables (strain $\boldsymbol{\epsilon}$, variation of fluid content $\zeta = (m_f - m_{f0})/\rho_{f0}$) by the state equations derivated from the free energy Ψ. This is the sum of the energy of the solid skeleton Ψ_s and on the fluid $m_f\psi_f$ (where ψ_f is the specific energy of the fluid f). Considering isothermal conditions, the proposed form for the free energy reads

$$\begin{aligned}\Psi(\boldsymbol{\epsilon}, \zeta, D, d) = \Psi_s + m_f\psi_f = \\ = \frac{1}{2}(1-D)\left\{2G(d)\mathbf{e} : \mathbf{e} + K(d)\left(\mathrm{tr}\boldsymbol{\epsilon}\right)^2 + M(d)b^2\left(\mathrm{tr}\boldsymbol{\epsilon} - \frac{\zeta}{b}\right)^2\right\} + \\ + \rho_f\zeta\psi_f\end{aligned} \tag{5.45}$$

In the above equation $\mathbf{e}$ is the deviatoric strain tensor, $G(d)$ and $K(d)$ are the shear and bulk moduli of the homogenized concrete skeleton affected by chemical damage, $M(d)$ and b are the Biot's modulus and the Biot's coefficient respectively. The shear modulus $G(d)$ is calculated from the expression of $K(d)$ (5.43) under the hypothesis of constant value of Poisson coefficient during the process:

$$G(d) = \frac{3}{2}\frac{(1-2\nu)}{(1+\nu)}K(d) \tag{5.46}$$

The state equations are obtained by partial derivation of the free energy whit respect to each kinematic variable

$$\boldsymbol{\sigma} = \frac{\partial\Psi}{\partial\boldsymbol{\epsilon}} = (1-D)\left\{2G(d)\mathbf{e} + K(d)\mathrm{tr}\boldsymbol{\epsilon}\mathbf{1} + M(d)b^2\left(\mathrm{tr}\boldsymbol{\epsilon} - \frac{\zeta}{b}\right)\mathbf{1}\right\} \tag{5.47}$$

$$\mu = \frac{1}{\rho_f}\frac{\partial\Psi}{\partial\zeta} = -\frac{1}{\rho_f}(1-D)M(d)b\left(\mathrm{tr}\left(\boldsymbol{\epsilon}\right) - \frac{\zeta}{b}\right) + \psi_f \tag{5.48}$$

$$Y_D = -\frac{\partial\Psi}{\partial D} \tag{5.49}$$

$$Y_d = -\frac{\partial\Psi}{\partial d} \tag{5.50}$$

Y_D and Y_d are the strain energy density release rates associated with the mechanical and the chemical damage respectively. The chemical potential μ is related to the fluid pressure p and the specific free energy as

$$\mu = \frac{p}{\rho_f} + \psi_f \tag{5.51}$$

Substituting this result into equation (5.48) the expression of fluid pressure is obtained

$$p = -(1-D)M(d)\left(b\mathrm{tr}\boldsymbol{\epsilon} - \zeta\right) \tag{5.52}$$

The macroscopic stress can hence be expressed in the final form

$$\boldsymbol{\sigma} = (1-D)\left[2G(d)\mathbf{e} + K(d)\mathrm{tr}\boldsymbol{\epsilon}\mathbf{1}\right] - bp\mathbf{1} \tag{5.53}$$

5.5 Balance of mass

Let us consider a reactive medium of R constituents under the hypothesis of infinitesimal transformation. The mass conservation can be expressed for each $\alpha = 1,\ ...,\ R$ component in the form:

$$\frac{dm_\alpha}{dt} = -\mathrm{div}\left(\rho_\alpha \mathbf{M}_\alpha\right) + \mathring{m}_{\to\alpha} \tag{5.54}$$

where $m_\alpha = \rho_\alpha \phi_\alpha$ is the mass content of constituent α, $\rho_\alpha \mathbf{M}_\alpha = \rho_\alpha \mathcal{N}_\alpha(\mathbf{v}_\alpha - \mathbf{v}_u)$ is the relative flow vector ($\mathcal{N}_\alpha$ is the eulerian porosity and $\mathbf{v}_\alpha - \mathbf{v}_u$ the relative flow velocity of component α respect the unreactive solid matrix u), $\mathring{m}_{\to\alpha}$ is the rate of mass formation (> 0) or consumption (< 0) of component α.

In the case of concrete subject to sulfate attack we consider these components and phases

Phase	component α
homogenized solid	nonreactive solid u
	reactive solid c
homogenized fluid	water w
	sulfate s
	expansive ettringite e

For the component α the mass concentration m_α is directly related to the molar concentration n_α through the molar mass $\mathcal{M}_\alpha$

$$m_\alpha = n_\alpha \mathcal{M}_\alpha \tag{5.55}$$

In diffusion-reaction problems equations (5.54) of mass balance are more conveniently expressed in terms of molar concentrations:

$$\frac{dn_\alpha}{dt} = -\text{div}\left(\mathbf{j}_\alpha\right) + \mathring{n}_{\to\alpha} \tag{5.56}$$

where $\mathbf{j}_\alpha$ is the flow of moles of component α

$$\mathbf{j}_\alpha = \frac{\rho_\alpha}{\mathcal{M}_\alpha}\mathbf{M}_\alpha \tag{5.57}$$

In a porous medium fully saturated with water and without electrochemical coupling phenomena the flow term can be modeled through the Fick's law. With this hypothesis, the diffusion is due to the concentration gradient only

$$\mathbf{j}_\alpha = -D_\alpha \text{grad}\left(n_\alpha\right) \tag{5.58}$$

5.5.1 Balance of moles during sulfate attack

The equations of balance (5.56) for each component can be written as

$$u: \quad \frac{dn_u}{dt} = 0 \tag{5.59}$$

$$c: \quad \frac{dn_c}{dt} = \mathring{n}_{\to c} \tag{5.60}$$

$$w: \quad \frac{dn_w}{dt} = -\text{div}\left(\mathbf{j}_w\right) + \mathring{n}_{\to w} \tag{5.61}$$

$$s: \quad \frac{dn_s}{dt} = -\text{div}\left(\mathbf{j}_s\right) + \mathring{n}_{\to s} \tag{5.62}$$

$$e: \quad \frac{dn_e}{dt} = -\text{div}\left(\mathbf{j}_e\right) + \mathring{n}_{\to e} \tag{5.63}$$

Note that the solid components, reactive c and non-reactive u, have zero relative velocity therefore in the balance equations the associated flow terms disappear: $\mathbf{j}_u = 0$, $\mathbf{j}_c = 0$. Furthermore by definition, for the non-reactive component the term $\mathring{n}_{\to u}$ is equal to zero.

To identify the other terms involved in the molar balances the chemical problem, described by the equations (2.2)-(2.3) and (2.5)-(2.7), must be analyzed. The first set of equations describes the reaction between sulfate anions and hydration products of cement paste (silicates and portandite) with consequent formation of gypsum. For each mole of sulfate reacted one mole of gypsum is formed. In the second set of equations the moles of gypsum react with the calcium aluminates forming ettringite. In the following we consider that the sulfate, spreading in the

material, completely reacts forming gypsum, hence equation (5.62) is capable to describe also the molar evolution of gypsum.

During the process of ettringite formation only calcium aluminates react with gypsum. For this reason, the equation (5.60) is used to model the depletion of aluminates. Following the approach proposed by [Tixier and Mobasher, 2003] and [Idiart et al., 2011(a)] the set of equation (2.5)-(2.7) can be expressed in the lumped form

$$C_{eq} + q\bar{S} + rH \rightarrow C_6A\bar{S}_3H_{32} \tag{5.64}$$

where $\bar{S}$ is the gypsum, H is water, q and r are the stoichiometric coefficients and C_{eq} is the equivalent grouping of calcium aluminates

$$C_{eq} = \sum_{i=1}^{4} \gamma_i P_i \qquad \gamma_i = \frac{n_{ci}}{\sum_{i=1}^{4} n_{ci}} \tag{5.65}$$

n_{ci} is the molar concentration of the single species of calcium aluminate P_i ($P_1 = C_4A\bar{S}H_{12}$ mono-sulphoaluminate, $P_2 = C_4AH_{13}$ tetra-hydrated aluminate, $P_3 = C_4AF$ alumino-ferrite and $P_4 = C_3A$ unreacted tricalcium aluminate) and $q = 2\gamma_1 + 3\gamma_2 + 4\gamma_3 + 3\gamma_4$ is the stoichiometric weighting coefficient of the sulfate phase.

During the process the moles of calcium, sulfate and water are transformed in ettringite. The terms of reaction present in equations (5.60), (5.61) and (5.62) are therefore only due to the consumption required for ettringite formation.

$$\mathring{n}_{\rightarrow c} = \mathring{n}_{e\rightarrow c} \tag{5.66}$$
$$\mathring{n}_{\rightarrow s} = \mathring{n}_{e\rightarrow s} \tag{5.67}$$
$$\mathring{n}_{\rightarrow w} = \mathring{n}_{e\rightarrow w} \tag{5.68}$$

where $\mathring{n}_{\beta\rightarrow\alpha} = -\mathring{n}_{\alpha\rightarrow\beta}$ denotes the number of moles of the α-component transformed into the β-component.

Using (5.58), (5.67) and (5.68) equations (5.60) and (5.62) can be written in the form

$$c: \qquad \frac{dn_c}{dt} = \mathring{n}_{e\rightarrow c} \tag{5.69}$$
$$s: \qquad \frac{dn_s}{dt} = \mathrm{div}\left(D_s \mathrm{grad}\left(n_s\right)\right) + \mathring{n}_{e\rightarrow s} \tag{5.70}$$

Assuming a second order reaction scheme the reaction term in (5.70) is expressed as

$$\mathring{n}_{e\rightarrow s} = -\mathring{n}_{s\rightarrow e} = -kn_cn_s \tag{5.71}$$

and accounting for (5.65) the reaction term in (5.69) reads

$$\mathring{n}_{e\to c} = -\mathring{n}_{c\to e} = -\frac{k}{q} n_c n_s \tag{5.72}$$

substituting into (5.69) - (5.69) we can obtain the final form of the diffusion reaction equations

$$c: \qquad \frac{dn_c}{dt} = -\frac{k}{q} n_c n_s \tag{5.73}$$

$$s: \qquad \frac{dn_s}{dt} = \mathrm{div}\left(D_s \mathrm{grad}\left(n_s\right)\right) - k n_c n_s \tag{5.74}$$

Since the diffusion of water inside the porous medium is much more rapid than the reaction, it can be assumed that the reacted moles of water are immediately replaced by the moles coming from the external environment and hence the water content remains constant.

5.6 Evolution laws

5.6.1 Reaction extent

The rate of reacting moles $\mathring{n}_{\to\alpha}$ can be expressed of a single reaction rate $\dot{\xi}$

$$\mathring{n}_{\to\alpha} = \nu_\alpha \dot{\xi} \tag{5.75}$$

where ν_α is the stoichiometric coefficient of component α involved in the reaction with the convention $\nu_\alpha > 0$ for a produced mole and $\nu_\alpha < 0$ for a reacting mole. For the reaction (5.64) one obtains

$$\dot{\xi} = -\mathring{n}_{\to c} = -\frac{\mathring{n}_{\to s}}{q} = -\frac{\mathring{n}_{\to w}}{r} = \mathring{n}_{\to e} \tag{5.76}$$

The evolution in time of the reaction can be obtained by integrating (5.69) from *0* to t and reads

$$\xi(t) = n_c(0) - n_c(t) \tag{5.77}$$

From (5.76) the molar concentration of ettringite at the time t and is equals $\xi(t)$. It is also convinient for later use to introduce the reaction extent $\bar{\xi}$ ranging from *0* to *1*

$$\bar{\xi} = \frac{\xi}{n_c(0)} \tag{5.78}$$

The variation of fluid content ζ can be directly related to the reaction extent of reaction through a material parameter a

$$\zeta = a\ \xi \tag{5.79}$$

For the parameter a we adopt the expression proposed in [Tixier and Mobasher, 2003] and used in several papers in recent years [Idiart et al., 2011(a)], [Campos et al., 2016], [Ikumi et al., 2014]

$$a = n_c(0) \sum_{i=1}^{4} \frac{\Delta V_i}{V_i} \mathcal{V}_i \gamma_i \qquad \frac{\Delta V_i}{V_i} = \frac{\mathcal{V}_e}{\mathcal{V}_i + \nu_i \mathcal{V}_{gyp}} - 1 \tag{5.80}$$

where $\mathcal{V}_i$, $\mathcal{V}_e$ e $\mathcal{V}_{gyp}$ are the molar volumes of each calcium aluminate, of ettringite and of gypsum, ν_i is the stoichiometric coefficient involved in reaction, γ_i is the ratio between the molar concentration of each aluminate $n_{c,i}$ and the total concentration of aluminates

$$\gamma_i = \frac{n_{c,i}}{\sum_{i=1}^{4} n_{c,i}} \tag{5.81}$$

5.6.2 Chemical damage evolution

The decalcification of material causes a microcracking which is described by an isotropic damage variable d. Similarly to what proposed in [Pignatelli et al., 2013], the evolution of chemical damage is expressed as a function of the reaction extent.

$$d = \frac{1 - \exp(-r_1 \bar{\xi})}{1 + \exp(-r_1 \bar{\xi} + r_2)} r_3 \tag{5.82}$$

5.6.3 Mechanical damage

The mechanical degradation of the material is described by two damage variables: D_t for damage due to prevailing tensile stress states and D_c for damage due to prevailing compression stress states. The evolution of these variables is governed by the loading-unloading conditions proposed in [Comi and Perego, 2001] and expressed in term of an inelastic effective stress $\boldsymbol{\sigma}'' = \boldsymbol{\sigma} + \beta p \mathbf{1}$, with β ($\beta \leq b$) a material parameter which tunes the level of material degradation.

$$f_i \leq 0; \qquad \dot{D}_i \geq 0; \qquad f_i \dot{D}_i = 0 \qquad \text{with:} i = t, c \tag{5.83}$$

The activation functions f_t and f_c depend on the first invariant of inelastic effective stress tensor I_1 and on the second invariant of deviatoric stress tensor J_2

$$f_t = J_2(\boldsymbol{\sigma}'') - a_t I_1^2(\boldsymbol{\sigma}'') + b_t h_t(D_t) I_1(\boldsymbol{\sigma}'') - k_t h_t^2(D_t) \tag{5.84}$$

$$f_c = J_2(\boldsymbol{\sigma}'') + a_c I_1^2(\boldsymbol{\sigma}'') + b_c h_c(D_c) I_1(\boldsymbol{\sigma}'') - k_c h_c^2(D_c) \tag{5.85}$$

where a_t, b_t, k_t, a_c, b_c, k_c are non negative parameters to be identified through experimental tests. The functions $h_t(D_t)$ and $h_c(D_c)$ govern the hardening and softening behavior

$$h_i(D_i) = \begin{cases} 1 - \left[1 - \left(\frac{\sigma_{ei}}{\sigma 01}\right)\right] \left(1 - \frac{D_i}{D_{0i}}\right)^2 & \text{for } D_i < D_{0i} \\ \left[1 - \left(\frac{D_i - D_{0i}}{1 - D_{0i}}\right)^{c_i}\right]^{0.75} & \text{for } D_i \geq D_{0i} \end{cases} \qquad i = t,\ c \tag{5.86}$$

where σ_{ei} and σ_{0i} are respectively the elastic limit stress and the peak stress. D_{0i} is the damage corresponding to the peak stress. The parameters c_c and c_c govern the softening stress-strain curve. In numerical analysis, depending on the mesh size, the parameters c_i are used to scale the fracture energy density in order to obtain the correct value of the fracture energy. This technique is called *fracture energy regularization* and avoids spurious mesh dependency of the numerical solution in the presence of softening.

6

Extension to partially saturation conditions

In the previous chapter a model for the description of sulfate attack in fully saturated condition is proposed. In many contexts the hypothesis of complete saturation is quite acceptable as in the case of dams or underground structures. In other cases significant variations in water content are present: this phenomenon causes variations of the state of stress and alters the kinetics of the chemical reaction.

Starting from the results presented in the case of fully saturated material an extension is here proposed to take into account the effect of the variation of water content.

6.1 Three phase formulation of concrete subject to sulfate attack

Concrete is represented as three-phase porous medium in which the solid skeleton and two fluid-like phases are superimposed. The first fluid phase (f) is constituted by liquid water (w) and by a mixture of air and vapor (g). The second fluid phase (e) is composed by the reaction products, in particular ettringite, assumed to exerts a hydrostatic pressure only (fluid-like assumption). The volume occupied by the solid skeleton is

$$V_s = V - \widetilde{\phi} V_0 \tag{6.1}$$

where $\widetilde{\phi}$ is the total porosity due to the initial ϕ and the additional ϕ_d porosities according to equation (5.10). The total porosity is filled by the two fluid-like phases

$$\widetilde{\phi}_e = \widetilde{\phi}_f = \widetilde{\phi} \tag{6.2}$$

The porosity of fluid phase f can by divided in two part: one filled by liquid water and the other occupied by air and vapor.

$$\widetilde{\phi}_f = \widetilde{\phi} = \widetilde{\phi}_w + \widetilde{\phi}_g \tag{6.3}$$

The relation between $\widetilde{\phi}_w$ or $\widetilde{\phi}_g$ and $\widetilde{\phi}$ can be expressed through the degree of saturation S_w

$$\widetilde{\phi}_w = S_w \widetilde{\phi} \tag{6.4}$$

$$\widetilde{\phi}_g = (1 - S_w)\widetilde{\phi} \tag{6.5}$$

The total pressure is given by the sum of the pressure exerted by the two coexisting fluid phases

$$p = p_e + p_f \tag{6.6}$$

Similarly to the case of total saturation the mesoscopic state of stress can be expressed as sum of the stress acting on the solid skeleton and the pressure inside the pores.

$$\frac{\mathrm{tr}\boldsymbol{\sigma}}{3} = (1 - \phi_0)\,\frac{\mathrm{tr}\boldsymbol{\sigma_s}}{3} - \phi_0\,(p_e + p_f) \tag{6.7}$$

The relation between the mean stress and the volumetric strain of the solid matrix is the same proposed in equation (5.19).

The expression of solid skeleton internal dissipation in incremental form is

$$d\Phi_s = \boldsymbol{\sigma} : d\boldsymbol{\epsilon} + p_w d\widetilde{\phi}_w + p_g d\widetilde{\phi}_g + p_e d\widetilde{\phi}_e - d\Psi_s \tag{6.8}$$

$$= \boldsymbol{\sigma} : d\boldsymbol{\epsilon} + p_w d\Big(S_w\widetilde{\phi}\Big) + p_g d\left[(1 - S_w)\widetilde{\phi}\right] + p_e d\widetilde{\phi}_e - d\Psi_s \tag{6.9}$$

We first derive the elastic formulation. In elasticity the dissipation is equal to zero. The derivative of the products between the degree of saturation and porosity is

$$d\Big(S_w\widetilde{\phi}\Big) = dS_w\widetilde{\phi} + d\widetilde{\phi}S_w \tag{6.10}$$

substituting the equation (6.10) in equation (6.9) one obtains

$$d\Phi_s = \boldsymbol{\sigma} : d\boldsymbol{\epsilon} + p_w\left(dS_w\widetilde{\phi} + d\widetilde{\phi}S_w\right) + p_g\cdot\left(-dS_w\widetilde{\phi} + d\widetilde{\phi}(1 - S_w)\right) + p_e d\widetilde{\phi}_e - d\Psi_s = 0 \tag{6.11}$$

Defining the equivalent pressure p^* and the capillary pressure p_c by

$$p^* = p_w S_w + p_g(1 - S_w) + p_e \tag{6.12}$$

$$p_c = p_g - p_w \tag{6.13}$$

the equation (6.11) can be expressed as

$$d\Phi_s = \boldsymbol{\sigma} : d\boldsymbol{\epsilon} + p^* d\widetilde{\phi} + p_c \widetilde{\phi} dS_w - d\Psi_s = 0 \tag{6.14}$$

p_c is the capillary pressure due to the interface between wetting (water) and non-wetting (air and vapor) phase. An energy U is associated to the interface and this term adds to the free energy of the solid ψ_s to give the skeleton free energy, see [Coussy, 2004] for details

$$\Psi_s(\boldsymbol{\epsilon}, S_w) = \psi_s(\boldsymbol{\epsilon}, \widetilde{\phi}) + \widetilde{\phi} U(S_w) \tag{6.15}$$

Replacing the equation (6.15) in equation (6.14) one obtains

$$\boldsymbol{\sigma} : d\boldsymbol{\epsilon} + p^* d\widetilde{\phi} + p_c \widetilde{\phi} dS_w - d\psi_s - d\widetilde{\phi} U - \widetilde{\phi} \frac{\partial U}{\partial S_w} dS_w = 0 \tag{6.16}$$

The last term is $\partial U / \partial S_w = -p_c$ and this leads to the final expression of dissipation

$$\boldsymbol{\sigma} : d\boldsymbol{\epsilon} + p^* d\widetilde{\phi} - U d\widetilde{\phi} - d\psi_s = 0 \tag{6.17}$$

$$\boldsymbol{\sigma} : d\boldsymbol{\epsilon} + \pi d\widetilde{\phi} - d\psi_s = 0 \tag{6.18}$$

where the pressure π is defined by

$$\pi = p^* - U \tag{6.19}$$

and in differential form

$$d\pi = dp^* - dU \tag{6.20}$$

Starting from the relations (6.12)-(6.13) one obtain

$$d\pi = dp_e + S_w dp_w + (1 - S_w) dp_g + p_w dS_w - p_g dS_w + p_g dS_w - p_w dS_w \tag{6.21}$$

$$= dp_e + S_w dp_w + dp_g - S_w dp_g \tag{6.22}$$

In this approach we consider a drained condition for the gas ($dp_g = 0$).
As in the case of total saturation we introduce the Gibbs potential $G_s = \Psi_s - \pi\widetilde{\phi}$

$$\boldsymbol{\sigma} : d\boldsymbol{\epsilon} - \tilde{\phi} d\pi - dG_s = 0 \tag{6.23}$$

from which we obtain the state equations for the elastic case

$$\boldsymbol{\sigma} = \frac{\partial G_s}{\partial \boldsymbol{\epsilon}}; \qquad \widetilde{\phi} = -\frac{\partial G_s}{\partial \pi} \tag{6.24}$$

Comparing the relations with (5.5), governing the bi-phase elastic behavior, on can observe that the only difference is that the pressure p is replaced by the equivalent pressure π. Differentiating relations (6.24) one obtains the incremental form of the state equations, fully analogous to relations (5.6) - (5.7)

$$d\boldsymbol{\sigma} = \mathbf{C}d\boldsymbol{\epsilon} - b\ d\pi\mathbf{1} \tag{6.25}$$

$$d\tilde{\phi} = b\ d\boldsymbol{\epsilon} : \mathbf{1} + \frac{d\pi}{N} \tag{6.26}$$

The relations between skeleton and matrix properties remains the same discussed in section 5.2.1, while since two separate fluid phases are considered, the relations between Biot's parameters and the fluids properties change and will be discussed in the following section.

6.2 Relation between Biot's parameters and fluids properties

Inside the pores are present three fluids grouped into two phases whose unit masses are given by the relations

$$m_w = S_w\tilde{\phi}\rho_w \tag{6.27}$$

$$m_e = \tilde{\phi}\rho_e \tag{6.28}$$

$$m_g = (1 - S_w)\tilde{\phi}\rho_g \tag{6.29}$$

The variation of fluid content for water and ettringite are

$$\zeta_w = \frac{dm_w}{\rho_w} = \frac{1}{\rho_w}\left(dS_w\widetilde{\phi}\rho_w + S_w d\widetilde{\phi}\rho_w + S_w\widetilde{\phi}d\rho_w\right) \tag{6.30}$$

$$\zeta_e = \frac{dm_e}{\rho_e} = \frac{1}{\rho_e}\left(d\widetilde{\phi}\rho_e + \widetilde{\phi}d\rho_e\right) \tag{6.31}$$

Substituting equation (6.26) into (6.30) and (6.31) we obtain

$$\zeta_w = S_w b d\boldsymbol{\epsilon} : \mathbf{1} + \frac{S_w}{N}d\pi + dS_w\widetilde{\phi} + S_w\widetilde{\phi}\frac{d\rho_w}{\rho_w} \tag{6.32}$$

$$\zeta_e = bd\boldsymbol{\epsilon} : \mathbf{1} + \frac{d\pi}{N} + \widetilde{\phi}\frac{d\rho_e}{\rho_e} \tag{6.33}$$

The quantities $d\rho_w/\rho_w$ and $d\rho_e/\rho_e$ can be related to the pressure and the stiffness of fluids through their respective bulk moduli K_w and K_e

$$\frac{d\rho_w}{\rho_w} = \frac{dp_w}{K_w}; \qquad \frac{d\rho_e}{\rho_e} = \frac{dp_e}{K_e} \tag{6.34}$$

The pressure π, under the assumption of $dp_g = 0$, is

$$d\pi = S_w dp_w + dp_e \tag{6.35}$$

This lead to the final expressions of fluid mass contents

$$\zeta_w = S_w b d\boldsymbol{\epsilon} : \mathbf{1} + \frac{S_w^2}{N} dp_w + \frac{S_w}{N} dp_e + dS_w \widetilde{\phi} + S_w \widetilde{\phi} \frac{dp_w}{K_w} \tag{6.36}$$

$$\zeta_e = b d\boldsymbol{\epsilon} : \mathbf{1} + \frac{S_w}{N} dp_w + \frac{1}{N} dp_e + \widetilde{\phi} \frac{dp_e}{K_e} \tag{6.37}$$

These equation can be rewritten in matrix form

$$\boldsymbol{\zeta} = \mathbf{b} \mathrm{tr} d\boldsymbol{\epsilon} + \mathbf{M}^{-1} d\mathbf{p} + d\mathbf{S} \tag{6.38}$$

where

$$\boldsymbol{\zeta} = \begin{bmatrix} \zeta_w \\ \zeta_e \end{bmatrix}; \qquad \mathbf{b} = \begin{bmatrix} bS_w \\ b \end{bmatrix} \qquad \mathbf{M}^{-1} = \begin{bmatrix} \left(\frac{S_w}{N} + \frac{\tilde{\phi}}{K_w} \right) S_w & \frac{S_w}{N} \\ \frac{S_w}{N} & \frac{1}{N} + \frac{\tilde{\phi}}{K_e} \end{bmatrix} \tag{6.39}$$

$$d\mathbf{p} = \begin{bmatrix} dp_w \\ dp_e \end{bmatrix} \qquad d\mathbf{S} = \begin{bmatrix} \tilde{\phi} dS_w \\ 0 \end{bmatrix} \tag{6.40}$$

The pressures exerted by water and ettringite can be related to the mass variation and skeleton deformation as

$$d\mathbf{p} = \begin{bmatrix} dp_w \\ dp_e \end{bmatrix} = \mathbf{M} \cdot \begin{bmatrix} \zeta_w - S_w b \mathrm{tr}\boldsymbol{\epsilon} - \tilde{\phi} dS_w \\ \zeta_e - b \mathrm{tr}\boldsymbol{\epsilon} \end{bmatrix} \tag{6.41}$$

If the extra diagonal terms of the matrix $\mathbf{M}$ are negligible respect the diagonal terms the two equation are uncoupled. In the simulation proposed in this thesis the extra diagonal terms are neglected.

Introducing the mechanical damage D and the chemical damage as in the biphase model (see Chapter 5) the pressure exerted by ettringite is computed by the relation

$$p_e = (1 - D) M_e(d)(\zeta_e - b \mathrm{tr}\boldsymbol{\epsilon}) \tag{6.42}$$

The pressure exerted by water can be computed by direct integration of the experimental capillary curve that links the capillary pressure $p_c = -p_w$ to the degree of saturation S_w

$$p_w = (1 - D) \int_{Sw_0}^{S_w} -S_w \frac{\partial p_c}{\partial S_w} dS_w \tag{6.43}$$

The macroscopic stress can be expressed in the final form

$$\boldsymbol{\sigma} = (1 - D) \left[2G(d)\mathbf{e} + K(d) \mathrm{tr}\boldsymbol{\epsilon}\mathbf{1} \right] - b(p_e + S_w p_w)\mathbf{1} \tag{6.44}$$

6.3 Transport of water in liquid form

The moisture transport in porous media can be treated rigorously by imposing a system of differential equations that take into account the exchange of mass between the different phases. In the case of weakly permeable materials, as in the case of concrete, it is possible to describe the transport of moisture through a simplified model in which the only variable is the degree of saturation S_w [Mainguy et al., 2001].

The water diffusion equations is obtained by combining the equation of the mass balance with the Darcy's law and considering negligible the contribution of the pressure variation of the gas inside the pores. The nonlinear equation of diffusion is

$$\phi \frac{\partial S_w}{\partial t} + \operatorname{div}\left(D_w \operatorname{grad} S_w\right) = 0 \tag{6.45}$$

where ϕ is the material porosity and D_w is the coefficient of diffusion of water which is a non linear function of

$$D_w = \frac{dp_c}{dS_w} \frac{\kappa \cdot k_{rw}(S_w)}{\eta_w} \tag{6.46}$$

where κ is the intrinsic permeability of concrete, k_{rw} is the relative permeability of water, η_w is the dynamic viscosity, p_c is the capillary pressure. The correlation between capillary pressure and degree of saturation can be obtained experimentally. [Mainguy et al., 2001] reports experimental curves that correlate water pressure and degree of saturation. At atmospheric pressure the water pressure is the opposite of the capillary pressure and an interpolation formula proposed by the same Authors is as follows

$$p_w = -p_c = -a(S_w^{-b} - 1)^{\left(1-\frac{1}{b}\right)} \tag{6.47}$$

$$k_{rw} = \sqrt{S_w}\left(1 - \left(1 - S_w^b\right)^{\frac{1}{b}}\right)^2 \tag{6.48}$$

with a and b material parameters to be calibrated by fitting the experimental curve, see figure 6.1. The equations proposed lead to a good interpolation of the curves for a degree of saturation between 0.1 and 0.6. For degrees of saturation close to unity the measured values deviate significantly from the fitting curve.

In practical cases presented in this work the initial degree of saturation of the specimens is generally high and during the process complete saturation is reached. For this reason we adopt an other interpolating expression that is well suited to the rage of degree of saturation typical of these problems.

$$p_c(S_w) = a_1 S_w^3 + a_2 S_w^2 + a_3 S_w + a_4 \tag{6.49}$$

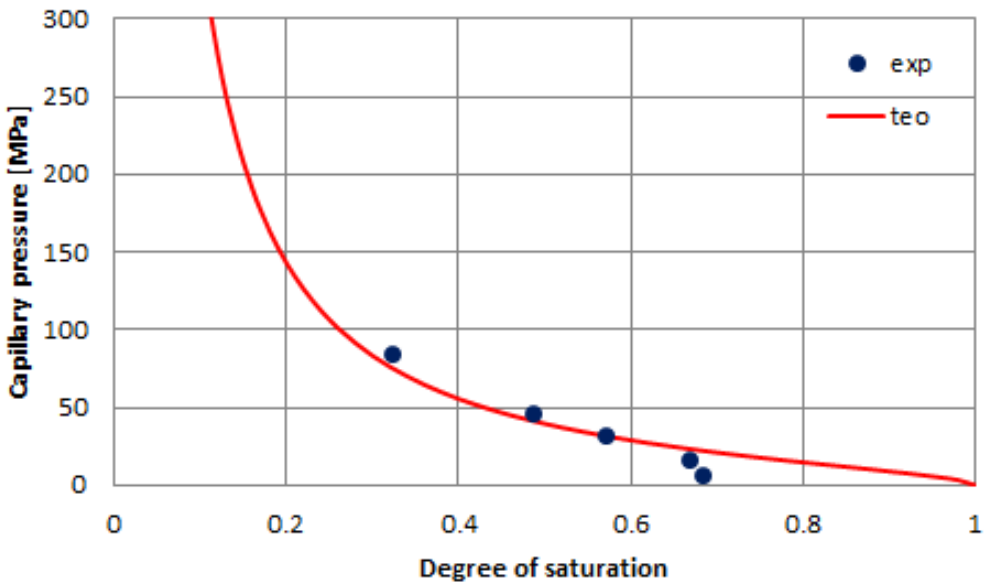

Figure 6.1: Capillary curve reported in [Mainguy et al., 2001]

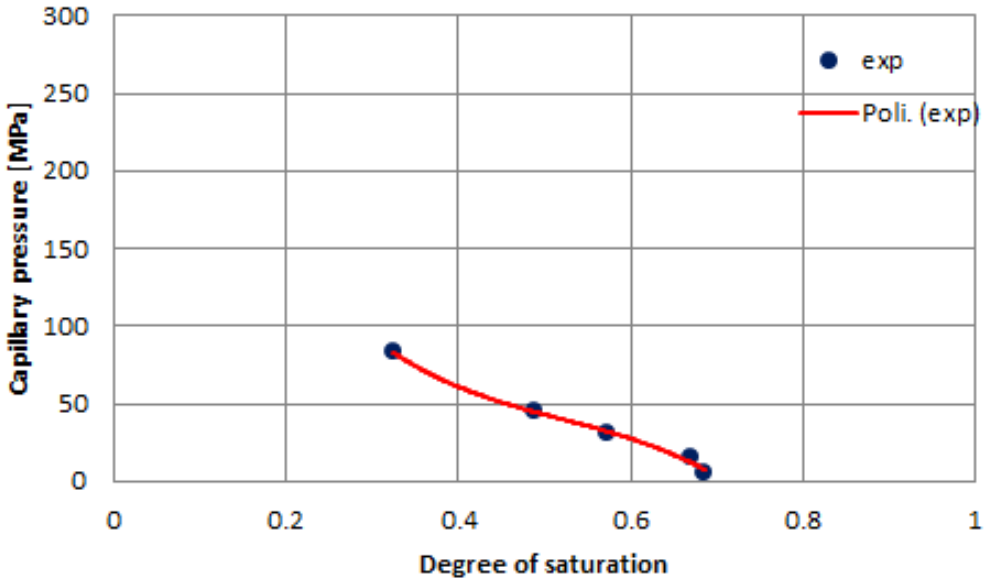

Figure 6.2: Polynomial interpolation of curve reported in [Mainguy et al., 2001] valid for $S_w > 0.3$

with a_i materials parameters to be calibrated by fitting the experimental curve, see figure 6.2

For given initial and boundary conditions on the degree of saturation, the solution of the nonlinear diffusion equation (6.45) provides the distribution of the degree of saturation, in time and space. In the above diffusion model of water the effect of salts present in the solution is neglected. This assumption is justified by the low influence that the salt concentration has on the capillary pressure [Samson et al., 2005].

The degree of saturation is an intrinsic quantity of the material and represents the ratio between the volume occupied by the liquid and the total volume of the pore. Generally the boundary conditions are expressed in terms of relative humidity defined as the ratio between the pressure of the vapor p_v and the saturated vapor pressure. The relationship between the degree of saturation and relative humidity h can be formulated by Kelvin's Law

$$\rho_w \frac{RT}{M_v} \ln(h) = p_w \tag{6.50}$$

where $R = 8.3145\ JK^{-1}mol^{-1}$ is the universal gas constant, T is the absolute temperature $[K]$, $M_v = 18.015\ g/mol$ is the molar mass of water vapor and p_w is the capillary pressure expressed by the relation (6.47). In figure 6.3 the relationship between relative humidity and degree of saturation is shown for a concrete with the capillarity curve reported in the figure 6.1 and at temperature $T = 293.15°\ K = 20°\ C$

6.4 Unsaturated diffusion-reaction process

Let us denote by $n_{sL} = n_{sL}(\mathbf{x}, t)$ the molar concentration of sulfate in the solution, varying in space $\boldsymbol{x}$ and time t, and by $n_s = n_s(\mathbf{x}, t)$ the molar concentration of sulfate referred to the unit material volume. In partially saturated media the latter depends on the degree of saturation and the relation between the two concentrations reads

$$n_s(\mathbf{x}, t) = n_{sL}(\mathbf{x}, t) S_w(\mathbf{x}, t) \widetilde{\phi} \tag{6.51}$$

The molar concentration $n_{sL}(\mathbf{x}, t)$ can be computed taking into account the diffusion process of sulfates within the pore solution and the consumption of sulfates due to the ettringite formation, then the problem can be formulated at the representative element volume level through a homogenized technique in terms of the molar concentration n_s, see [Samson et al., 2005], [Samson and Marchand, 2007]. The diffusion of sulfates within the homogenized material is driven by the gradient of concentration and by the fluid movement under the effect of the water content

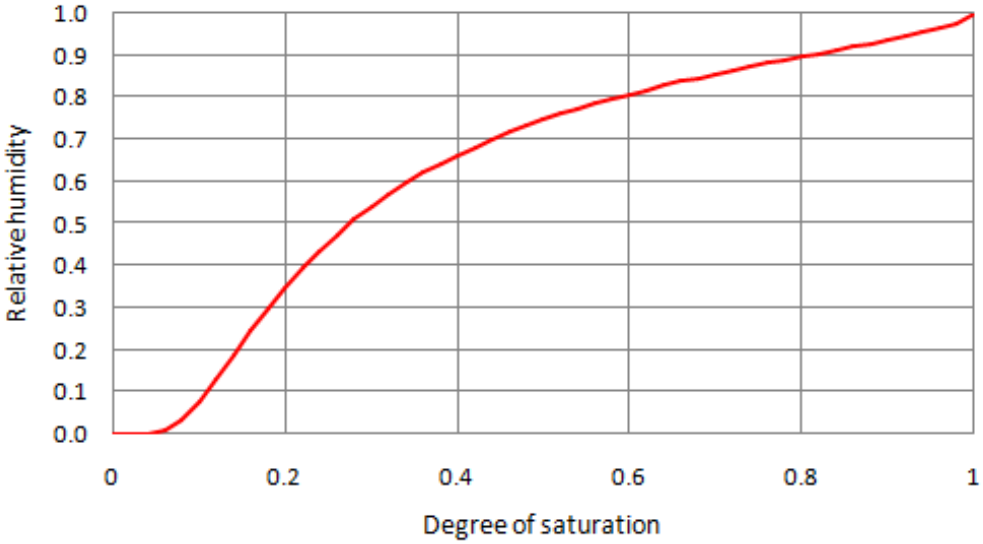

Figure 6.3: Relationship between the degree of saturation and relative humidity ($T = 293.15°\ K$)

gradient. This second advection term is not present in the fully saturated case. The consumption of sulfates is modeled considering a second order reaction between sulfates and aluminates. Denoting by $n_c = n_c(\mathbf{x}, t)$ the molar concentration of aluminates referred to the volume of the material, the evolution of both the concentration of sulfates and aluminates is governed by the following system

$$\begin{cases} \frac{\partial n_s}{\partial t} - \text{div}\left(\bar{D}_s S_w \text{grad}\left(\frac{n_s}{S_w}\right)\right) - D_w \frac{n_s}{S_w} \text{grad} S_w\Big) = -k n_c n_s \\ \frac{\partial n_c}{\partial t} = -\frac{k}{q} n_c n_s \end{cases} \tag{6.52}$$

In previous equation k is the rate of sulfates take up and $\bar{D}_s$ is the coefficient of diffusion of the sulfates depending, for partially saturated media, on the degree of saturation. When the material is unsaturated, the reduction in aqueous phase volume decreases the diffusion properties; as in [Samson et al., 2005], the following expression is assumed in this work

$$\bar{D}_s = D_s S_w^{7/3} \tag{6.53}$$

where D_s is the diffusion coefficient for the saturated material.

7 Numerical analyses

The constitutive model presented in previous chapters has been implemented in an ad-hoc finite element code developed in Matlab. The simulations has been perform in two or three dimensions using constant strain triangles, axis-symmetric 3 nodes elements and constant strain tetrahedra. To validate the model proposed we simulated the experimental concerning mortar and concrete samples affected by ESA and mortar prism subject to ISA. The experimental data have ben taken both from the literature ([Akpinar and Casanova, 2010], [Bouzabata et al., 2012]) and the new campaign performed during the present work and described in Chapter 3. Finally the model has been used to simulate the experimental data on a reduced scale tunnel lining subject to ESA [Lei et al., 2013].

7.1 Weakly coupled numerical approach

The numerical solution of the problem is obtained by a weakly coupled numerical approach whose algorithm is schematically shown in figure 7.1. A moisture diffusion analysis is performed to compute the degree of saturation distribution in space and time. Then the chemical reaction-diffusion problem, governed by equations (6.52), is solved to compute the evolution of the aluminates content and hence, through equation (5.78), the reaction extent $\bar{\xi}$. The degree of saturation and the reaction extent are the input of the subsequent mechanical analysis which allows to obtain strain, stress and damage. The weakly coupled approach greatly simplifies the numerical solution and is justified by two experimental based assumption. First, the water consumption due to the reaction of ettringite formation does not

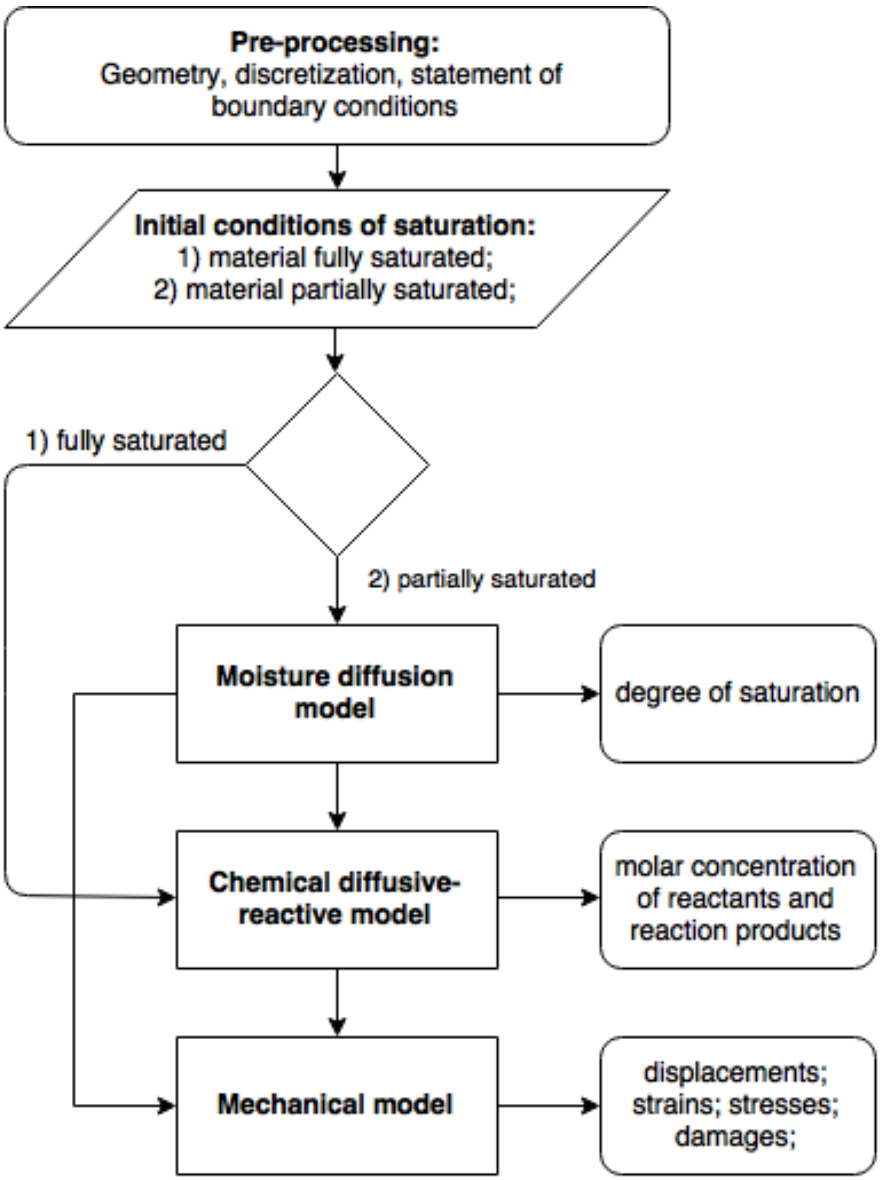

Figure 7.1: Weakly coupled numerical approach

alter significantly the degree of saturation, so that the moisture diffusion analysis is independent from the reaction-diffusion analysis. Second, the saturation process is generally very fast when compared to the kinetics of the reaction, thus often saturates before cracks formation therefore the permeability can be assumed as constant.

The time integration of the problem of diffusion-reaction was implemented with a staggered iterative scheme. First the sulfate concentrations is computed from

equation the firs equation of system (6.52) considering the value of the concentration of the aluminates of the previous iteration, then the new value of aluminates concentration is obtained from the second equation of system (6.52). This process is repeated until the difference between the concentration at two subsequent iterations are smaller than a given tolerance. The diffusion coefficient of sulfate can be kept constant over time or modified to take account chemical damage.

The mechanical response of concrete is governed by the chemo-elastic constitutive model with isotropic damage in tension and in compression proposed in previous chapters.

7.2 ESA on mortar samples: simulation of experiments by [Akpinar and Casanova, 2010]

The experimental campaign presented in [Akpinar and Casanova, 2010] was carried out on mortar prism $2.5 \times 2.5 \times 8.5\ cm^3$ fully immersed in sodium sulfate solution (mass concentration 5%). Two different types of cement were employed: one with low content of aluminate (CEM I 52.5N / SR) and one with high content (CEM I 52.5R). Numerical simulations of the transport process and of the mechanical response were performed in 3D considering three symmetry planes. In the moisture diffusion analysis the initial value of RH was assumed equal to 65%, corresponding a degree of saturation $S_w = 0.4$ at $T = 20°C$. The evolution of the degree of saturation at different exposure time (t = 20 days, 40 days, 60 days and 80 days) in the central section of specimen is show in figure 7.3. Figure 7.3 displays the contour plots of the degree of saturation at different time of one eight of the specimen. The complete saturation of the specimen is reached at about 70 days.

Then the diffusion-reaction analysis was performed to evaluate changes in chemical species within the material. A constant sodium sulfate concentration is imposed at the outer surfaces and no flux is allowed through the symmetry planes. The initial concentration of equivalent aluminates are 100 mol/m^3 for CEM I 52.5N/SR and 200 mol/m^3 for CEM I 52.5R. Figure 7.4 shows the evolution of molar concentration of sulfate and of ettringite at different exposure time (t = 60 days, 200 days, 400 days and 600 days).

The comparison between the results of the diffusion of moisture and the diffusion-reaction of chemical species shows that the first process is much faster than the second: after 60 days of immersion the specimen is almost fully saturated while the reaction has still very little effect.

Figure 7.5 shows the comparison between the molar mass of calcium aluminate computed in the case of material fully saturated material (sat) and in the case of progressive saturation (ns) at different times. In the case of material initially

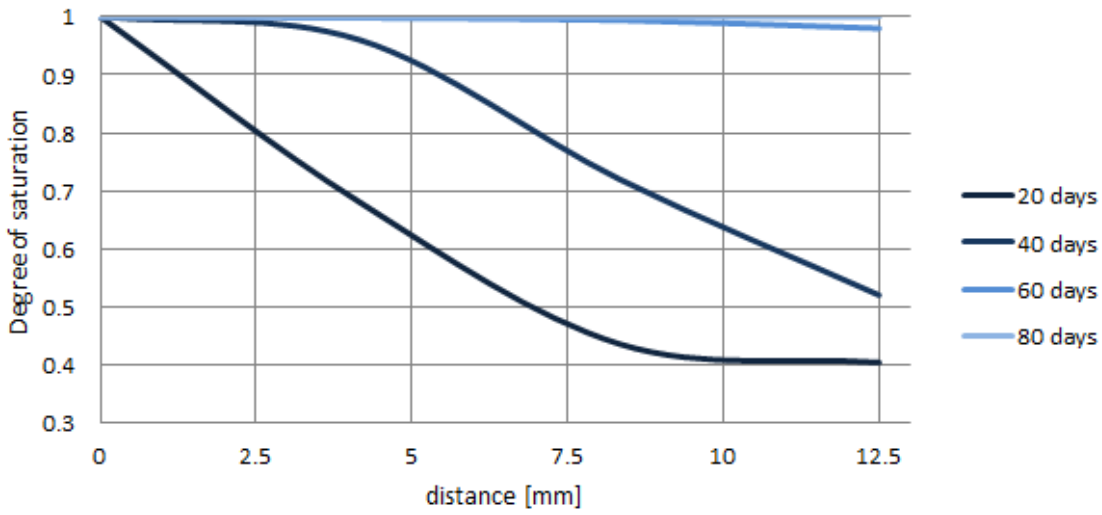

Figure 7.2: Evolution of the degree of saturation in the central section of the specimen in times (the distance is taken from the external surface).

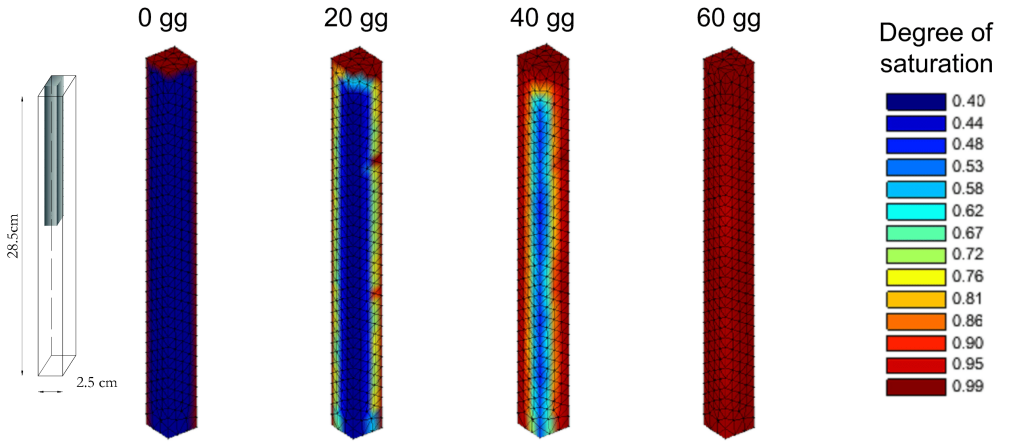

Figure 7.3: Evolution of the degree of saturation at different times ($t = 0$; 20 days; 40 days; 60 days)

saturated the kinetics of reaction is faster, and therefore the consumption of aluminate is greater. The difference between the two cases is pronounced during the first period. After complete saturation the difference progressively decreases.

The mechanical problem is solved by considering for mortar the elastic and damage parameters reported in table 7.1

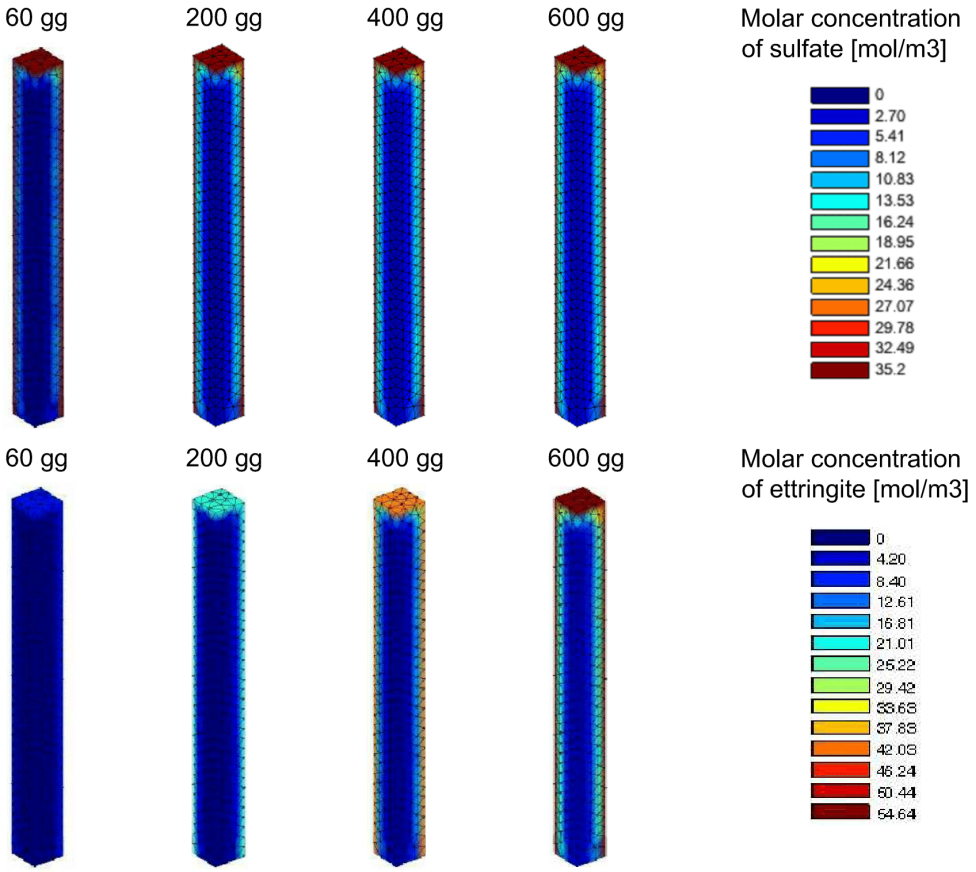

Figure 7.4: Molar concentration of sulfate and ettringite in time

Elastic parameter	Mechanical damage parameter	Chemical parameter
E=27000 MPa	$a_t = 0.25$	$r_1 = 45$
$\nu = 0.2$	$b_t = 4.3MPa$	r2=5.1
b=0.4;	$k_t = 18.6MPa^2$	$r_3 = 1$
	$D_{0p} = 0.5$	$\omega = 0.2$
	$\sigma_e/\sigma_0 = 0.6$	$\beta = 0.0$

Table 7.1: Parameters used in the simulation of the experiments reported in [Akpinar and Casanova, 2010]

In this problem mechanical damage only activates in tension, therefore only the parameter defining f_t are reported in table 7.1.

The patterns of damage reported in figure 7.6 show that the chemical damage

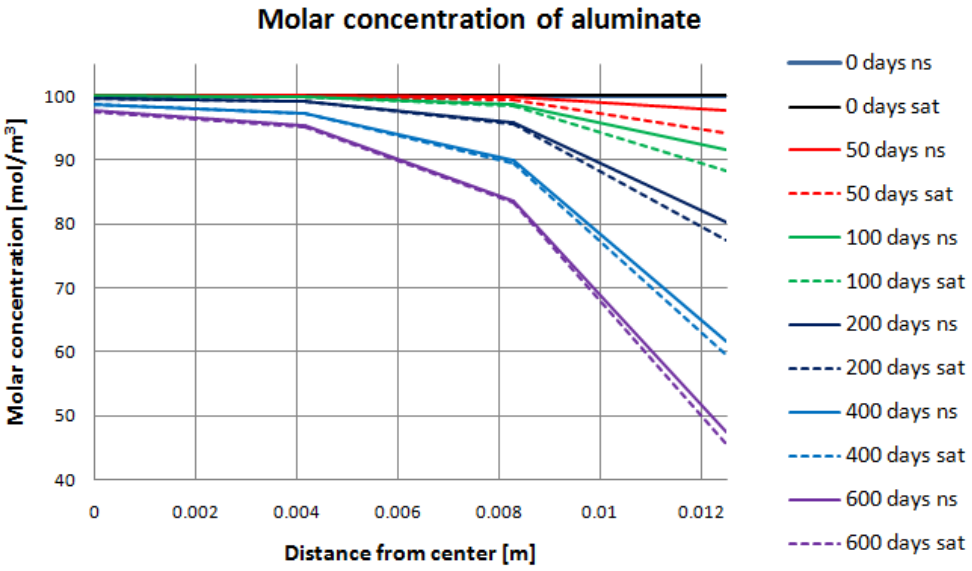

Figure 7.5: Molar concentration of aluminate at different times; dashed lines: saturated conditions, continuous lines: partially saturated conditions

of the material evolves only in the outer portion of material, in direct contact with the solution, while the mechanical damage develops in the inner part in which the state of stress is of prevailing tension. This is in agreement with the experimental observations reported in chapter 2 in which it is shown as external cracking is mainly due to the leaching while internal damage is due to the stress. Figure 7.7 show the comparison between the experimental points and the simulations of the free expansion of specimens cast with cements with different initial concentration of calcium aluminates. After the first phase, in which the swelling is due to absorption of the water, there is a second phase of expansion caused by the formation of ettringite. The simulations of the model correctly describe the experimental behavior.

Figure 7.8 shows the comparison between the contour plot of the pressure at 600 days for the high aluminate content specimen computed by the present model and the crystallization pressure p_c computed by the equation proposed in [Yu et al., 2013].

$$p_c = \frac{RT}{\mathcal{V}_e} \ln\left(\frac{n_s}{n_s^{eq}}\right) \tag{7.1}$$

where n_s and n_s^{eq} are the current and equilibrium molar concentrations of sulfate.

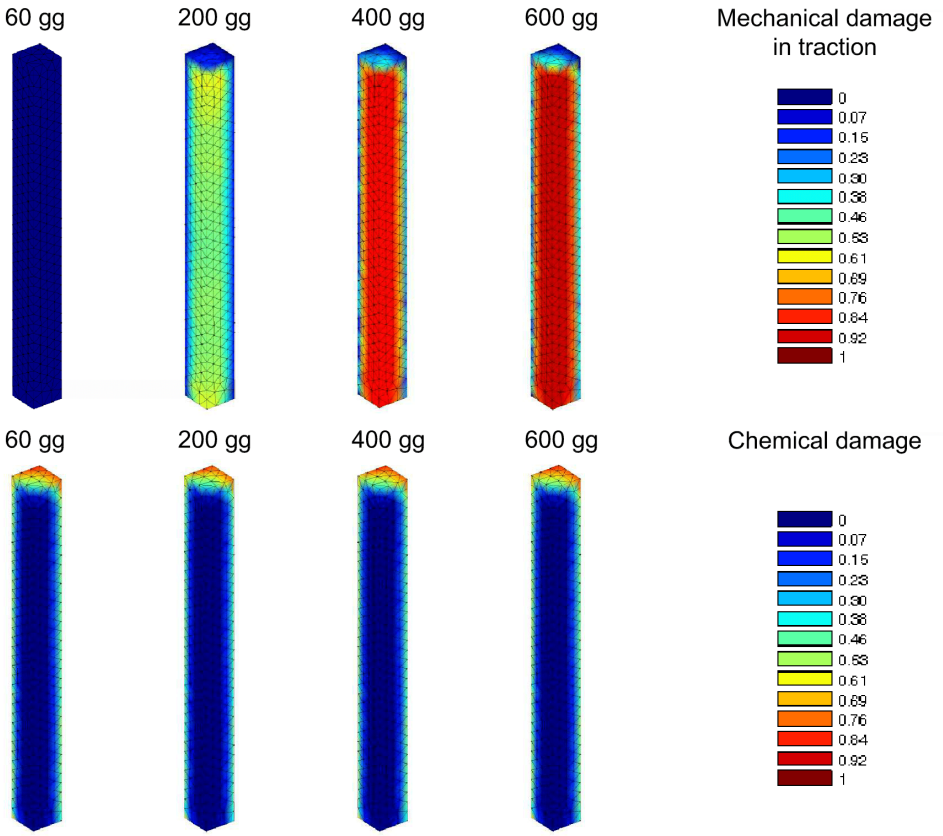

Figure 7.6: Mechanical and chemical damage on mortar prism at different time ($t = 60$ days; 200 days; 400 days; 600 days)

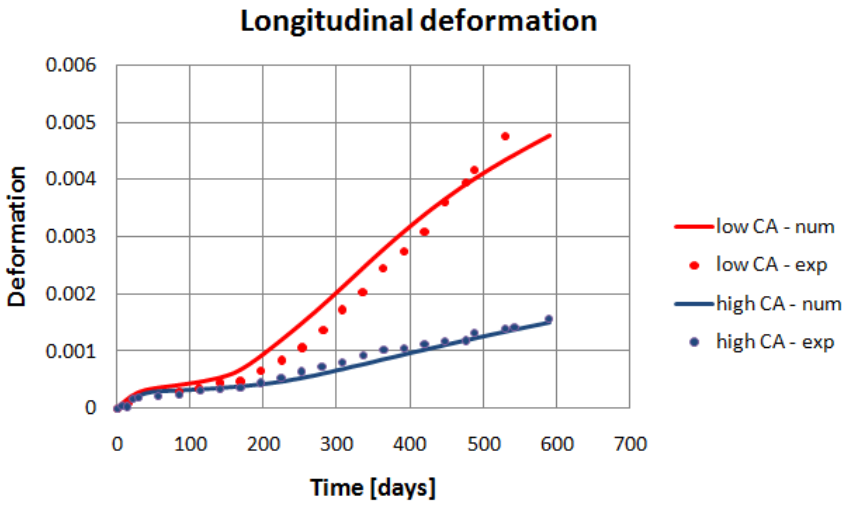

Figure 7.7: Longitudinal deformation of mortar prism: experimental and numerical comparison

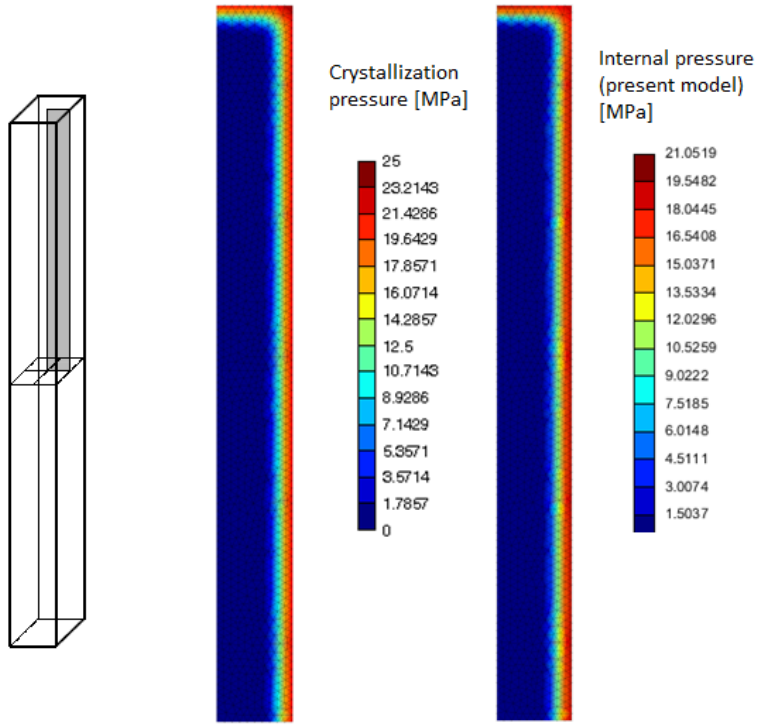

Figure 7.8: Comparison between the pressure computed by equation (7.1) proposed in [Yu et al., 2013] and by the present model

7.3 ESA on fully immersed concrete samples

7.3.1 Cylindrical samples

The experimental campaign presented in chapter 3 of this thesis of fully immersed cylinder has been simulated by the developed model and the result are collected in this paragraph. The possibility to perform a separate preliminary experimental identification of many material parameters required for the numerical simulation has allowed a significantly reduction of arbitrariness in the choice of material parameters and hence has allowed for a real validation of the model developed in present work. All the analyses are performed using triangular axisymmetric elements. The water-diffusion parameter are first calibrated through the data obtained in capillary tests conducted in a climatic chamber at constant temperature and humidity ($T = 20°C$ and $RH = 50\%$). The comparison between experimental measurement and simulation after material calibration are reported in figure 7.9 in term of mass variation evolution in time. The same picture also shows the contours plots of the degree of saturation at different times.

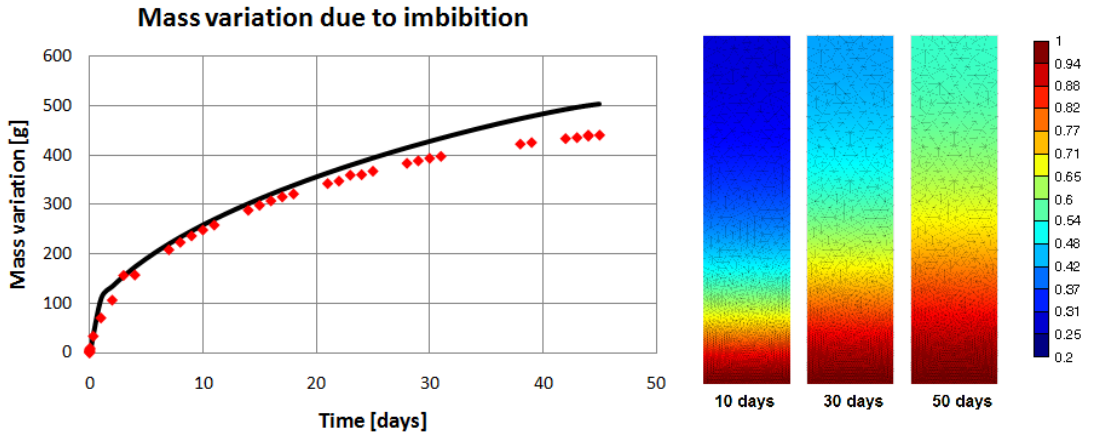

Figure 7.9: Comparison between experiment and simulation of the capillary test

The parameters governing the problem of diffusion-reaction have been calibrated in a qualitative way through the profiles of salt penetration obtained cutting and drying the cube stored for 400 days in the 10% sodium sulfate solution. Using a diffusion coefficient for sulphates $D_S = 7.2 \times 10^{-2} mm^2/days$, a reaction coefficient $k = 1.12 \times 10^{-4} m^3/(mol\ days)$ and a initial concentration of equivalent aluminate $n_c(0) = 76 mol/m^3$ the comparison in figure 7.10 is obtained. The figures 7.11, 7.12 and 7.13 show the simulations of longitudinal and radial expansions

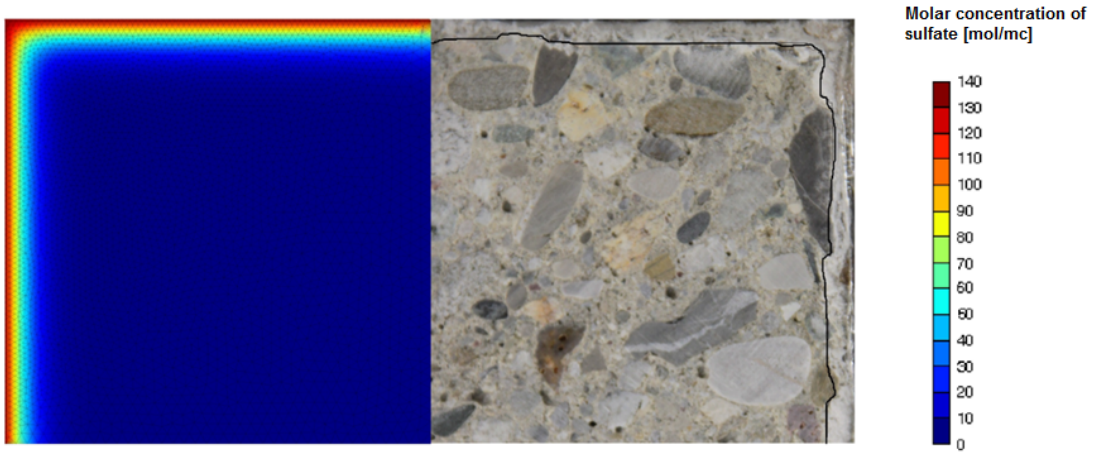

Figure 7.10: Penetration front of sulfate after 400 days of immersion: numerical solution and experimental profile

of the cylinders fully immersed in water, in 5% sodium sulfate solution and in 10% sodium sulfate solution respectively. The only input data varied in numerical simulations is the sulfate concentration at the edges. The proposed model is able to provide an estimate of the deformations in good agreement with the experimental observations. In particular the influence of the sulfate concentration and the effect of geometry on the difference between the longitudinal and radial deformation are well simulated.

Figure 7.14 shows the pattern of damage calculated by the model on a cylinder after 400 days of exposure in 10% sodium sulfate solution. The region most damaged by tensile stress is near of the upper corner. This prediction is in agreement with the experimental observation that shows large cracks in correspondence of this region, see fig. 2.1 (b).

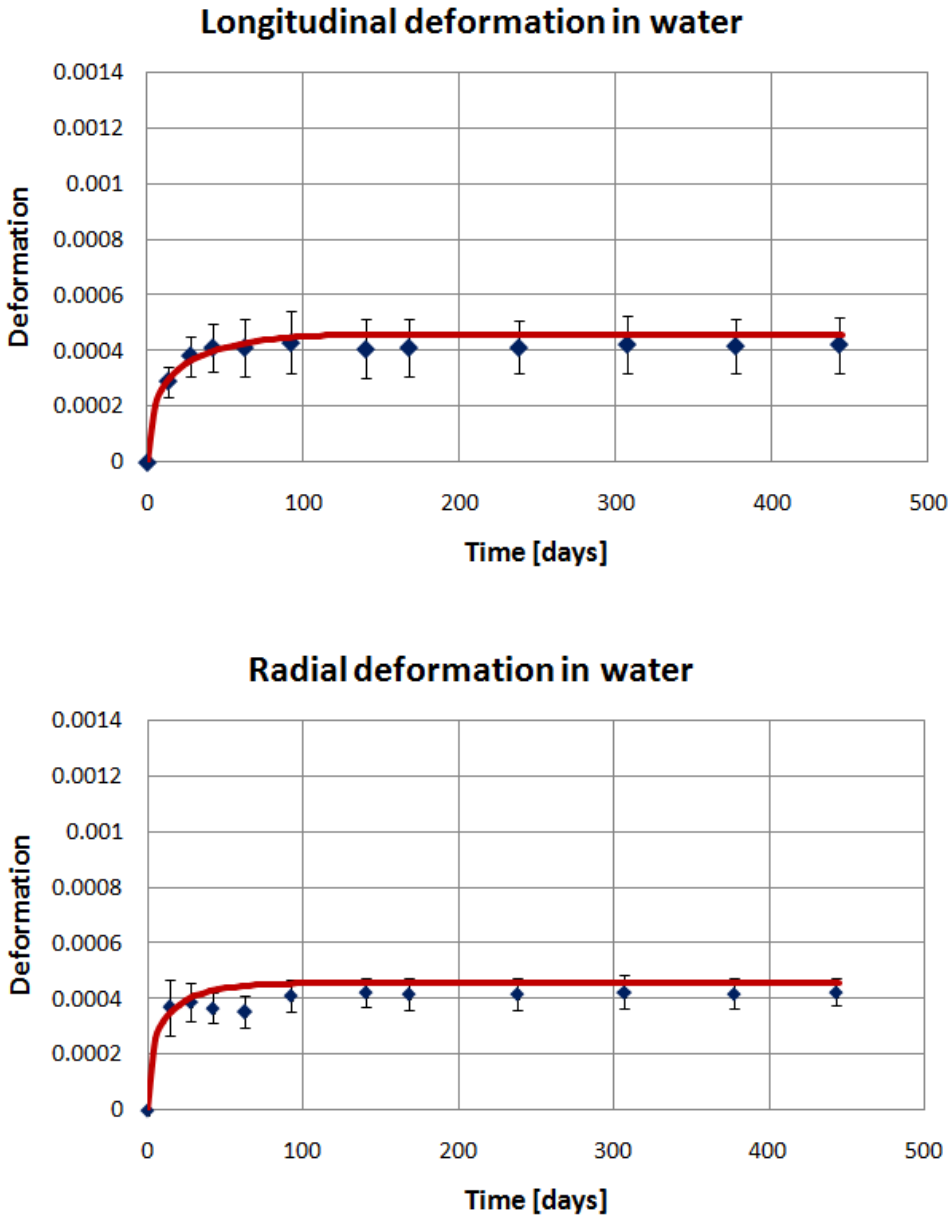

Figure 7.11: Cylinders immersed in pure water. Time evolution of longitudinal and radial deformation: experimental value on 4 specimens and model simulation

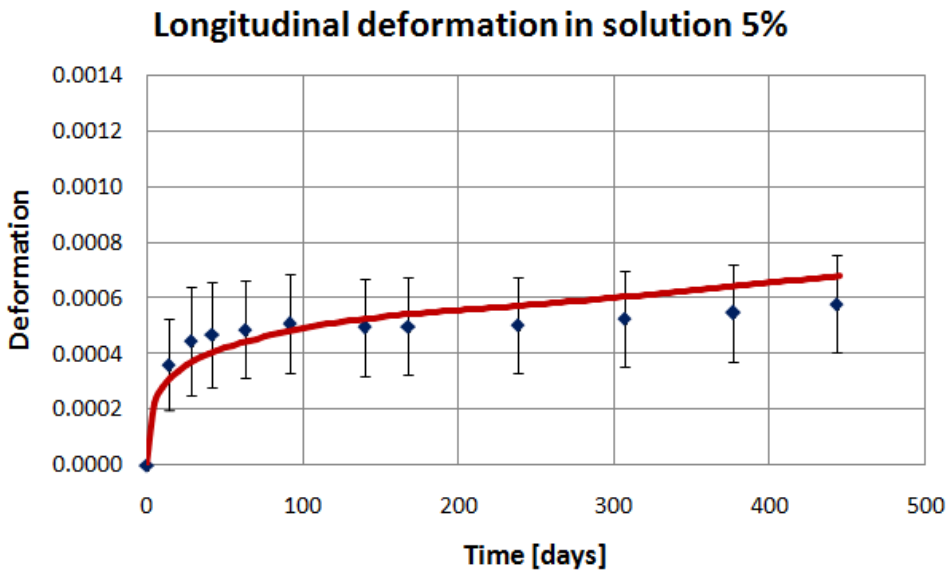

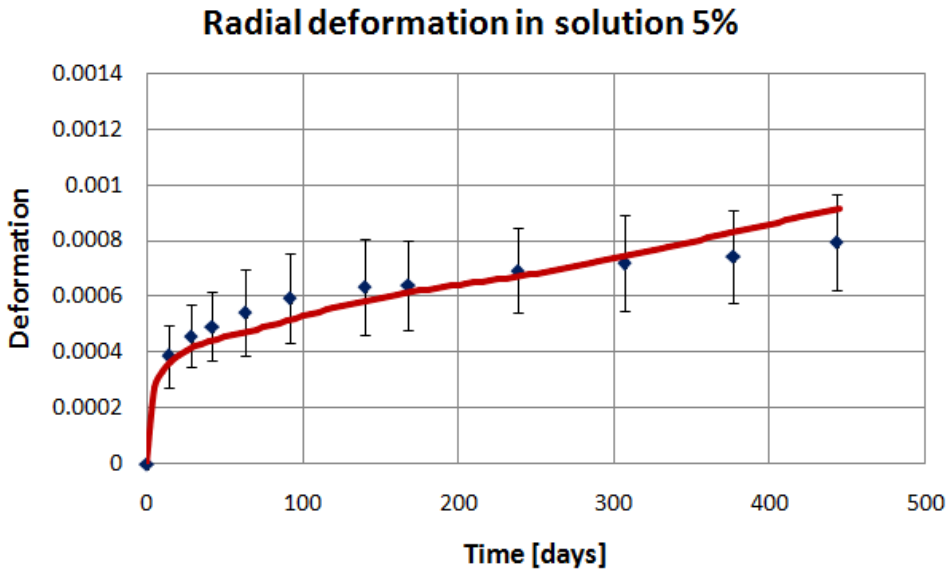

Figure 7.12: Cylinders in 5% sodium sulfate solution. Time evolution of longitudinal and radial deformation: experimental value on 4 specimens and model simulation

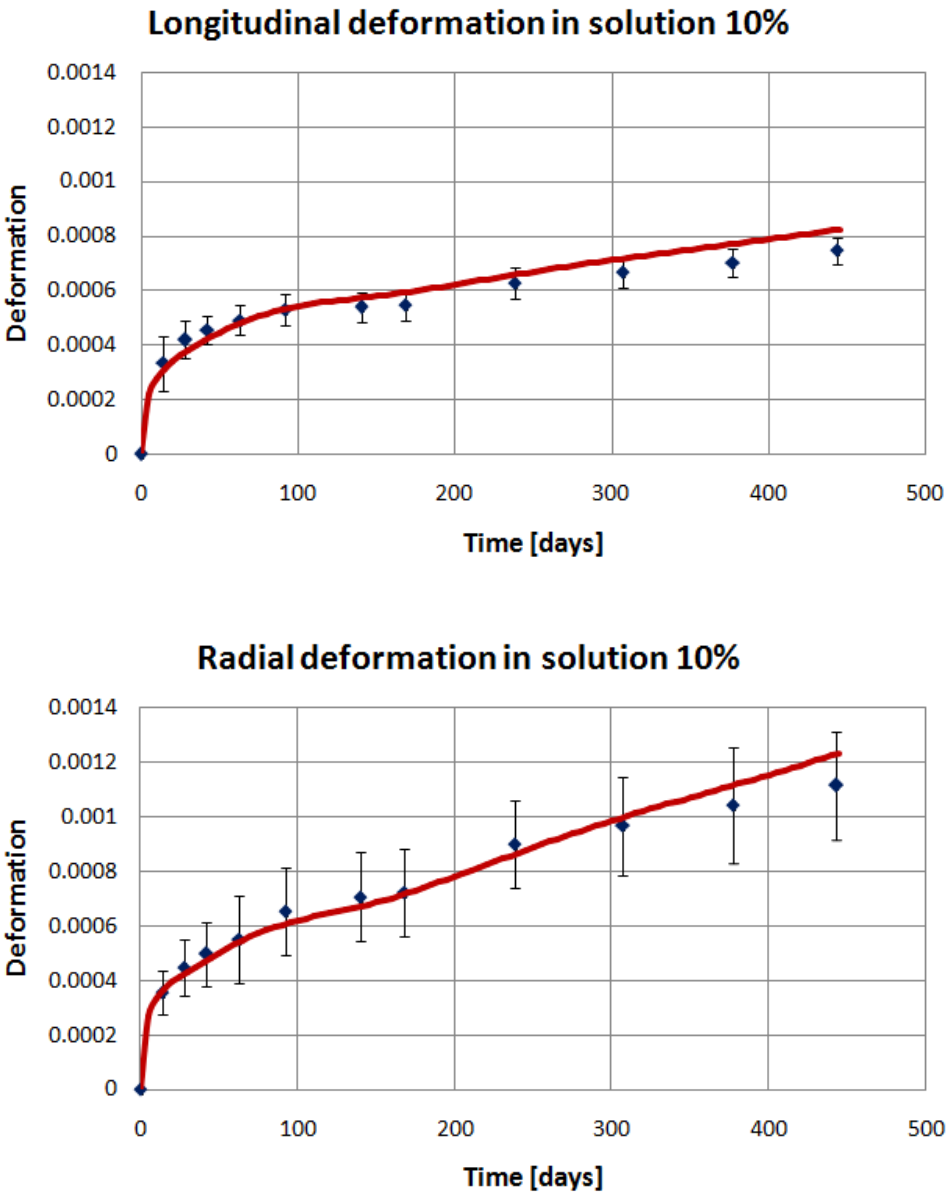

Figure 7.13: Cylinder ins 10% sodium sulfate solution. Time evolution of longitudinal and radial deformation: experimental value on 4 specimens and model simulation

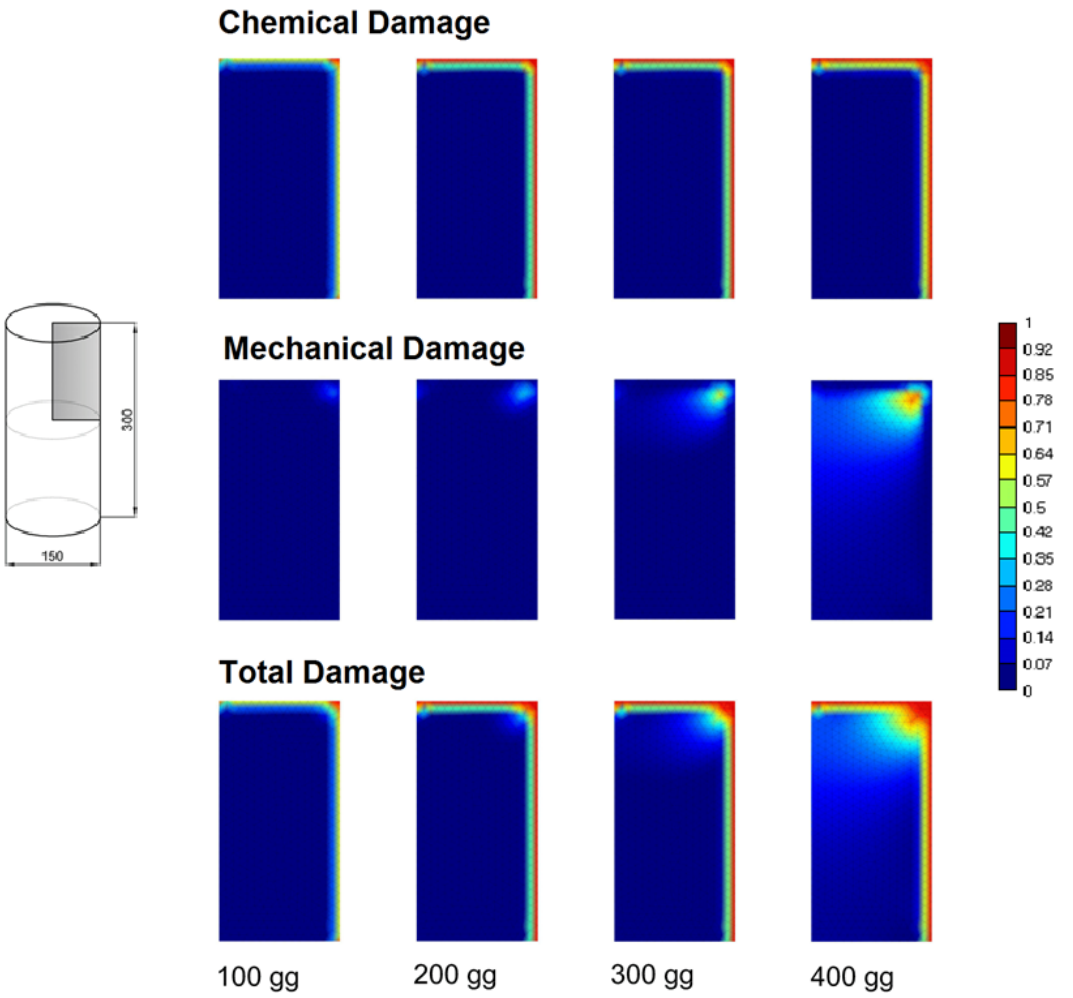

Figure 7.14: Chemical, mechanical (traction) and total damage in a cylinder immersed in a 10% sodium sulfate solution

7.3.2 Prismatic samples

As a further validation, also the experimental results obtained on the prisms, cast with a more reactive cement, have been simulated by the present model. In particular the free expansion tests of prismatic specimens totally immersed in water and sodium sulfate solution at molar concentration 10% have been considered. The mechanical parameters used in numerical simulation are the same of section 7.3.1. The initial concentration of equivalent aluminates are $n_c(0) = 96 mol/m^3$. These parameters have been changed to take into account the different chemical properties of cement.

Figure 7.15 shows the comparison between the experimental and numerical predicted evolution of transversal and longitudinal deformation for specimens immersed in pure water, while figure 7.16 shows the same comparison for specimen fully immersed in 10% sodium sulfate. A good agreement is obtained in all cases.

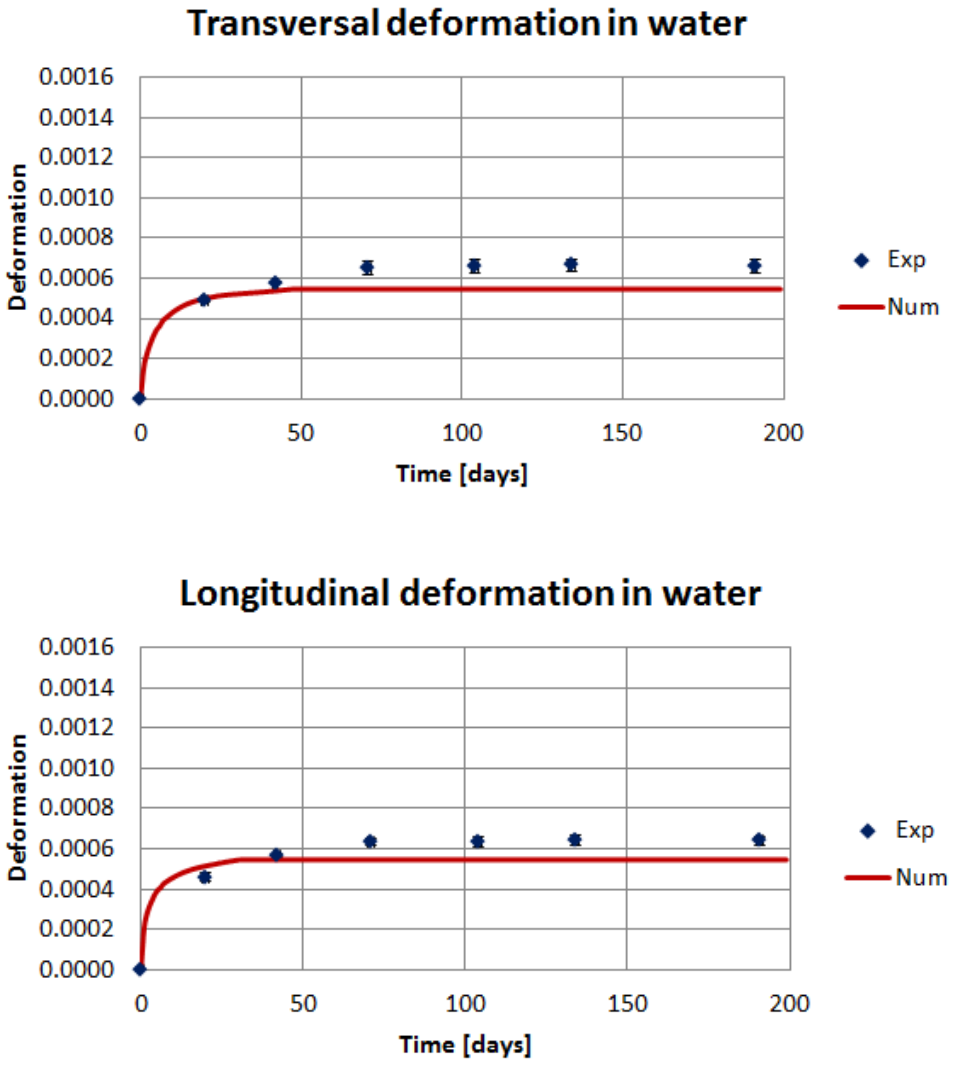

Figure 7.15: Transversal and longitudinal deformation of prism fully immersed in water

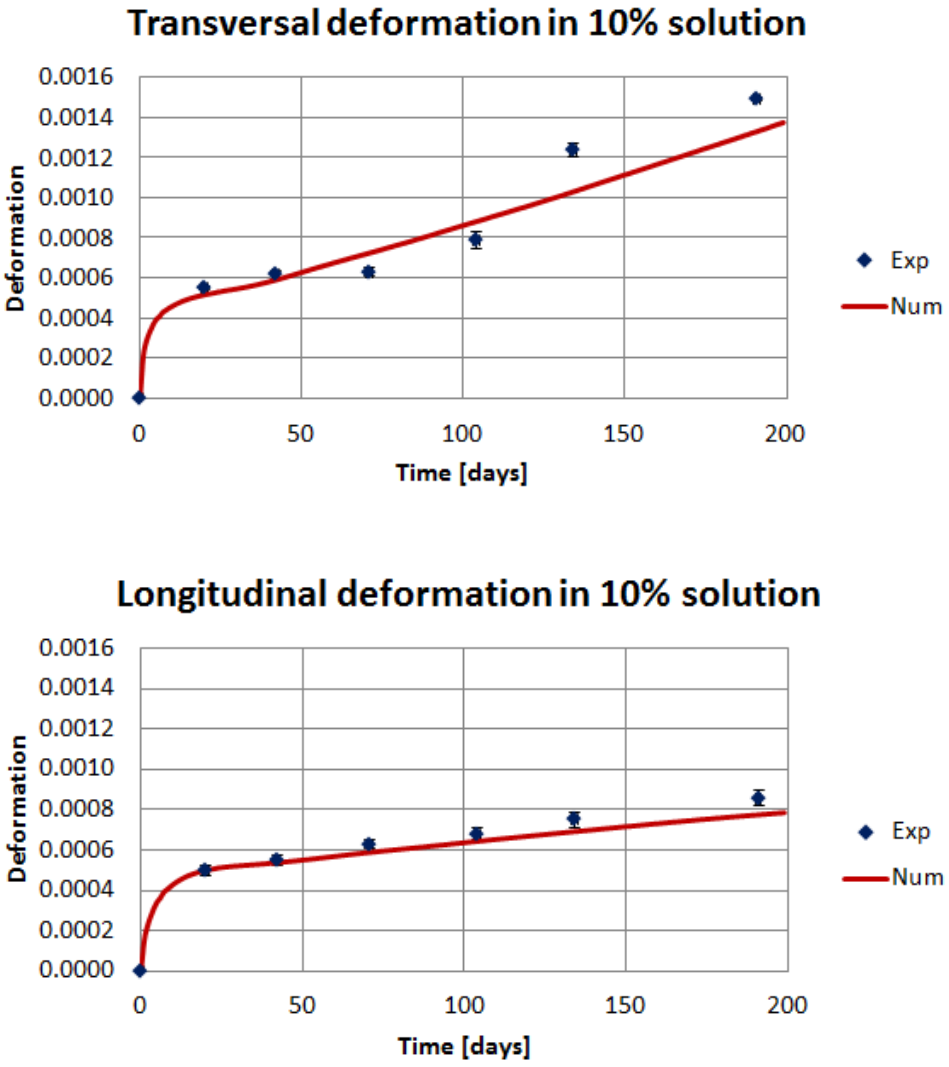

Figure 7.16: Transversal and longitudinal deformation of prisms fully immersed in 10% sodium sulfate solution

7.4 ESA on partially immersed Prisms

In this chapter the simulation of longitudinal and radial deformation of partially immersed prism reported in chapter 3 are perform. The prism are immersed in water and in 10% sodium sulfate solution for half height and stored in climatic chamber at constant humidity and temperature ($RH = 90\%$, $T = 20°C$). These prisms has been cast in the same time of the totally immersed prisms, thus the same parameters are used in the numerical simulations.

Figures 7.17 and 7.18 show the comparison between experimental and numerically predicted evolution of longitudinal deformation and of bottom and top transversal deformation for specimens partially immersed in sodium sulfate solution.

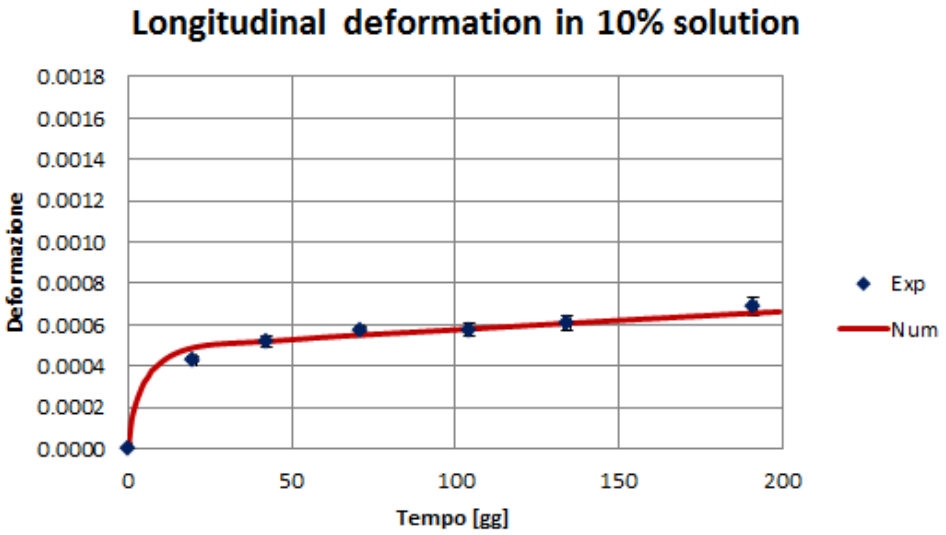

Figure 7.17: Prisms partially immersed in 10% sodium sulfate solution. Time evolution of longitudinal deformations: experimental mean value on 2 specimens and model simulations

In all case the model can predict the response of material: the transversal deformation of top point is not appreciably influenced by the chemical reactions and the overall effect is mainly due to the water imbibition, the transversal deformation of the bottom point is appreciably influenced by the reaction so much so is quite similar to the same observed in the total immersed prisms, the rate of longitudinal deformation is intermediate respect the two transversal deformation and it is due to the fact that the reacted and un-reacted part in this direction are connected in series.

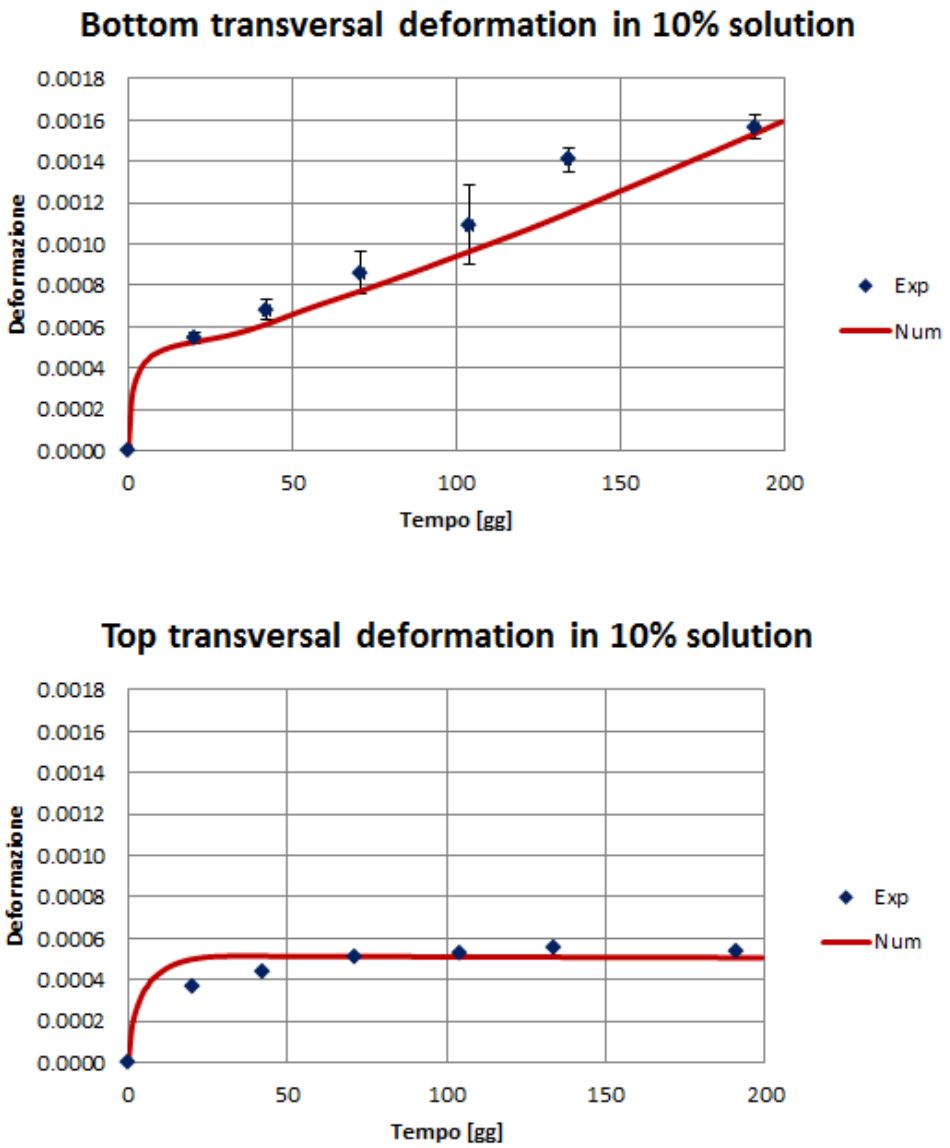

Figure 7.18: Prisms partially immersed in 10% sodium sulfate solution. Time evolution of top and bottom transversal deformations: experimental mean value on 2 specimens and model simulations

7.5 ISA on restrained mortar samples: simulation of experiments by [Bouzabata et al., 2012]

In this section the experimental tests presented in [Bouzabata et al., 2012] are simulated. Those tests were performed on mortar prism in which 3.1% of Na_2SO_4 was added to the mixture water. The experiments have been conducted on prism $40mm \times 40mm \times 160mm$ with water concrete ratio $a/c = 0.55$.

After casting some specimens were subjected to a heat treatment consisting of a first step at the temperature $20°C$ for $1h$, a second heating step from $20°C$ to $80°C$ in 4 h, a third step at constant temperature of $80°C$ for 10 h and a fourth stage of cooling up to $20°C$ in 10 h. The samples were cured in steam chamber within metal mold and covered by plastic sheets to prevent water evaporation. In addition another set of samples was stored at a constant temperature of $20°C$. After the thermal process, all the specimens were stored in plastic film at $20°C$ for 28 days.

After 28 days of curing the specimens have been inserted in a constraint device consisting of two steel plates connected by four stainless steel bars. In order to obtain two different levels of constraint bars with different diameter have been used:$2mm$ (4D2) and $5mm$ (4D5).

In this case an internal sulfate attack occurs, the sulfate concentration is homogeneous in space and varies in time due to the reaction with the aluminates. The comparisons between the experimental curves and numerical simulations are shown in figures 7.20 and 7.21 in terms of radial and longitudinal strains in different constrain conditions: free expansion, four restrain bars $\oslash = 2mm$, four restrain bars $\oslash = 5mm$). With increasing diameter of the steel bars there is a reduction of the longitudinal deformation and a small increase of the radial one.

The model is able to correctly simulate the reduction of the asymptotic longitudinal expansion due to the compressive stress acting on the restrained specimens. The real strain evolution at early stages of the reaction is smoother than the one predicted by the model. This is could be due to the fact that the material in inhomogeneous at the mesoscale and thus the reaction does not start simultaneously in all points of the specimen. Moreover, the chemical reactions leading to delayed ettringite formation in ISA are not exatly the same of those characterizing ESA, therefore kinetic is be different.

The compressive strength of material not subject to degradation phenomena increases over time due to the hydration. On the contrary the compressive strength of mortar subject to sulfate attack decreases in time due to leaching and cracking in a first phase. The a limited increase due to the progress of hydration is observed, see the experiment present in figure 7.22. The model correctly describes the decrease while the consequent increase for hydration is non considered, see

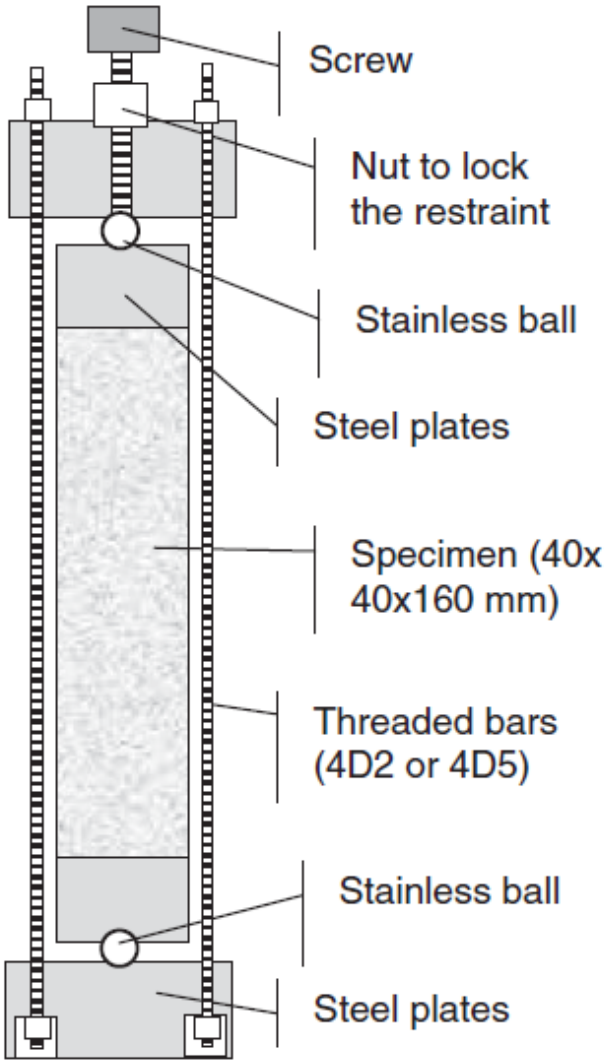

Figure 7.19: Constraint device used in [Bouzabata et al., 2012]

continuous line in figure 7.22.

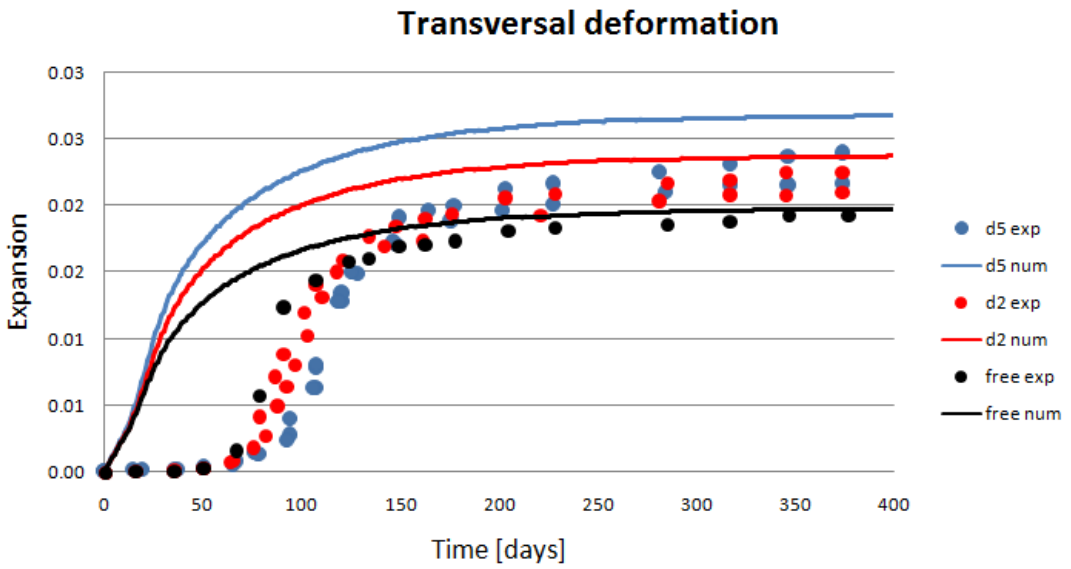

Figure 7.20: Transversal deformation of constrained mortar prisms affected by ISA

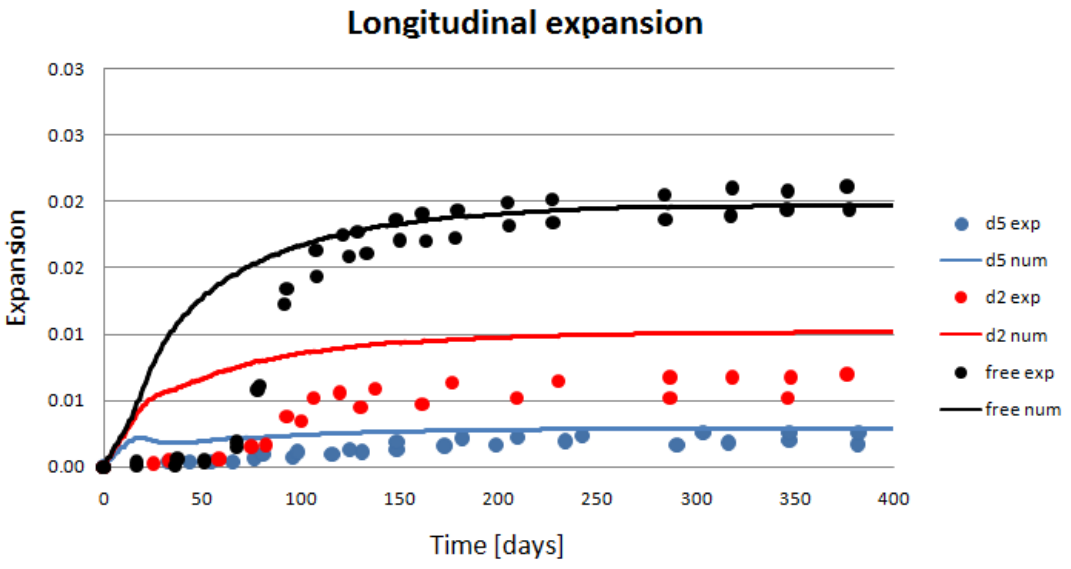

Figure 7.21: Longitudinal deformation of constrained mortars prisms affected by ISA

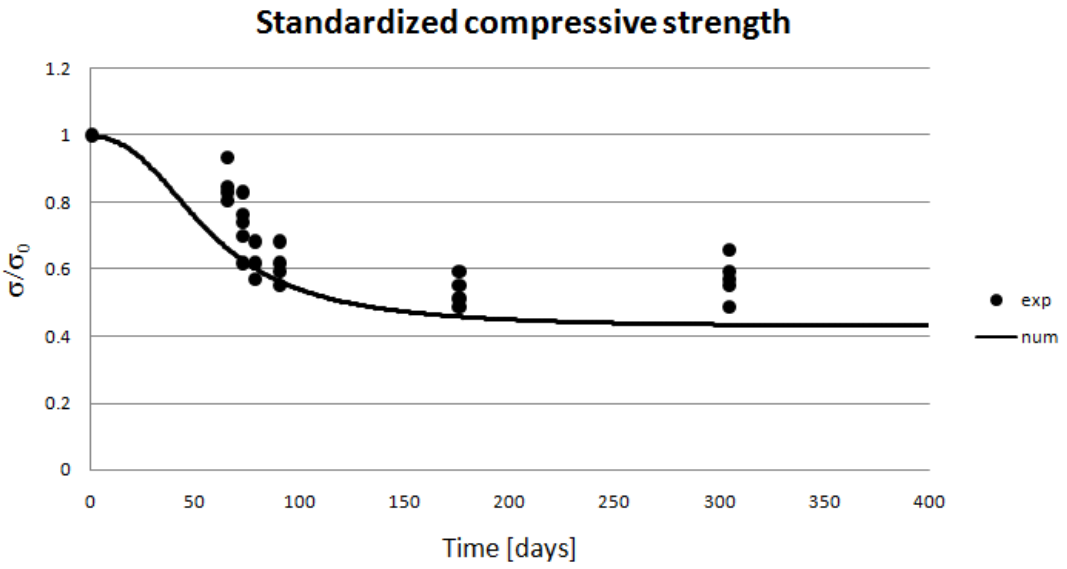

Figure 7.22: Normalized strength of mortar prisms affected by ISA

7.6 Tunnel subject to ESA

Tunnels for transport infrastructures or for hydroelectric plants are a typical class of structures often placed in contact with aggressive soils and therefore subject to external sulfate attack. A significant example, reported in [Lei et al., 2013], is represented by the Chengdu-Kunming railway in China, where numerous tunnels built in 1960s and 1970s exhibit a severe damage, mainly due to sulfate attack.

Field investigations showed that the sulfate anions entered in the tunnel lining and caused damage by erosion and spalling. The penetration of sulfates was very fast, as the concrete used for the realization of these structures has low strength and high porosity.

In [Lei et al., 2013] an experimental campaign aimed to study the mechanical response in time of these tunnels is presented. Some reduced scale models have been cast and placed in an artificial environment test system constituted by a box filled with soil and closed at the top by a steel plate, on which different values of mechanical loads were applied, see Fig. 7.23. Inside the tunnel a temperature of $25°C$ and a relative humidity of 80% were fixed. A 5% sodium sulfate solution was periodically injected into the soil in order to produce the sulfate attack in the tunnel lining. The tests were performed by imposing different constant vertical loads and evaluating the displacements of the vault and of other characteristic points of the lining. We have simulated these tests by the proposed approach, considering a plane strain approximation of the tunnel-soil-box system.

Figure 7.24 shows the comparison between the experimental and numerical values of the vault settlement at different load levels. The symbols represent the experimental values periodically measured on the scaled model at different load levels while the solid lines are the results of the simulation. The numerical results are in good agreement with the experimental observations for values of external load $q = 160kN$ and $q = 190kN$. For higher loads the results provided by the model, though qualitatively consistent, are less accurate when compared with the measured values. We note, however, that at these loads the experimental values are more dispersed.

Figure 7.25 shows the comparison in terms of displacements of characteristic points of the vault and of the flanks of the tunnel after 6 months of exposure and for different load levels. The comparison between the results of simulations and the experimental observations is, also in this case, reasonably good especially for low load levels.

After two months of exposure, the experimental tests already showed the appearance of cracked areas with some spalling in about the 10% of the lining surface, mainly concentrated in the upper part of the vault. After six months, a very large degraded area was observed.

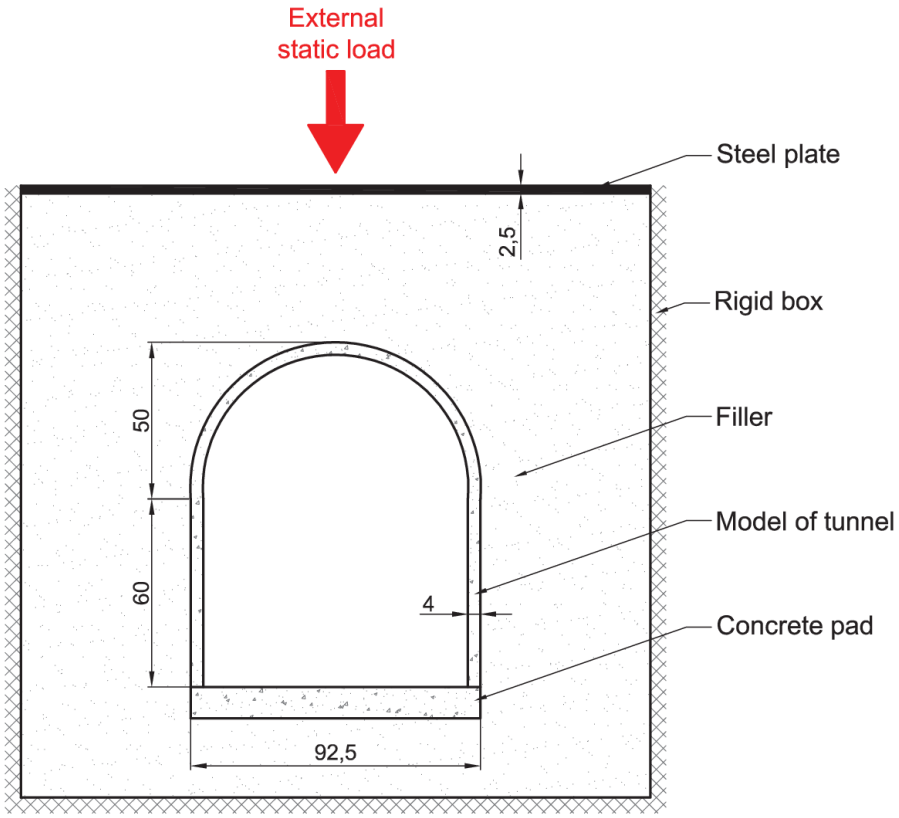

Figure 7.23: Geometry of the reduced scale 1:10 model of the tunnel lining structure tested in [Lei et al., 2013], (measures in [cm]).

The model proposed in this thesis qualitatively accounts for these phenomena by damage evolution. Figure 7.26 shows the contour plots of the chemical and mechanical damage in tension and compression after 2 and 6 months, for the test with $240kN$. It can be observed that the chemical damage progressively develops, starting from the surface in contact with the aggressive soil and then spreads through the whole thickness of the tunnel. The mechanical damage in tension concentrates at the upper part of the vault and reaches high values already after 2 months of exposure. Another highly damaged part develops at the interface between concrete and soil at one third of the arch. The mechanical damage in compression is very limited, less than 0.06 in the whole structure. Figure 7.27 reports the evolution of the overall stiffness reduction, accounting for both chemical and mechanical damage of the measurements points indicated in figure 7.25. The high value, close to 1, at the upper point of the vault simulates in the present continuous approach the real crack formation.

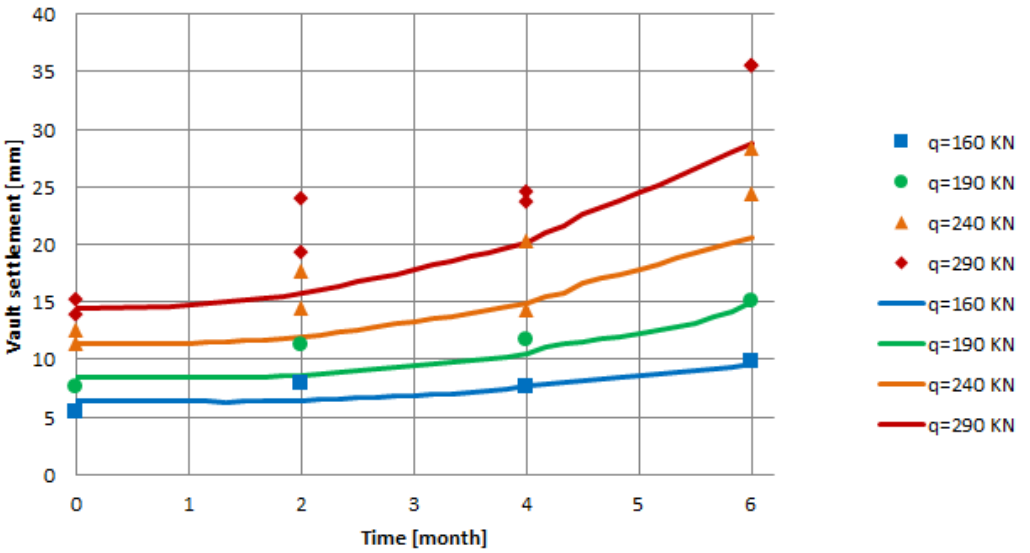

Figure 7.24: Comparison between experimental (symbols) and numerical (continuous lines) evolution in time of vault settlements

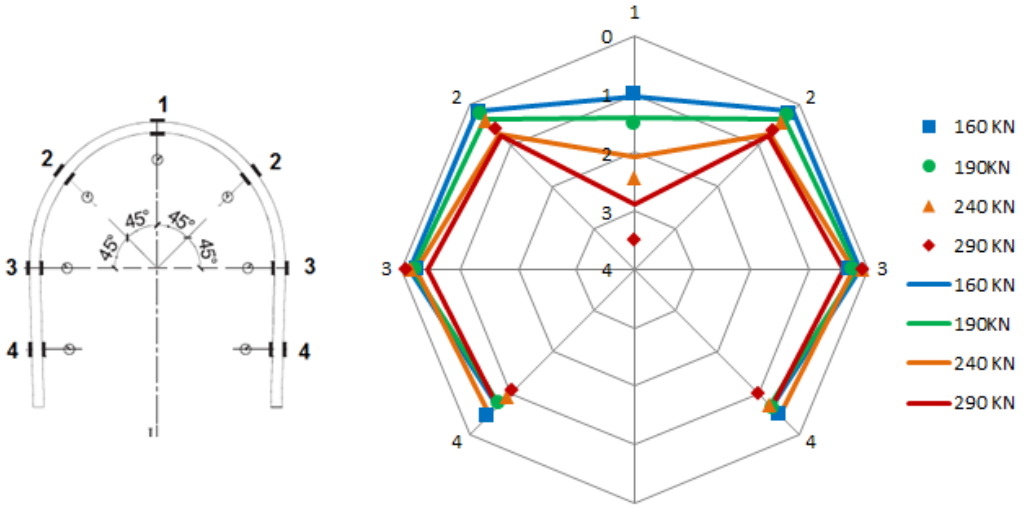

Figure 7.25: Comparison between the experimental and numerical displacement of the vault

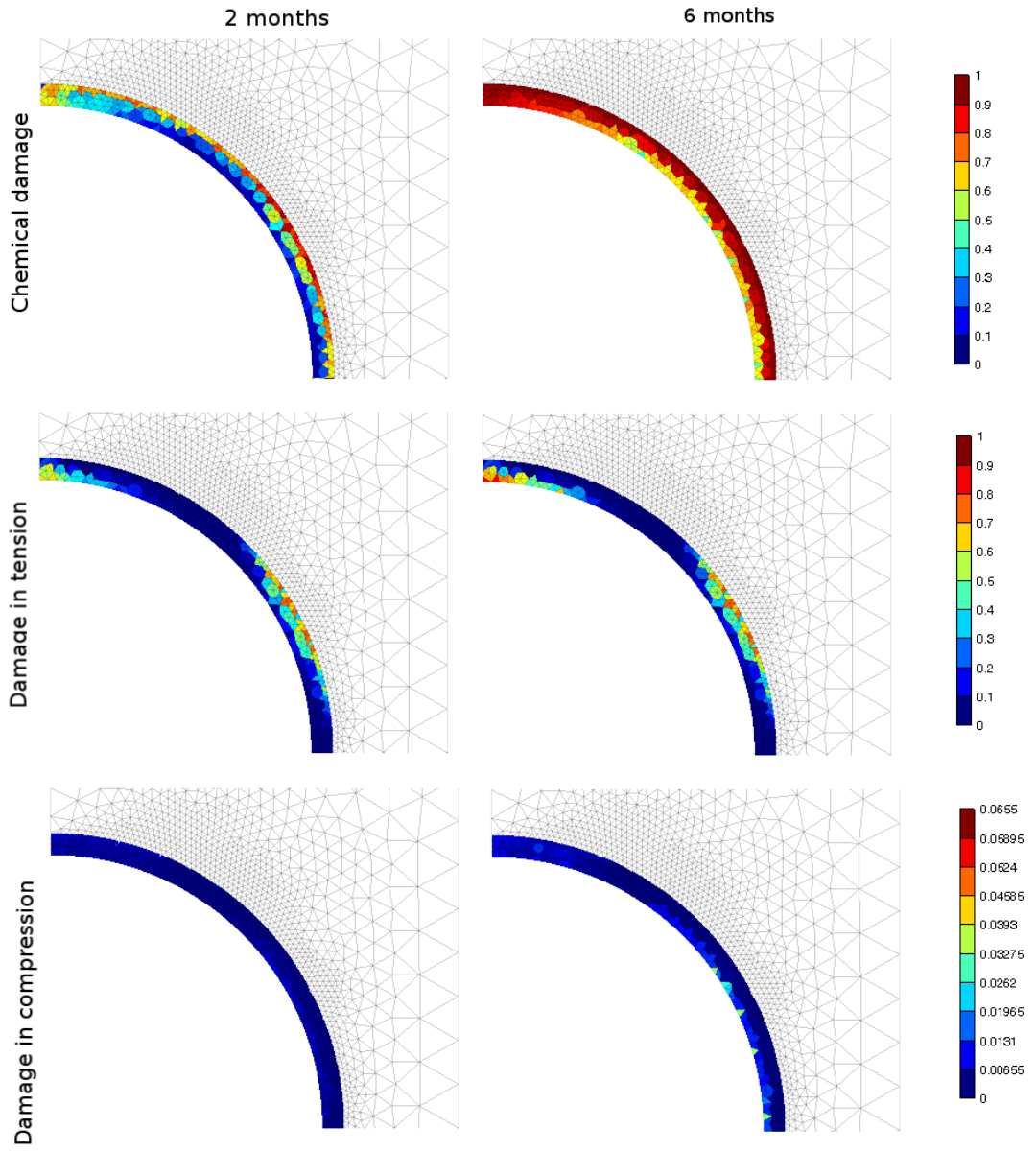

Figure 7.26: Pattern of chemical and mechanical damage in tension and compression after two and six months of exposure, external load of $240kN$.

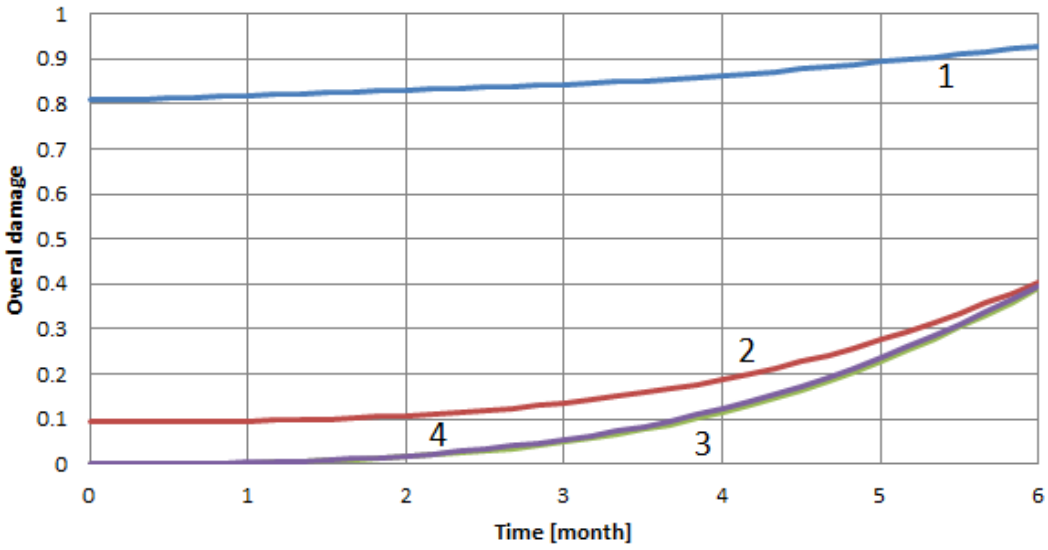

Figure 7.27: Evolution of the overall damage of the measurements points, load of $240kN$.

8

Concluding remarks and further developments

In this work an experimental, theoretical and numerical study of the mechanical effect of sulfate attack in concrete is presented.

During the experimental campaign presented in chapter 3 a wide number of specimens in concrete have been subjected to external sulfate attack in different conditions of exposure. The evolution of the phenomenon has been periodically monitored through various measurements of weight, of length variations and of ultrasonic wave propagation. In addition, after 400 days of exposure, a series of chemical and physical test (depth of salts penetration, porosimetry and XRD/EDS observations) have been performed to identify the effect of the reactions inside the material. Through this experimental campaign we have obtained significant data concerning the behavior of two different types of concrete subject to external sulfate attack. At difference from the majority of the experimental data available in the scientific literature which concern mortar specimens, in the present campaign two structural concretes, with maximum aggregate size of 32 mm and 16 mm, respectively, have been used. This allows to obtain reliable data for the calibration of a model intended to describe the behavior of concrete structures subject to sulfate attack.

The measurements carried out on the different samples have shown how the exposure conditions, the chemical properties of the cement and the geometry of the sample play a key role in the overall mechanical response. The effect of the geometry of the sample in the case of ESA and of the molar concentration of sodium sulfate in solution is well represented by the time evolution of deformation

of the fully immersed cylinders. In fact, the ratio between the length of the reactive external layer and the total length in the radial direction is higher than the same ratio in longitudinal direction. This leads to radial deformations higher than the longitudinal one. Also the effect of the sulfate concentration in solution is crucial: the cylinders stored in the 5% sodium sulfate solution show a deformation, both in the radial and longitudinal directions, appreciably lower than those stored in the 10% sodium sulfate solution. The same trend can be found on the mean level of damage on the material evaluated through the propagation time of the ultrasonic waves which is higher in the first case.

As for the theoretical and numerical description of sulfate attack, two different models have been developed and implemented in the present work. The firs model is a bi-phase chemo-elastic damage model for the description of the mechanical response in fully saturated conditions. In the context of the Biot's theory of porous media, the concrete subject to sulfate attack is represented as a continuous medium consisting of two phases: the solid skeleton of concrete and the expansive products of the reaction. In this formulation, in line of the models proposed in [Comi et al., 2009] and [Pignatelli et al., 2013] for the concrete subject to alkali-silica reaction, a new model based on two kinds of damage is introduced. An internal variable of chemical damage describes the leaching of hydration products (calcium silicate hydrate and calcium hydroxide) and two internal variable of mechanical damage describe the degradation due to the state of stress (tension and compression) caused by the expansion of the reaction products and/or by the external loads. The evolution of the phenomenon and the macroscopic effects on the material depend of the rate of ettringite produced during the reactions. A proper diffusive-reactive model, based on mass balances, is formulated and implemented for the simulation of the sulfate diffusion and the aluminate depletion. The quantity of ettringite produced during the reactions is directly related to the amount of aluminates consumed.

The second model is based on a three-phase formulation and allow to consider partially saturated conditions. The description of moisture diffusion is performed through a simplified model presented in [Mainguy et al., 2001] and valid in the case of weakly permeable materials. Also the diffusion-reaction model is properly modified for take in account the effect of partially saturated conditions. The mechanical effect of water imbibition is modeled by a internal pressure computed by direct integration of capillary curve. This new model effectively predicts not only the overall expansion due to the chemical reactions but also the real pore pressure arising within the material. A weakly coupled approach for the analysis of concrete structures subject to SA has been proposed and implemented in a finite element code fully developed in Matlab. Several different tests taken from the literature as well as those obtained in this work have been numerically simulated:

a good agreement has been obtained in all cases.

Future developments

The experimental data considered in this thesis and the numerical simulation are limited to concrete and mortar specimen and small scale structures subject to sulfate attack in laboratory conditions. An interesting development of the present work consists in the study of the response of real structures (dams, tunnels, underground storage structures) under sulfate attack. The main problem is to find complete monitored data on real structures subject to sulfate attack. Moreover often the SA is accompanied by other deleterious chemical reaction like e.g. the alkali-silica reaction or by other physical degradation phenomena as in the case of freeze than cycles.

A further very important aspect for engineering applications consists in the development of identification techniques allowing to extract, from available monitoring data, the material parameters to be used in a numerical analysis to predict the subsequent structural behavior and to perform a reliable safety assessment analysis.

Another important development of the present work consists in the introduction of non-local strategy for damage regularization.

Bibliography

[Akpinar and Casanova, 2010] Akpinar, P., Casanova, I., A combined study of expansive and tensile strength evolution of mortars under sulfate attack: implications on durability assessment. *Materiales de Construccion* , 60-297 (2010) 59-68. 1.1, 2.4, 3, 7, 7.2

[Al-Amoudi, 2002] Al-Amoudi, O. S. B., Attack on plain and blended cements exposed to aggressive sulfate environments. *Cement and Concrete Composites* , 24-3 (2002) 305-316. 2.2

[Al Shamaa et al., 2014] Al Shamaa, M. , Lavaud, S., Divet, L., Nahas, G., Torrenti, J.M., Coupling between mechanical and transfer properties and expansion due to DEF in a concrete of a nuclear plant. *Nuclear Engineering and Design* , 266 (2014) 70-77. 1, 2.3

[Bard et al., 2003] Bard, A. and Stratmann, M. and Calvo, E. Encyclopedia of Electrochemistry, vol.2. *Wiley* , (2013) 4.1

[Bary, 2008] Bary, B. Simplified coupled chemo-mechanical modeling of cement pastes behavior subjected to combined leaching and external sulfate attack. *Int J Numer Anal Meth Geomech* , 32 (2008) 1791-816. 1.1, 4, 4.2.2, 4.2.2

[Basista and Weglewski, 2008] Basista, M., Weglewski, W. Micromechanical modeling of sulphate corrosion in concrete: influence of ettringite forming reaction. *Theoretical and Applied Mechanics* , 35 (2008) 29-52. 1.1, 2.4, 4.2.1, 4.2.2, 4.2.2

[Batic et al., 2000] Batic, O. R., Milanesi, C. A., Maiza, P. J., Marfil, S. A. Secondary ettringite formation in concrete subjected to different curing conditions. *Cement and Concrete Research* , 30 (2000) 1407-1412 2.3

[Berriman et al., 2000] Berriman, J., Purnell, P., Hutchins, D.A., Neild, A. Humidity and aggregate content correction factors for air-coupled ultrasonic evaluation of concrete. *Ultrasonics*, 43 (2005) 211-217 3.3.4

[Bockris e Reddy, 2013] Bockris, J.O.M. and Reddy, A.K.N. Modern Electrochemistry: Ionics. *Kluwer Academic Pub* , (2013) 4.1

[Bouzabata et al., 2012] Bouzabata, H., Multon, S., Sellier, A., Houari, H. Effects of restraint on expansion due to delayed ettringite formation. *Cement and Concrete Research* , 42 (2012) 1024-1031 3, 7, 7.5

[Campos et al., 2016] Campos, A., Lopez, C. M. and Aguado, A. Diffusion-reaction model for the internal sulfate attack in concrete. *Construction and Building Materials* , 102 (2016) 531-540 5.6.1

[Carbó, 2009] Carbó, A.D. Electrochemistry of Porous Materials *CRC Press* , (2009) 4.1

[Carol et al., 2001] Cefis, N. and Comi, C., Micromechanical analysis of quasi-brittle materials using fracture-based interface elements. *International Journal for Numerical Methods in Engineering*, 52.1-2 (2001) 193-215. 4

[Cefis and Comi, 2014] Cefis, N. and Comi, C., Damage modelling in concrete subject to sulfate attack. *Fracture and Structural Integrity* , 29 (2014) 222-229. 4

[Collepardi, 1991] Collepardi, M., Scienza e tecnologia del calcestruzzo. *Hoepli editore*, (1991). 2.1

[Collepardi, 2003] Collepardi, M., A state-of-the-art review on delayed ettringite attack on concrete. *Cement and Concrete Composites*, 25-4 (2003) 401-407. 1.1, 2.2, 2.3, 2.4

[Comi et al., 2009] Comi, C., Fedele R. and Perego U., A chemo-thermo-damage model for the analysis of concrete dams affected by alkali-silica reaction. *Mechanics of Materials*, 41.3 (2009) 210-230. 4, 5, 8

[Comi and Perego, 2001] Comi, C. and Perego, U., Fracture energy based bi-dissipative damage model for concrete. *International Journal of Solids and Structures*, 38 (2001) 6427-6454. 4, 5.4, 5.6.3

[Coussy, 2004] Coussy, O., Poromechanics. *John Wiley Sons*, (2004). 5, 5.1, 6.1

[Coussy and Monteiro, 2018] Coussy, O., Monteiro J.M., Poroelastic model for concrete exposed to freezing temperatures. *Cement and Concrete Research*, 38.1 (2008) 40-48. 4

[El-Hachem et al., 2012] El-Hachem, R., Roziére, E., Grondin, F., Loukili, A., Multi-criteria analysis of the mechanism of degradation of Portland cement based mortars exposed to external sulphate attack. *Cement and Concrete Research*, 42 (2012) 1327-1335. 2.2

[Escadeillas et al., 2007] Escadeillas, G., Aubert, J. E., Segerer, M., Prince, W., Some factors affecting delayed ettringite formation in heat-cured mortars. *Cement and Concrete Research*, 37 (2007) 1445-1452. 1.1

[Gawin et al., 2007] Gawin, D., Pesavento, F., Schrefler, B. A., Modeling of cementitious materials exposed to isothermal calcium leaching, considering process kinetics and advective water flow. Part 1: Theoretical model. International journal of solids and structures. Part 2: numerical solution. International Journal of Solids and Structures. *International journal of solids and structures*, 45.25 (2007) 6221-6240, 6241-6268 4

[Gawin et al., 2009] Gawin, D., Pesavento, F., Schrefler, B. A., Modeling deterioration of cementitious materials exposed to calcium leaching in non-isothermal conditions. *Computer Methods in Applied Mechanics and Engineering*, 198.37 (2009) 3051-3083. 4

[Hewlett, 2003] Hewlett, P., Lea's chemistry of cement and concrete. *Butterworth-Heinemann.*, (2003). 2.1

[Idiart et al., 2011(a)] Idiart, A.E. and Lopez, C.M. and Carol, I., Chemo-mechanical analysis of concrete cracking and degradation due to external sulfate attack: a meso-scale model. *Cement Concrete Composites* , 33 (2011) 411-423. 1.1, 2.4, 4, 4.2.1, 4.2.1, 4.2.1, 5.5.1, 5.6.1

[Idiart et al., 2011(b)] Idiart, A.E. and Lopez, C.M. and Carol, I., Modeling of drying shrinkage of concrete specimens at the meso-level. *Materials and structures*, 44.2 (2011) 415-435. 4

[Ikumi et al., 2014] Ikumi, T., Cavalaro, S. H., Segura, I. and Aguado, A., Alternative methodology to consider damage and expansions in external sulfate attack modeling. *Cement and Concrete Research*, 63 (2014) 105-116.. 5.6.1

[Kendall et al., 1983] Kendall, K., Howard, A. J., Birchall, J. D., Pratt, P. L., Proctor, B. A. and Jefferis, S. A., The relation between porosity, microstructure and strength, and the approach to advanced cement-based materials [and discussion]. *Philosophical Transactions of the Royal Society of London A: Mathematical, Physical and Engineering Sciences*, 310 (1983), 139-153. 5.2.1, 5.2.1, 5.4

[Krajcinovic et al., 1992] Krajcinovic, D., Basista, M., Mallick, K., Sumarac, D. Chemo-micromechanics of brittle solids. *Journal of the Mechanics and Physics of Solids*, 40.5 (1992) 965-990. 4.2.1, 4.2.1

[Lamond, 2006] Lamond, J. F., Significance of tests and properties of concrete and concrete-making materials . *ASTM International*, 169 (2006). 3.1

[Leemann and Loser, 2011] Leemann, A., Loser, R. Analysis of concrete in a vertical ventilation shaft exposed to sulfate-containing groundwater for 45years. *Cement and Concrete Composites*, 33 (2011) 74-83. 2.3

[Lei et al., 2013] Lei, M., Peng, L., Shi, C., Wang, S. Experimental study on the damage mechanism of tunnel structure suffering from sulfate attack. *Tunnelling and underground space technology* , 36 (2013) 5-13. 1, 2.2, 7, 7.6

[Lydon and Balendran, 1986] Lydon, F. D., Balendran, R. V.. Some observations on elastic properties of plain concrete. *Cement and Concrete Research* , 16-3 (1986) 314-324. 3.1

[Mainguy et al., 2001] Mainguy, M., Coussy, O., Baroghel-Bouny, V., Role of air pressure in drying of weakly permeable materials. *Journal of engineering mechanics* , 127.6 (2001) 582-592 6.3, 6.3, 8

[Marchand, 2003] Marchand, J., Odler, I., Skalny, J.P. Sulfate Attack on Concrete. *CRC Press* , (2003). 2.4

[Neville, 2004] Neville, A. The confused world of sulfate attack on concrete. *Cement and Concrete Research* , 34.8 (2004) 1275-1296. 1.1

[Ohdaira and Masuzawa, 2000] Ohdaira, E. Masuzawa, N., Water content and its effect on ultrasound propagation in concrete - the possibility of NDE. *Ultrasonics* , 8.1 (2000) 546-552. 3.3.4

[Oliveira et al., 2013] Oliveira, I., Cavalaro, S. H., Aguado, A. New kinetic model to quantify the internal sulfate attack in concrete. *Cement and Concrete Research*, 43 (2013) 95-104. 2.3

[Ouyang et al., 1988] Ouyang, C., Nanni, A., Chang, W. F. Internal and external sources of sulfate ions in Portland cement mortar: two types of chemical attack. *Cement and Concrete Research*, 18-5 (1988) 699-709 2.4

[Pajares et al., 2003] Pajares, I., Martínez-Ramiŕez, S., Blanco-Varela, M. T., Evolution of ettringite in presence of carbonate, and silicate ions. *Cement and Concrete Composites*, 28-5 (2003) 861-865. 2.4

[Pesavento et al., 2012] Pesavento, F., Gawin, D., Wyrzykowski, M., Schrefler, B. A., Simoni, L., Modeling alkali-silica reaction in non-isothermal, partially saturated cement based materials. *Computer Methods in Applied Mechanics and Engineering*, 2225 (2012) 95-115. 4

[Piazza e Parola, 2008] Piazza, R. and Parola, A. Thermophoresis in colloidal suspensions. *J. Phys.: Condens. Matter*, 20 (2008) 153102. 4.1

[Pignatelli et al., 2013] Pignatelli, R., Comi, C., Monteiro, P. J. A coupled mechanical and chemical damage model for concrete affected by alkali-silica reaction. *Cement and Concrete Research*, 53 (2013) 196-210. 5.6.2, 8

[Planel et al., 2006] Planel, D., Sercombe, J., Le Bescop, P., Adenot, F., Torrenti, J. M. Long-term performance of cement paste during combined calcium leachingâsulfate attack: kinetics and size effect. *Cement and Concrete Research* , 36.1 (2006) 137-143. 1.1, 3

[Powers, 1958] Powers, T. C. Structure and physical properties of hardened Portland cement paste. *Journal of the American Ceramic Society* , 41 (1958), 1-6 2

[Roziére et al., 2009] Roziére, E., Loukili, A., El Hachem, R., Grondin, F. Durability of concrete exposed to leaching and external sulphate attacks. *Cement and Concrete Research* , 39 (2009) 1188-1198 1.1

[Samson et al., 2005] Samson, E., Marchand, J., Snyder, K. A., Beaudoin, J. J. Modeling ion and fluid transport in unsaturated cement systems for isothermal conditions. *Cement and Concrete Research* 35.1 (2005) 141-153. 6.3, 6.4, 6.4

[Samson and Marchand, 2007] Samson, E. and Marchand, J. Modeling the transport of ions in unsaturated cement-based materials. *Computers and Structures* 85(2007) 1740-1756 4.1, 6.4

[Santhanam et al, 2002] Santhanam, M., Cohen, M. D., Olek, J., Mechanism of sulfate attack: a fresh look: part 1: summary of experimental results. *Cement and concrete research* 32-6 (2002) 915-921 2.5

[Sarkar et al., 2010] Sarkar, S., Mahadevan, S., Meeussen, J. C. L., Van der Sloot, H., Kosson, D. S. Numerical simulation of cementitious materials degradation under external sulfate attack. *Cement and Concrete Composites* 32 (2010) 241-252 2.2, 4.2.1

[Scrivener and Young, 1997] Scrivener, K. L., Young, J. F.. Mechanisms of chemical degradation of cement-based systems. *CRC Press* , (1997) 2.2

[Schrefler et al., 2002] Schrefler, B. A., Brunello, P., Gawin, D., Majorana, C. E., Pesavento, F., Concrete at high temperature with application to tunnel fire. *Computational Mechanics*, 29.1 (2002) 43-51. 4

[Segura and Carol, 2004] Segura JM and Carol I., On zero-thickness interface elements for diffusion problems. *Int J Numer Anal Meth Geomech*, 28.9 (2004) 947-962. 4

[Taylor, 1997] Taylor, H. F. Cement chemistry. *Thomas Telford*, (1997). 2.1

[Tixier and Mobasher, 2003] Tixier, R. and Mobasher, B., Modeling of Damage in Cement-Based Materials Subjected to External Sulfate Attack, I: Formulation. *ASCE J. Mater. Civ. Eng*, 15 (2003) 305-322. 1.1, 2.4, 4.2.1, 4.2.1, 5.5.1, 5.6.1

[Tarcy et al., 2004] Tracy, S. L., Boyd, S. R., Connolly, J. D. Effect of Curing Temperature and Cement Chemistry on the Potential for Concrete Expansion Due to DEF. *PCI journal* , 49 (2004) 46-57. 1.1

[Ulm et al., 2000] Ulm, F. J., Coussy, O., Kefei, L., Larive, C., Thermo-chemo-mechanics of ASR expansion in concrete structures. *Journal of engineering mechanics* , 126.3 (2000) 233-242. 4, 5

[Wee et al., 2000] Wee, T. H., Suryavanshi, A. K., Wong, S. F., Rahman, A. A. Sulfate resistance of concrete containing mineral admixtures. *ACI Materials Journal* , 97 (2000) 536-549. 1.1, 2, 2.4

[Yu et al., 2013] Yu, C., Sun, W., Scrivener, K. Mechanism of expansion of mortars immersed in sodium sulfate solutions. *Cement and Concrete Research* , 43 (2013) 105-111. 3, 4.2.2, 7.2